Development and Characterization of New Non-evaporable Getter Coatings : to achieve extreme high vacuum

By

RAJENDRA KUMAR SHARMA

(Enroll. No. PHYS01200804016)

Bhabha Atomic Research Centre, Mumbai

Under the guidance of

Prof. S. C. Gadkari

A thesis submitted to the
Board of Studies in Physical Sciences
In partial fulfillment of requirements
For the Degree of

DOCTOR OF PHILOSOPHY

Of

HOMI BHABHA NATIONAL INSTITUTE

OCTOBER 2014

Homi Bhabha National Institute

Recommendations of the Viva Voce Board

As members of the Viva Voce Board, we certify that we have read the dissertation prepared by **Rajendra Kumar Sharma** entitled **"Development and Characterization of New Non-evaporable Getter Coatings: to achieve extreme high Vacuum"** and recommend that it may be accepted as fulfilling the dissertation requirement for the Degree of Doctor of Philosophy.

Chairman- **Prof. B. N. Jagatap**		**Date:** 29/10/2015
Guide / Convener- **Prof. S. C. Gadkari**		**Date:** 29/10/2015
External Examiner- **Prof. B. R. Mehta**		**Date:** 29/10/15
Member 1- **Prof. D. S. Patil**		**Date:** 29/10/15
Member 2- **Prof. D. Srivastava**		**Date:** 29/10/2015

Final approval and acceptance of this dissertation is contingent upon the candidate's submission of the final copies of the dissertation to HBNI.

I hereby certify that I have read this dissertation prepared under my direction and recommend that it may be accepted as fulfilling the dissertation requirement.

Date: 29/10/2015

Place: HBNI, Mumbai

29/10/15

Prof. S. C. Gadkari

(Guide)

STATEMENT BY AUTHOR

This dissertation has been submitted in partial fulfillment of requirements for an advanced degree at Homi Bhabha National Institute (HBNI) and is deposited in the Library to be made available to borrowers under rules of the HBNI.

Brief quotations from this dissertation are allowable without special permission, provided that accurate acknowledgement of source is made. Requests for permission for extended quotation from or reproduction of this manuscript in whole or in part may be granted by the Competent Authority of HBNI when in his or her judgment the proposed use of the material is in the interests of scholarship. In all other instances, however, permission must be obtained from the author.

Rajendra Kumar Sharma

Declaration

I, hereby declare that the investigations present in this thesis has been solely carried out by me. The work presented is original and has not submitted earlier as a whole or in part for a degree/diploma at this or any other Institution/University.

Rajendra Kumar Sharma

Dedicated To My Family and Friends

ACKNOWLEDGEMENT

My heartly thanks to all who have helped and inspired me during period of accomplishment of this thesis. This thesis would not have been possible without the encouraging support of my adviser **Prof. S. C. Gadkari**. His continuous motivation and guidance helped a lot to execute the work in the thesis. I would also like to express my gratitude to the members of my doctoral committee;**Prof. B. N. Jagatap, Prof. S. C. Gadkari, Prof. D. S. Patil and Prof. D. Srivastava** for attending all the long review sessions and remarking the essential comments and suggestions.

I would like to thank **Prof. S. K. Gupta, Head, TPD** and **Mr. M. R. Singh**, **Head, S&LTPS** for encouraging to finish my thesis.

I am very thankful to **Dr. K. G. Bhushan & Dr. Shashwati Sen** for helping me to initial setting of deposition facility and suggestions during writing my thesis.

I am very grateful to **Dr. Jagannath**, **Mrs. Nidhi Gupta** for characterizing my samples on XPS facility which took number of days to complete a single sample. I am very thankful to **Mr. Haridas Patil** who has given full support during all the UHV work which needs a tremendous effort. I am thankful to **Mr. R Pradeep**, **Mr. Kaushik Dutta, Mr. R. K. Nair, Mr. U. K. Goutam, Mr. V. Nataraju, Dr. R. Mukund, Dr. K. C. Rao, Dr C. L. Prajapat, Mr. S. M. Rodrigues** for their support.

I would like to thank **Dr. S. Bhattacharya**, **Atul K Sinha**, **Dr. C. B. Basak** and **Mr. R. B. Tokas** for their necessary support during the experiments on the samples.

Finally, I would like to offer my gratitude to my family and friends who have always motivated and supported me.

Rajendra Kumar Sharma

CONTENTS

CHAPTER 6

Synopsis

Development and Characterization of New Non-evaporable Getter Coatings: to achieve extreme high Vacuum

Getters are well known for their unique property of high affinity for chemical bonding with different gases or chemisorbing gas molecules on their surfaces. They are used in many applications such as in vacuum tubes, field – emission displays, inert gas purification systems, plasma purification, hydrogen species recycling as in Tokamak Fusion Test Reactor, Particle accelerators, Synchrotron Source and highly surface sensitive application. Getters, however have very limited pumping capacity for inert gases such as noble gases and methane ($CH_{4)}$. All adsorbed gases remain on the getter surface, H_2 can diffuse into the bulk after adsorption even at room temperature.

Getter materials are classified in two families depending on the production of active surfaces (evaporable and non-evaporable) [1]. The concerned topic of this report is non evaporable getters (NEG) in the form of thin films or coatings. NEG coatings which are basically alloy of different getter materials are known to act to achieve extreme high vacuum (XHV) (range of pressure below 10^{-11} mbar). In spite of producing extreme high vacuum, the NEG coated surfaces shows many other beneficial properties over conventional material surfaces. NEG coated surfaces undergo very low out gassing as compare to material surface in conventional form, e.g., SS, Cu and Al etc. Secondary electron yield (SEY) of NEG coated surfaces 30-40% lower than material surfaces in conventional form [2]. Photo desorption studies revealed the reduction of 1-2 order in the photo desorption yield [3]. Action of the NEG coating starts after heating it to its activation temperature which depends on the composition of the coatings. NEG coatings once activated apart from providing an ideal linear pumping for

conductance limited pipes distributed over all the system, it may also inhibit the desorption of gas molecules from the vacuum chamber which is not possible with conventional materials(SS, Cu, Al). Most of the advanced accelerator and large detectors like LHC(CERN), ESRF (France) [4], Elletra (Italy) [5], Diamond (U.K.) [6], Soleil [7], MaxIII (Sweden) [8] and CATRIN (Germany) are utilizing NEG coated pipes in order to get the better UHV conditions. In LHC where the ring is 27 km long is mostly using the vacuum pipes coated with the NEG materials. In the interaction region of LHC, the extreme high vacuum of the order of 10^{-13} mbar was achieved by using NEG coating. Our group is also involved in the development many high precision sub-systems, e.g., electron energy spectrometers (Hemispherical type, Toroidal type) and Photo electron emission microscope (PEEM) which will be later benefitted with development of NEG coatings and pumps.

There are no. of getter coatings which have been already used, e.g., St101, binary alloy in the form Zr 84 Al 16 (wt%) (Activation temperature of 750°C) [7,8], St707, ternary alloy in the form of Zr 70 V 24.6 Fe 5.4 (wt%) (Activation temperature of 450°C)[9], ternary alloy NEG coatings (TiVZr) [10]. This thesis presents the study of NEG coatings and later it is being deployed for in-house development of NEG coatings and pumps.

Literature confirmed about group IVB elements (Ti, Zr, Hf) (hcp structures) in periodic table shows the maximum solubility [11, 12, 13] for oxygen and VB(V, Nb, Ta) (bcc structures) shows maximum diffusion length for oxygen [14, 15] inside the bulk. Different combination of these elements were studied and tested. A high solubility limit is essential to accommodate oxygen accumulation due to many activation air-exposure (so-called venting) cycles [16]. The thickness of the oxide layer formed during air exposure is 2 – 3 nm. A 1µm thick film would present an oxygen concentration of 2–3% after 10 such cycles. Solubility limit

of at least of 10% is desirable for better performance [17]. The ternary form of TiVZr and TiNbZr in different stoichiometry getter films were DC-magnetron sputtered coated and studied. The TiNbZr film in stoichiometry of $Ti_{20}Nb_{55}Zr_{25}$ in at.% was studied which showed the activation after heating at 250ºC[18]. Among many tested Non-Evaporable Getter (NEG) materials, the lowest Activation temperature (T_A) in the range(160-180°C) [19] has been achieved for TiVZr alloy in suitable stoichiometry of $Ti_{27}V_{45}Zr_{28}$. So the TiVZr coatings will be the principal part of this thesis. The aim of the thesis to study and investigate the properties that are in the benefit of the optimization of the film quality for the better performance in terms of gettering action. These properties are microstructure, surface roughness, grain size of the NEG coatings and optimize their surface properties to act efficiently for the creation of extreme high vacuum (XHV). X-ray Photoelectron spectroscopy used as a main tool to get the Activation temperature of NEG films. Scanning Electron Microscopy (SEM) provide the microstructure of the film which plays the crucial role in adsorption and diffusion of the oxygen from surface to the bulk and across the grain boundaries efficiently. Atomic Force microscopy attributes the surface roughness of the film. Rougher is the surface more no. of active adsorption sites will be present. The DC magnetron sputtering deposition technique was used for coating. This technique provides many benefits over other techniques in terms of mechanical strength due to higher energy of the sputtered species (1 eV-10 eV) [20] than those of the other deposition techniques such as thermal evaporation and chemical decomposition. The sputtering process achieves the deposition of variety of materials without heating the source materials. The in-house cylindrical type DC-magnetron sputtering system designed and developed which has fulfilled our requirements to coat the NEG materials on inner walls of the vacuum pipes, large area stainless steel sheets. These sheets were to used to make prototype NEG pumps.

The secondary electron yield (SEY) of these NEG films is low as compared to material in natural form . The secondary electrons which are generated in a multiplication process by highly charged bunches [21], play a large part in the formation of an electron cloud, especially at a large bunch-current region. One promising way to suppress the ECI (Electron Cloud Instability) is, therefore, to apply a surface with a low secondary electron yield (SEY) to an inner surface of a beam duct [22, 23]. The SEY plays very important role in the accelerators as it lead to multi-pacting effect with the main beam. It is advisable to have material with low SEY to avoid the multi-pacting effect. For SEY measurement we have designed and assembled in-house secondary electron measurement setup under ultra high vacuum condition. The SEY of NEG coated and uncoated samples was measured for different primary electron energies (0 – 2.5 KeV). The results showed the reduction of SEY of coated samples than those of uncoated. The measurement of coated sample was also taken after heating the sample at different temperatures in the range (140 - 180 ^{0}C). SEY of coated samples decreased after activation temperature of 180 ^{0}C.

NEG pumps was produced by deploying the long NEG coated SS304 strip. The pump was facilitated with in-vacuum resistive heating of the NEG strip. A K-type thermocouple was integrated to monitor the temperature of the NEG strip. The whole assembly was mounted on a DN100CF flange. The NEG pump was directly mounted on a XHV testing set up. After 24 hrs activation of NEG pump at 180^{0}C by applying DC current of 12A , the lowest pressure of the order of $<10^{-12}$ mbar was achieved.

The summary of the work has been divided in six chapters.

Chapter 1 : It has been divided in two parts. The first part describes the fundamental aspects and brief introduction of getter materials, different types of available non evaporable getters such

alloy 101 (Zr-Al), alloy707 (Zr-V-Fe), alloy 185 etc. The physical and chemical properties of NEG materials e.g., electron affinity, dissociation energy, solubility, diffusivity etc. that make them useful in-terms of getter materials and renders to the creation of extreme high vacuum. The second part describes the brief introduction and some fundamental aspects of vacuum physics, brief description of vacuum pumps and type. It also consists of measurement of different ranges of pressures and materials used for vacuum application. Last portion of the chapter briefs about the role of solubility and solubility limit of IVB elements for oxygen and the fundamental concept of diffusion, calculation of diffusion coefficient for the materials which is very relevant in describing the action of NEG material.

Chapter 2 : In this chapter a brief introduction about the different type of coating methods with advantages and disadvantages is given. Fundamentals of the sputtering deposition and the brief introduction of Physics of sputtering is included. The description of the simulation, design and the development of in-house cylindrical DC-magnetron sputtering system has been included. This chapter also covers the fundamentals steps of the film deposition, different types of film growth and factors affecting the quality of the film such as, deposition pressure of the sputtering gas, purity of the sputtering gas, type of sputtering gas, temperature of the substrate, effects of type of the substrate, adhesion of the film.

Chapter 3: The brief introduction of different types of surface characterization techniques, e.g., X-ray Photoelectron Spectroscopy (XPS), Scanning Electron Microscopy (SEM) and Atomic Force Microscopy (AFM). Grazing Incidence X-ray Diffraction technique benefits a lot over normal angle x-ray diffraction in case of the structural analysis of thin film which were used in the characterization of the films, the description of this technique has been also covered in this chapter. The comparative studies regarding to microstructure benefited to better adsorption, have

been shown using micrograph of Scanning Electron microscope of film deposited in different stoichiometry.

Chapter 4: It describes the thermal activation studies both qualitatively and quantitatively based on the X-ray photoelectron spectroscopy of NEG films has been described. Different steps of the process which were involves during the surface characterization are contented. Heating of the film in a controlled manner with a constant increase in temperature and then keep it at the same temperature for 2-3 hours and then cool it down to room temperature to get the film in equilibrium. After reaching to room temperature, XPS spectra in angle integrated mode has been taken. This all sequential study was done at different temperature from 100ºC to 350ºC to all the NEG coatings that had studied in this thesis. In this process we do the activation studies of the NEG film which is linked with the shift in the B.E. of the NEG materials present at the surface of the film. The temperature at which the shift in the B.E. of the elements starts is known as Activation temperature of the NEG film.

Chapter 5: This chapter enunciates the design, development and assembly of the test set up to achieve XHV using combination of TSIP & NEG pumps after heating later to Activation temperature. The evolution of partial pressures with time after activation for different gases, e.g., H_2, CO_2 etc. has been also depicted.

Chapter 6: CONCLUSION

Coatings of NEG materials in the form of ternary alloy were prepared using in-house developed cylindrical type DC-magnetron sputtering system. Cylindrical DC-magnetron Sputtering system was developed to deposit the NEG film on internal surfaces of longer UHV compatible pipes and big size SS sheets. Surfaces of these coatings in as-deposited as well as after heating at different temperatures were characterized deploying XPS. Activation temperature which was based on the

shift in the characteristic B.E. peaks of the constituent elements of these films was achieved. Microstructure of the prepared films was studies on SEM. Stoichiometry of the coatings was produced using EDX and XRF techniques. The evolution of pressure with time has been shown. Nature of the film was achieved with GIXRD measurements which shows the polycrystalline form of the film with average grain size of 28 - 38 nm.

List of Publications arising from the thesis

Journals

1. "Thin film of ternary transition metals in alloy form : path to achieve very low vacuum, **R. K. Sharma**, Jagannath, Sovit Bhattacharya, SC Gadkari, R. Mukund, V. K. Handu, Asian J Physics Vol 17, No.2 (2010)1-6.

2. "Deposition and in-situ characterization of Ti-Zr-V alloy thin films annealed at different temperatures under ultra-high vacuum conditions", **R. K. Sharma**, Jagannath, S. Bhattacharya, R.B. Tokas, K.G. Bhushan, Shashwati Sen, S.C. Gadkari, S.K. Gupta, Journal of Alloys and Compounds 651 (2015) 375-381.

Conferences

1. " Ti-Zr-V thin films as Non-Evaporable Getters(NEG) to produce extreme high vacuum"**,** **R.K. Sharma**, N. Mithal, Jagannath, K.G. Bhushan, D. Srivastava, **H.** R. Prabhakara, S. C. Gadkari, J.V. Yakhmi and V. C. Sahni**,** *Journal of Physics: Conference Series* 114(2008)012050.

2. " Characterization of NEG coating for the production of Extreme high vacuum", **R. K. Sharma**, Jagannath, Nidhi Mithal, S.C. Gadkari, K. G. Bhusan, R. Mukund and J. V. Yakhmi *published in BARC Newsletter, October 2010 p.291*.

3. " Thin films of Ti–Nb–Zr as non-evaporable getter films", **R. K. Sharma**, Jagannath, S. Bhattacharya, S.C. Gadkari, R. Mukund and S. K.Gupta, *Journal of Physics: Conference Series* 390 (2012) 012041

4. "Activation studies of NEG coatings by surface techniques", **R. K. Sharma**, Jagannath, K. G. Bhushan, S. C. Gadkari, R. Mukund , AIP Conf. Proc. 1512, 790 (2013); doi: 10.1063/1.4791275*).*

5. "Studies of thin films of Ti- Zr -V as non-evaporable getter films prepared by RF sputtering", Nidhi Gupta, Jagannath**, R. K. Sharma**, S. C. Gadkari, K. P. Muthe, AIP Conf. Proc. 1512, 794 (2013); doi: 10.1063/1.4791277.

6. "Secondary electron measurement and XPS characterization of NEG coatings", **R. K. Sharma**, Atul K. Sinha, Nidhi Gupta, J. Nuwad, Jagannath, S.C. Gadkari, M. R. Singh, S.K. Gupta, AIP Conf. Proc. 1591, 916 (2014); doi: 10.1063/1.4872801.

7. "Surface studies and measurement of pumping characteristic of NEG coating (Ti-V-Zr)", **R. K. Sharma**, Atul K Sinha, Jagannath, D.C. Basak, S.C. Gadkari, M.R. Singh, S.K.Gupta, XXVI Int. Symp on Discharges and Electrical insulation in vacuum- 2014, p.529.

LIST OF FIGURES

LIST OF TABLES

CHAPTER-1

1.1 Introduction to Getter materials

Getters are a class of materials that have strong chemical affinity towards gas species such as H_2, CO_2, O_2, N_2 and H_2O. In general, getter materials react chemically with gas molecules to form stable low vapour pressure compounds that result in the removal of the residual gas molecules from a within a sealed-off vacuum system, thereby reducing the total pressure in the system. Hence these chemically active metals or alloys are called getter metals or just getters in short. Different types of evaporable and non-evaporable getters have been developed over the years, such as Ba getters used as flash getters at room temperatures [1-3], Ti getters in bulk form are used in the titanium sublimation pumps [4]. The Zr and Ti based alloys can be binary, ternary or multi-component, comprising the elements such as Ni, Fe, Al, Co, rare earth etc. to obtain specific gettering characteristics and other required physiochemical features. Getter materials do not pump inert gases (He, Ne, Ar, Kr) as well as methane effectively. Several getter materials either as a single element or in the form of alloys (binary, ternary or quaternary) have been reported in literature that are being utilized in the form of evaporated and non-evaporated getters. Thorium and uranium have also been found to be useable as getter materials but their radioactivity and pyrophoricity limit their applicability [5]. Hafnium also exhibits some interesting gettering capability but availability, cost and stability limits its use in real getters [5]. Different types of non-evaporable getters are used in the form of alloys, such as alloy of Zr/Al (commercially called St101), ternary alloy of Zr/V/Fe (commercially called St707), alloy Zr/Co, alloy Ti/Zr, alloy of Ti/Nb/Zr, alloy of Ti/Zr/V, alloy of Ti/Zr/V/Hf, etc.

1.2 Importance of getter materials

Getters play a very important role in variety of applications such as vacuum tubes [6] with sealed-off vacuum of the order of 10^{-4} to 10^{-6} mbar to remove the residual gases to avoid the fall in cathode emission, screen spots, variation of applied potentials due to contaminated surfaces, arcing due to high voltage, etc. Getters improve the effective vacuum inside the vacuum tubes in the range of 10^{-5} to 10^{-7} mbar. Some of the systems that require UHV / XHV are linear accelerators, synchrotron accelerators, large hadron collider (LHC), low energy photoelectron diffractions etc. [7]. In accelerators, getter coated surfaces provide linear distributed pumping resulting in nearly uniform pressure throughout the length of the vacuum pipe, which otherwise is not possible with localised conventional pumps. The NEG coated surfaces also provide a low secondary electron yield and low photo-desorption yield, thereby enhancing the storage lifetimes of charged particles beams circulating inside vacuum pipes. In inert gas purification system, getters are utilized to reduce the impurities down to ppm levels for long periods, as required in fusion devices [8,9, 10]. The gettering process is also important in the solid storage of hydrogen [9].In this thesis work, we focus our attention on those getters that are used in the production of ultra high vacuum(UHV) and extreme high vacuum(XHV)(range of pressure below 10^{-11} mbar).

1.3 Requirement of getter materials

Getter materials in thin film or bulk form are used to create XHV in a sealed-off system where they are utilized to capture residual gas molecules as evaporable or non-evaporable getters. A good example of evaporable getter is titanium. Titanium in the form of thin filaments are used in titanium sublimation pump which is sublimed with high current to form freshly prepared Ti films that chemisorbs the active residual gases to make chemically stable, low vapour pressure compounds. This action leads to net removal of residual gas species

thereby decreasing the ultimate pressure in the system. The problem with evaporable getters is that they are used for localized pumping and require additional vacuum piping which increases the total volume and surface area. The Non-evaporable getters (NEG) materials, on the other hand, can be coated on the inner walls of vacuum pipes or chambers so that they provide linear distributed pumping at every point in a sealed-off vacuum system. These materials do not add any extra volume to the main chamber. The NEG coatings need to be thermally activate din order to initiate capture of residual gas molecules. This is usually done during the baking of vacuum chambers or pipes to temperatures of the order of 300ºCwhich also activates the NEG coatings, e.g., St707alloy, has an activation temperature of about 450ºC [11] while NEG coatings of Ti/Zr/V can be activated around 160ºC.

1.4 Historical perspective

Most of the residual gases in atmosphere such as, H_2, CO_2, O_2, N_2 and even H_2O will react with many solids to form stable, strongly bound compounds through the gettering process. Such gettering processes were initially studied in the late 19^{th} century to improve the vacuum within carbon filaments and improve its useful life time [12].Getter materials in different forms and combinations have later been utilized in the vacuum technology as well as in other applications such as inert gas purification, in field emission displays and in H_2 storage devices etc. for the last 4-5 decades. Apart from different applications of getter materials, in this thesis work we concentrate only in the ultra high vacuum/extreme high vacuum applications of NEG materials. Initially single element getters such as Ba and Ti were used in the bulk form. Kindl and Robusin [13] first proposed the idea of a binary alloy of Zr-Al as a non-evaporable getter in the form of thick film coatings. It was found that this getter performed better that Ba getters in terms of regenerations. The coating of St101 alloy was also used in CERN vacuum pipeline of 27 km LEP as the main UHV pumping element. For

activation of the coating, a heating (resistive) of more than 750ºC is required [14] which is quite high for the electrical feed-throughs and welding of the systems. Since group VB(V, Nb, Ta) elements shows greater diffusivity, a ternary alloy of Zr/V/Fe (St 707) was developed as NEG coating. The St707 alloy showed an activation temperature of 450ºC [11] which was much less than that of the St101 alloy. The bulk getter Zr/Co has a large capacity for hydrogen storage [15]. Coatings of binary alloy of Ti/Zr showed the activation temperature of 250-300ºC [16, 17]. The coating of ternary alloy of Ti/Nb/Zr showed the activation temperature of 250ºC [18].

1.5 Current research in getter materials

In the search for low activation temperature NEG materials with good sorption/storage capacity, the combination of IVB and VB materials either in ternary or quaternary form have emerged as the most suitable and preferential candidates. A few low temperature activated NEG coatings have already been developed e.g. Ti-Zr (activation at 250 - 300ºC) [16, 17], Ti/Zr/V(activated at 180-200ºC). Recently, Malyshev et al [19] developed a quaternary coating of Ti-Z-Hf-V NEG materials, where they have provided a comparative study of dense film and columnar film and have reported the lowest activation temperature of 150ºC for a quaternary coating of columnar type of morphology. They have also reported on the role of morphology for lowering the electron-stimulated desorption of the coating.

1.6 Low activation temperature getters

Evaporable getters such as Ti and Ba are high temperature getters where the getter materials need to evaporate first then deposited to some surfaces in the form of fresh active film. The residual active gas molecules are chemisorbed on the surface thereby net removal of residual

gas molecules takes place in a sealed-off system. On the other hand, the non-evaporable getters both in bulk and coating form, removes the residual molecules inside of a sealed-off system by heating them only to their activation temperatures that ranges from 160ºC to 200ºC for different type of alloy NEG coatings. These types of getter materials are called low temperature getters. The alloy St101 activates at a temperature of 700ºC and other ternary alloy St707 is fully activated at temperatures about 450ºC. There are other NEG coatings such as binary alloy of Ti-Zr that can be activated at lower temperature around 250ºC and ternary alloy of Ti-Nb-Zr can be activated at temperature below 250ºC [18]. Most recently, the lowest activation temperature in the range 160-180ºC has been achieved for the ternary film Ti-V-Zr.

1.7 Physics of Getter materials

1.7.1 Different classes of getter materials

Getter materials are classified in two families namely, *evaporable* or *non-evaporable,* depending on the production of active surfaces. In principle, all getters can be used either as *evaporable* or as *non-evaporable*. It is easier or more convenient to use certain getter materials in the *evaporated* mode and others in the *non-evaporated* mode.

Evaporable Getters: In the case of *evaporated getters*, the getter material is heated to a sufficiently high temperature to evaporate and form a film onto a surface inside the vacuum system. This film is immediately ready to absorb gases. The geometric area and the real area of the film determine the speed and capacity of the getter. Particularly Ba, Ca, Sr, Ti, P are generally used as *evaporable* getters.

Non-Evaporable Getters (NEG): In the case of *non-evaporated* getter which is also the topic of the present thesis, there is no evaporation or sublimation of the getter material; the gases react on the available surface of the material and, if sufficient energy is supplied, diffuse into

the bulk. The metals of the IVB group and particularly Zr and Ti, in pure or alloy form, are generally used as *non-evaporable* getters. Ti is also used as an evaporable getter in the so-called sublimation pumps. Multi-component thin films, and bulk alloys consisting of combinations of various elements like Ni, Fe, Al, Ti, Zr, V, etc Co have been studied and reported in literature.

1.7.2 How do getters actually work

When a molecule interacts with a solid surface a number of phenomena (shown in Fig.1.1) can take place. Out of these phenomena, the adsorption and later diffusion of the molecules are important in the consequence of gettering action. The getters eliminate active gases from a vacuum environment by chemically binding the gaseous molecules to their surfaces. Generally, the reaction proceeds by dissociative chemisorptions, followed by a reaction to form the resulting oxide, carbide, or nitride:

CO (gas) + 2 M<=>CO (adsorbed) + 2M + M-C + M-O

CO_2 (gas) + 3 M<=>CO_2 (adsorbed) + 3M + M-C + **2** M-O

N_2 (gas) + 2 M<=>N_2 (adsorbed) + 2M + 2M-N

NO (gas) + 2 M<=>NO (adsorbed) + 2M + M-O + M-N

Where, M represents the constituents of the NEG getter alloy. Hydrogen compounds seem to be an exception, with the hydrogen dissociates and chemisorbed then dissolved into the bulk;

H_2 (gas) + M<=> 2 H (adsorbed) + M <=> 2 H (M bulk)

H_2 (gas) + 3M <=> 2 H (adsorbed) + M-O + 2 M<=>M-O + 2 H (M bulk)

The criteria for the working of a getter material are governed by the *solubility* and *diffusivity* of the getter materials for oxygen at elevated temperature. Solubility for oxygen helps to create active surfaces through adsorption by dissolving the superficial surface oxide in the bulk of the coating after elevating temperature. Transition metals of IVB and VB have the

property to make solid solution readily with oxygen. Systematic variation in the oxygen solubility from one group to other having same crystalline structure and lattice parameter, suggests, that it may be governed by their electronic structure. The mechanism associated with gas solution [20, 21] in a getter material is usually described by a three step process:

(a) dissociation of the gas molecules at the gas surface interface;

(b) sorption at the superficial, or near surface, sites; and

(c) dissolution in the bulk of getter material, through diffusion mechanisms.

A solid solution of gas metal system is formed with the adsorbed gas species usually located at the interstitial sites of the lattice of the host metal. The structural effects caused by gas dissolution are generally limited to some expansion of the lattice, with increase of lattice parameters. Solid solution(α phase) is thermodynamically stable until the solubility limit is reached.

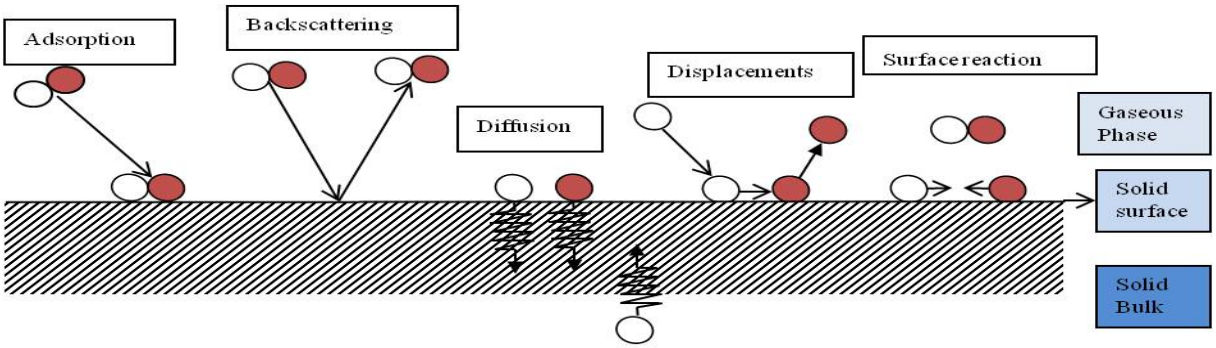

Fig.1.1: Some type of gas surface interaction.

In the case of the dissolution of a di-atomic gas species, the solid solution in a getter material can be shown by the reaction below:

$$X_{2(g)} \rightarrow 2\,[X]_{(s)} \qquad ----------(1)$$

Where *g* and *s* denote gas phase and solid solution, respectively.

After reaching the thermodynamic equilibrium, the pressure P is proportional to the square r of the gas species concentration in the material, q:

$$P = K\,q^2 \qquad \text{---------(2)}$$

Gas concentration related to gas pressure and to the getter temperatures by Sievert law [22] is given as:

$$log\ P_{X_2} = A + 2\log C_X + \frac{B}{T} \qquad \text{--------(3)}$$

Where A and B are gas constant parameters depending on gas type and getter material which can determined experimentally. This Eq. (3) is valid for any solute gas. The solid solution is thermodynamically stable until the solubility limit is reached. Approaching this concentration, the interaction between the solute atoms tend to increase, nucleation and growth of solid phases co-exist and the isotherms shows a plateau, which depends on temperature, according to Van'T Hoffs law:

$$\frac{1}{2}\ln P = -\frac{\Delta S}{RT} + \frac{\Delta H}{RT} \qquad \text{---------(4)}$$

Where P is the pressure, T is the getter temperature in K, and ΔS and ΔH are, respectively, the entropy and enthalpy of formation of the β phase. In high-vacuum (HV) and ultrahigh-vacuum (UHV) applications of getter materials, the amounts of gases involved in the sorption process are relatively small and therefore they typically form dilute solid solutions.

Group IVB elements (Ti, Zr, Hf) in the periodic table shows maximum solubility limit for oxygen at room temperature [23] as shown in Table1.1and Table 1.2 which will enhance the life time of a getter materials so that it can be utilized for number of cycles.

Table1.1: Solubility limit of different elements at room temperature [24].

IIIB	Solubility	IVB	Solubility	VB	Solubility
Sc	1%	Ti	20%	V	1%
Y	1%	Zr	20%	Nb	1%
La	1%	Hf	20%	Ta	1%

Table 1.2: Numerical values of solubility limit of oxygen (x_o) for the elements of the 3rd, 4th and 5th groups.

Group	Metal	Solubility(Atom %)	T[K]	Refs.
3rd	Sc	2	400	[25]
	Y	0.33	673	[26]
		4.2	773	26]
		18	1453	[26]
4th	Ti	33	600-900	[25]
		30	—	[27]
		32	0-1800	[26]
	Zr	29	473-773	[26] [28]
		35	2338	[26]
	Hf	17	1000-2200	[25]
5th	V	4	200 - 600	[25]
		3.5	473-573	[26]
		$\log x0 = -3.918 + 7.383 \times 10^{-3} T - 6.711 \times 10^{-6} T2 + 2.083 \times 10^{-9} T^3$	935 - 1415	[29]
		$\log x0 = -77 + (383/T)$		[29]
		7	973	[30]
		$\log x_0$ weight = 0.705 – (515/T)	473-1023	[30]
	Nb	$\log x_0 = -0.33 - (1680/T)$	1073-1773	[31]
		0.013	1123	[31]
		$-\log x_0 = (8600 \text{ cal } g-1/RT) + 0.516$	973-1823	[32]
		0.20	973	[33] [34]
		0.40	1173	[33] [34]
		0.33	418	[35]
		$\log x_o$ weight $= -32 + 3.33 \times (1000/T)$	1050-1373	[36]
		1.15	973	[37]
		6	2048	[38]
		1	973	[30]
	Ta	$\log x_o = -0.78 - (980/T)$	873-2153	[38]
		4	1600	[25]
		0.4	823	[39]
		0.10	1000	[33][34]
		0.30	1373	[33] [34]
		5	1323	[40]
		$\log x_o(ppm) = 4.130 - (1279/T)$	873-1173	[41]
		2	973	[30]

1.7.3 Diffusivity and diffusion length of oxygen for IVB and VB elements:

Diffusivity is the other important factor in the working of NEG materials as it provides an easy path for surface oxygen to diffuse inside the bulk which is governed by the

concentration gradient under thermal energy. The numerical values of diffusivity of oxygen can be calculated by using the formula,

$$D(T) = D_o\, e^{\frac{-E_O}{R.T}} \qquad ---------(5)$$

where, D(T) is the diffusion coefficient (or diffusivity) of the oxygen in metal at temperature T, D_o is a constant ($cm^2\ s^{-1}$), E_o is the activation energy for diffusion of the element oxygen ($J\ mol^{-1}$) and R is the molar gas constant ($8.314\ JK^{-1}mol^{-1}$).

The diffusion length L during the time t at temperature T is given by [42]:

$$L = \sqrt{D(T).t} \qquad ---------(6)$$

The diffusion coefficients of various gas metal systems are given in Table 1.3.

Table1.3: Numerical values of diffusivity for oxygen Metal Systems at Different Temperatures.

Group	Metal	D_0[cm^2s-1]	E_0[Jmol-1]	T[K]	Refs.
3rd	Sc(α)	D = 2.8 × 10−6		1498	[43]
		1.16 X 1010	448 530	1470–1700	[44]
	Y(α)	9.4 × 10−3	86 700	1173–1733	[43]
	La	D = 6.6 X 10-7		1083	[43]
4th	T i(α)	0.45	201 000	573 – 1223	[43]
		0.8	200 830	673 – 1123	[45]
		2.03 X 10^5	315 168	1199 - 1423	[46]
	Zr(α)	6.61 X 10^{-2}	184 200	563 – 923	[43]
		6.61 X 10^{-2}	184 100	563 – 923	[47]
		9.13 X10^{-5}	124 770	< 973	[48]
	Along [0001]	0.115	186 046	523 – 773	[49]
	Along[0001]	1.07	193 286	523 – 773	[49]
	Hf(α)	0.66		773 – 1323	[43]
		0.66	212 800	1073	[43]
		D = 3.8 X10^{-11}			[47]
		0.66 212 800		773 - 2073	
5th	V	2.46 X 10^{-2}	123 490	333 – 2098	[43]
		1.90 X 10^{-2}	122 850	333 – 2098	[40]
		1.3 X 10^{-2}	121 600	489 - 774	[49]
	Nb	5.86 X 10^{-3}	109 650	296 – 1823	[43]
		6.95 X 10^{-3}	110 000	296 – 1823	[43]
		4.2 X 10^{-3}	107 200	303 – 1773	[43]
		1.38 X 10^{-2}	111 530	296 – 1873	[50]
		8.0 X 10^{-2}	116 320	403 -1073	[50]
	Ta	1.05 X 10^{-2}	110 430	298 – 1673	[43]
		1.14 X 10^{-2}	110 940	298 – 1873	[41]
		1.9 X 10^{-2}	114 819	700 – 900	[51]

Table 1.2 shows that the solubility limit of metals of group IVB is maximum, so they have higher storage capacities for oxygen. IVB elements can be used for more number of cycles when used as NEG materials and alloy coating of such materials sustained for longer times.

In Table 1.4 the calculated values of diffusion lengths of IVB and VB are given after two hours of heating at 300ºC which indicate that metals of group VB have a higher diffusivity. Alloying with VB materials provides easy diffusion of surface oxygen at lower temperatures. It is concluded that NEG coatings prepared by alloying of IVB and VB elements can be very efficient and have a longer life. In addition, the activation temperature is lower due to structure of alloy and density of grain boundaries as compared to other NEG materials.

Table 1.4: Numerical values of diffusion length of oxygen (*L*), in nanometres, for the elements of the 4thand 5th groups for 2 hours heating at 300°C.

S.N.	**IVB group**			**VB group**		
Elements	Ti	Zr	Hf	V	Nb	Ta
Diffusion length (nm)	0.39	0.87	0.14	312	652	804

1.8 Preparation and activation of getters

Coating of non-evaporable getters on some vacuum compatible substrates can be prepared by pressing, sintering or by a physical vapor deposition technique. The St101 was prepared by pressing the powder of Zr and Al. Young Joon Yoon et.al.[53] prepared alloys of Zr-V-Fe and Zr-Co in bulk form by plasma arc melting and electron beam melting. Benvenuti et.al.[16, 23]prepared NEG coatings of binary and ternary alloys by using different combinations of IVB and VB elements such as Ti-Zr, Ti-Hf, Ti/V/Z etc. The Ternary alloy coating of NEG material Ti/V/Zr and Ti/Nb/Zr on stainless steel substrates are prepared in our lab by a DC-magnetron sputtering system. Malyshev et. al. [19] prepared the quarternary alloy Ti-Zr-Hf-V, through DC- magnetron sputtering by using a composite alloy target of Ti-Zr-Hf-V. Inevitably, a thin oxide layer is formed on the surface of any non-evaporable getter after the preparation of coatings when exposed to atmosphere. This thin oxide layer is very

stable and prevents the atmospheric gases from reacting with the bulk of the alloy. When the coated system is sealed off, it is necessary to remove this surface oxide film from the getter surfaces.

The concept of activation of any getter material is as follows. The surface of the powder form of any getter material or thin film is readily covered mainly by oxide layer when surface is exposed to air for the first time. This layer passivates the getter materials thus inhibiting further adsorption of gases. The getter material, therefore, is not immediately active and ready to act when introduced in the vacuum environment. In order to make the getter material to chemisorb different gaseous species, the passivating layer has to be removed which occurs automatically in *evaporable* getter during heating because a new fresh metal surface is formed during the evaporation under vacuum, with oxygen and carbon atoms being dissolved in the evaporated film mass. In the case of non-evaporable getters, the removal of passivating layer to get clean, essentially metallic surface is usually necessary before the getters starts working, this process is called *activation* [54, 55] of the getter materials. It is generally performed by heating the material for sufficient time to promote the diffusion of superficial oxygen and carbon atoms into the bulk of the materials. The process is regulated by the diffusion laws and can be performed using suitable combinations of temperature and time. The partial and full activation of the *non-evaporable* getters are possible as per the level of the obtained metallic surfaces. After full activation, the pumping speed of gettering reaches a maximum due to the availability of maximum number of adsorption sites. H_2 can diffuse easily through the porous and cracked oxide layer and later absorbed by the getter metal surface immediately underneath. The activation process has been schematically represented in Fig.1.2.

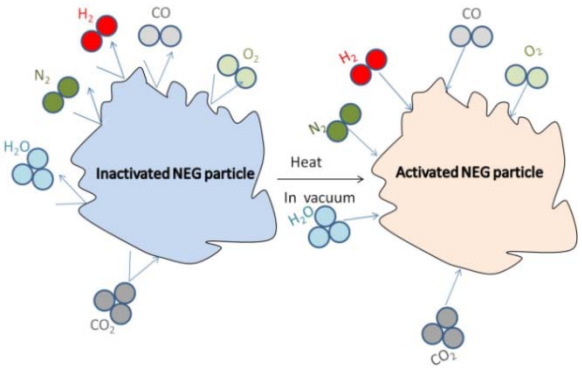

Fig.1.2: Representation of the activation process for a *non-evaporable* getter.

1.9 Storage / sorbing capacity of getters

The gettering capacity of a getter material is called its storage or sorption capacity and measured in mbar.litre. The maximum sorption capacity corresponds to formation of stoichiometric compounds such as ZrO_2, TiO_2, V_2O_5 in case of Ti/V/Zr getter coatings. NEG materials have a chemical affinity toward the active residual gas species when they are freshly prepared. After forming a passive oxide layer on the surface during exposure to atmosphere, they do not adsorb residual molecules at room temperature inside a sealed-off vacuum system. When the materials or surfaces coated with NEG materials are heated tothe activation temperature, the NEG starts adsorbing and then sorbing the residual gas species inside the chamber. This happens due to diffusion of the present surface oxygen into the bulk at elevated temperatures. Every time when the NEG is exposed to atmosphere it will behave as inactive unless it is activated. The number of cycles of the sorption of residual gases depends on its storage/sorption capacity. The two important factors that play the essential role in storage capacity are the solubility and diffusion length of the getter materials in the particular temperature range. Thickness of the NEG coatings matters for higher sorption capacity and number of activation – venting cycles. The group IVB elements (Ti, Zr, Hf) show higher solubility and consequently, higher storage capacity. The group VB elements (V,

Nb, Ta) show higher diffusion length in the same temperature range as the group IVB and have higher solubility. So coatings prepared by alloying these elements in binary, ternary or quaternary form will provide better gettering action with high storage capacity due to structure of the alloy and the grain boundaries. The sorbing capacity decreases with each cycle of exposure of the NEG surfaces.

1.10 Pumping speed for different gases

The NEG materials are useful for the removal of residual gases/pumping inside a sealed-off system after activation at elevated temperatures. These materials show variation in the pumping action for different gases due different chemical affinity and diffusion rate for different gases. In 1985, J.L. Cecchi et.al.[56] reported a measured pumping speed of 99.8 m^3/sfor H_2 for St101 alloy, after heating to 700ºC for 45 minutes and then lowered the temperature to 400ºC.The NEG was then allowed to cool down to room temperature, the pumping speed reduced to 69m^3/s. They also reported a pumping speed of 54 m^3/s for oxygen. In the year 1995, Benvenuti et.al. reported the pumping speed of alloy St707 at room temperature both for individual gases and for gas mixture as a function of the quantity of gas pumped and concluded that heating at 400ºC for one hour, or at 350ºC for one day results in pumping speeds of about 1000 $ls^{-1}m^{-1}$ for hydrogen, 2000 $ls^{-1}m^{-1}$ for CO and 450$ls^{-1}m^{-1}$ for N_2; these values are very close to those obtained after activation at higher temperature of 740ºC. Benvenuti et. al. also reported the pumping speed measurement of coating of binary alloy Ti-Zr at 20ºC after heating the alloy at 300ºC for two hours [16]. The measured pumping speed of hydrogen and carbon monoxide (CO) were 550 $ls^{-1}m^{-1}$ and 900ls^1m^{-1} respectively. The same group also measured the pumping speed of thin film of Ti-Zr-V in ternary alloy form after heating the film at 180ºC. They have also shown the dependence of pumping speed and surface saturation capacity on the film morphology.

1.11 Production of XHV with getter materials

1.11.1 Materials for XHV

Materials used in XHV applications are specific in class and should have very low outgassing as well as tolerant to the long baking hours in a temperature range from 300ºC to 400ºC. The materials can outgas by several mechanisms. Molecules of gas and water can be adsorbed on the surface of the materials and therefore materials with low affinity to water should be chosen. Material may sublimate in vacuum on heating and so alloy of cadmium and zinc should also be excluded. The gases can be trapped and released from porous materials or from cracks and crevices at low pressures so such surfaces should also be excluded. The gases liberated from the materials can be reabsorbed and diffuse on the other surfaces inside the vacuum chamber such as helium diffuse through Pyrex glass. In spite of all these requirements material should have enough strength through the entire required temperature range and maintain their physical properties (elasticity, plasticity, electrical and thermal conductivity). It should also be easy for machining and have low cost too.

The austenitic stainless steels SS304L and SS316L which are resistant to all above mentioned properties are generally used in the construction of UHV and XHV systems. Aluminium can also be used as XHV material but problem of its low melting point which decrease the mechanical strength at the baking temperature (more than 200ºC) and also due to relativity high thermal conductivity that poses problem in welding as compared to stainless steel. Aluminium welds have a tendency to crack from excessive shrinkage stresses due to their high rate of thermal contraction. Copper is also suitable for UHV/XHV applications but again the problem comes in welding Cu due to very high thermal conductivity which requires high welding speed, excellent material purity(OFE copper) and cleanliness and welding must

be done in an inert environment. Heating causes the copper to re-crystallize forming large grain size and annealing and cost is another issue in case of copper.

1.11.2 Limitations of normal pumping schemes

The normal pumping systems such as turbo-molecular pump (TMP) and TSIP(Triode sputter ion pumps) are not suitable stand alone for XHV type of pressure because all of them are conductance dependence. They show pressure bumps in longer pipes and pressure is not uniform as shown in Fig. 1.3. All these pumps when integrated to the system also add extra volume to the system that need to evacuate. The turbo-molecular pump that works on the principle of the transfer of directional momentum by a high speed rotating body to the molecules (as shown in Fig. 1.4) to the residual gas species present inside a sealed-off system. The turbo molecular pump is not able to pump H_2 beyond a certain low pressure due to small compression ratio for light gases and cause back streaming. TSIP that works on the principle of penning discharge in cross electric and magnetic fields (diagram schematic shown in Fig. 1.5) is not stable at very low pressure due to independence of discharge current and the pressure. At very low pressure the discharge current varies strongly with anode voltage and lead to field emission.

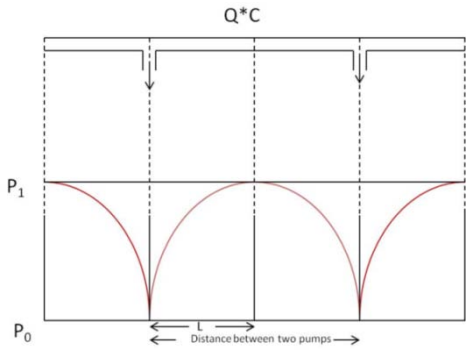

Fig.1.3: Pressure bump between the two pumps

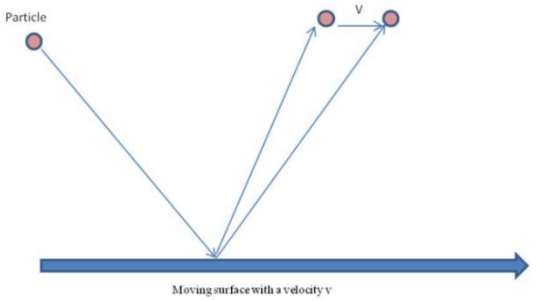

Fig.1.4: Principle of operation of turbo molecular pump.

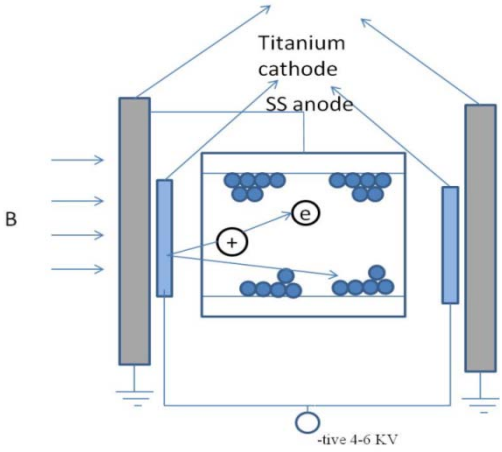

Fig.1.5: Schematic of a Sputter Ion Pump.

In case of NEG getters which are coated on the inner walls of a vacuum system pump, H_2can be pump by diffusion in the bulk and make solid solution after activation. The hydrogen partial pressure can be achieved down to 10^{-14} mbar that decreases the ultimate pressure of the sealed-off system in XHV range.

1.11.3 Advantages of getter materials for XHV

The NEG materials are very useful for the systems where UHV/XHV kind of pressure is required. Unlike other UHV pumps such as TSIP/TMP, it does not add extra volume to the system. There are no pressure bumps in case of pumping by NEG materials because they can be coated on the inner walls of the chamber or pipes and the walls itself converted into pumps. Power requirement is another issue in these pumps because NEG pumps do not need continuous power source for pumping as in the case of other available UHV pumps. These pumps can be activated at relatively lower temperatures of 160 - 180º C in case of ternary alloy of TiVZr. NEG pumps are free from any kinds of vibration like mechanical turbo pumps and cryosorption pumps. Unlike TSIP, NEG pumps do not affect the field of circulating beam in an accelerator or low energy electron detector due to absence of magnetic

or electric fields. The other important benefit of the NEG coating is a low secondary electron yield as compared to bare surfaces of conventional materials (SS, Cu, Al etc.) which avoids the multipacting effect in the accelerators. The secondary electrons which are generated in a multiplication process by highly charged bunches [57], play a large part in the formation of an electron cloud, especially at a large bunch-current region. One promising way to suppress the ECI(Electron Cloud Instability) is, therefore, to apply a surface with a low secondary electron yield (SEY) material to an inner surface of a beam duct [58, 59]. The studies revealed the reduction of 1-2 order in the photo-desorption yield [60].

1.11.4 Selective sorption capacity of getters

Sorption capacity of the getter materials or coatings depends on their crystalline structure and number of phases. In case of thin films the polycrystalline films with nanocrystalline grains are more suitable for better sorption capacity. In nanocrystalline films, the number of grain boundaries is more as compared to bigger grain size films and grain boundaries are more helpful in the diffusion of the adsorbed gas species.

1.12 Overview of present research work

1.12.1 Choice of materials

The choice of materials was done after a thorough study of existing literature on getter materials and study of the physical and chemical properties of available NEG materials. The basic properties of IVB elements (Ti, Zr, Hf) shows the highest solubility for oxygen as given in Table-2 which is highest 20% (approx.) for these materials. The materials with higher solubility are promising to make solid solution with present superficial surface oxide formed at lower temperatures and have higher capacity for storage and leave the NEG surface with unsaturated bonds which are the leading sites for adsorption of the residual gases. Higher

storage capacities for oxygen lead NEG materials to work for more number of evacuation cycles. The types of phases present in the getter materials also affect its chemical affinity, solubility and diffusivity etc. Diffusivity and diffusion length are another beneficial properties of materials to be used as NEG materials. It can also be seen from previous studies that the diffusivity and diffusion length of group VB elements (V, Nb, Ta) are higher than the other elements, as given in Tables-3. The calculated diffusion lengths of some of the elements at 300ºC given in Tables-4 are also maximum for VB elements. Alloying with VB materials provides easy diffusion of surface oxygen at lower temperatures. It is concluded that NEG coatings prepared by alloying of IVB and VB elements can be very efficient, have longer life, low activation temperature and large number of cycles as compared to other NEG materials.

1.12.2 Existing literature on NEG materials

Getter materials, in both, bulk and thin film forms have been utilized for UHV/XHV in sealed-off systems over the last 4-5 decades. There are number of groups which are working and developed many useful getter worldwide. The first work in the area of NEG materials was started in 1967 by B. Kindl and E. Rabusin et.al. of Italy who prepared the Zr-Al alloy in bulk form[13]. Later Della Porta et.al. of Italy in 1969 and Boffito et.al. in 1981 developed the binary alloy Zr-Al and ternary alloy Zr/V/Fe with trademark names as St101 and St707 [61, 62] which have been efficiently used in CERN. Benvenuti et. al. later prepared the thin film of binary alloy of getter material Ti-Zr, Ti-Hf, Zr-Hf in1998 and achieved much lower activation temperatures of 250ºC (for 24h of heating) for Ti-Zr compared to other available getters materials [16]. The same group also prepared thin films of ternary alloy TiVZr in the 2001 and reported a much lower activation temperature of 180ºC (for 24h of heating) [63].

1.12.3 Techniques to prepareNEG materials

A variety of techniques have been used to produce the NEG materials by different research groups. P. Della Porta et.al. of SAES Getter (Italy) prepared alloy of Zr (84%)Al(16%) with a trademark name St101 [64, 65] and coated this material by cold pressing of the powders of the alloy on the constantan strips [66]. St101 was studied by studied by Benvenuti et. al. from CERN. Sancrotti et. al. studied the ternary alloy of NEG materials in bulk form in the stoichiometry of $Zr_{57}V_{36}Fe_7$[St707] which was also prepared by SAES getter(Italy) by the technique of arc melting in water-cooled copper crucibles under argon atmosphere and used purity of raw materials of 99.9%, 99.95% and 99.99% for Zr, V and Fe [67]. Benvenuti et.al. from CERN prepared 1.5 µm thick coatings of binary alloy of NEG materials Ti-Zr on stainless steel, copper and Aluminium substrates by using cylindrical DC-magnetron sputtering technique where they used a target made by twisting together the 1 mm wires of materials Zr and Ti[68]. Later, Benvenuti et. al. also prepared 1-1.5µm thick coating of ternary alloy of NEG materials Ti-Zr-V on the same substrate by using the sputtering deposition technique and reported the activation temperature of 180ºC [65]. Chien-Cheng Li et. al. group of Taiwan also prepared 1-3µm thick films of ternary alloy Ti-Zr-V on Si(110) substrates by the glancing angle dc-magnetron sputtering technique in the Ar environment at different pressures and showed the porosity of the coatings increases with increasing glancing angle [69].

1.12.4 Working of NEG materials such as activation temperature, sorbing capacity and pumping speed for different gases, etc.

The NEG films of Zr-Al (trademark name St101) 0.2 mm thick were prepared by SAES Getters (Milano, Italy) on Constantan by cold sintering and studied by Benvenuti et.al. [68].It was tested and found that full activation of the film needed a heating at 700ºC for 1hour and

continuous heating of 400ºC during operation. Laboratory testing showed that this NEG film may withstand 50 such cycle without any noticeable deterioration. Measurements showed that all the present gases CO, CO_2, N_2, H_2 were pumped by this NEG except noble gas and methane.

Ternary alloy of Zr-V-Fe in the trademark name St707 by SAES Getter, Milano (studied by Sancroti et.al.) was prepared as a substitute for St101 alloy due to its very high activation temperature. Core level XPS study of this alloy showed the full activation at a lower temperature of 500ºC [70] as compared to St101 where the metallic carbide found at the surface even after heating at 700ºC. Benvenuti et.al. studied the characteristics of thin film of binary quasi-equiatomic alloys TiHf, HfZr and TiZr and concluded that their activation temperature is below 400ºC. They also concluded that TiZr alloy shows the activation temperature of 250ºC based on XPS measurements. The lowest ultimate pressure of about 7 X 10^{-14} Torr, was measured after 24h, bakeout at 350ºC of 2m long and ϕ 60mm coated chamber by combination with Ti sublimation /sputter-ion pump through an orifice of 25 l/s conductance for H_2 [71].The sticking coefficient of 10^{-2} of these coating for $H_2$was reported based on Monte Carlo simulation which results in a specific pumping speed of 0.5 l/s.cm^2 for H_2. Benuvenuti et.al. also studied the characteristic properties of ternary coating of Ti30%Zr20%V50% (at.%) and reported the complete activation of the film at 180ºC after 24h of heating[65].It is reported that this coating can work for more than 25 air exposure cycle with increased activation temperature of 350ºC.

1.13 Arrangement of thesis

This thesis presents the development of NEG coatings that have low activation temperatures of around 160ºC. Similar coatings with different stoichiometry have already been developed, but with higher activation temperatures of around 180ºC. For this purpose, we have

developed an in-house cylindrical type DC-magnetron sputtering system which can be used for coating big substrate in the form of sheet and longer pipes. The NEG coatings of ternary alloy Ti-V-Zr in different stoichiometry on stainless steel and Si substrates have been prepared with different deposition parameters. These coatings were characterized by different techniques such as XPS, FESEM, EDX, GIXRD etc. to understand the activation mechanism and activation temperature and effect of the morphology on the activation temperature. The results of the pumping action of the activated NEG coatings in a sealed-off vacuum system have been also reported. The development of secondary electron yield measurement system has been described and results of a comparative study of secondary electron yield of some of the coated and uncoated substrates are reported.

The motivation behind the current thesis is to develop low temperature activated NEG coating and pumps. Our group at BARC is involve in the development of high precision equipment such as hemispherical type high energy analyser [72], toroidal shape analyser [73], high energy X-ray photoelectron spectroscopy(HXPES) beam line [74], X-ray Photo emission electron microscopy(X-PEEM) beamline on Indus-2 synchrotron source [75]. All these high precision systems need UHV/XHU to work efficiently. The indigenous development of NEG getter pumps is expected to help in efficiently working of all these systems.

Chapter-2: In this chapter a brief introduction about different type of coating methods with advantages and disadvantages is given. Fundamentals of the sputtering deposition and a brief introduction of Physics of sputtering is included. The description of the simulation, design and the development of in-house cylindrical DC-magnetron sputtering system have been included. This chapter also covers the fundamentals steps of the film deposition, different types of film growth and factors affecting the quality of the film such as, deposition pressure

of the sputtering gas, purity of the sputtering gas, type of sputtering gas, temperature of the substrate, effects of type of the substrate, adhesion of the film.

Chapter-3: A brief introduction of different types of surface characterization techniques, e.g., X-ray Photo electron Spectroscopy (XPS), Scanning Electron Microscopy (SEM) and Atomic Force Microscopy (AFM) is given. Grazing Incidence X-ray Diffraction technique benefits a lot over normal angle X-ray diffraction in case of the structural analysis of thin film which was used in the characterization of the films; the description of this technique has been also covered in this chapter. A comparative study regarding the microstructure useful for a better adsorption has been carried out using the Scanning Electron microscope of film deposited in different conditions.

Chapter-4: It describes the thermal activation studies both qualitatively and quantitatively based on the X-ray photoelectron spectroscopy of NEG films. Different steps of the process which were involved during the surface characterization are described. Procedure to heat the film in a controlled manner at a constant rate and then soaking at different temperatures for 2-3 hours before cooling it down to room temperature to get the film in equilibrium has been described. The XPS spectrum in an angle integrated mode has been recorded after each heat cycle. The activation temperatures in each case were determined in a range from 100ºC to 350ºC.The shift in the binding energy (B.E.) from metal-oxide to metal has been considered to find out the activation temperature.

Chapter-5: This chapter enunciates the design, development and assembly of a test set up to achieve XHV using combination of TSIP and NEG pumps after heating later to the activation

temperature. The evolution of partial pressures with time after activation for different gases, e.g., H_2, CO_2 etc. has been also depicted.

Chapter-6: Conclusions

Coatings of NEG materials in the form of ternary alloy were prepared using in-house developed cylindrical type DC-magnetron sputtering system. Cylindrical DC-magnetron Sputtering system was developed to deposit the NEG film on internal surfaces of longer UHV compatible pipes and big size SS sheets. Surfaces of these coatings in as-deposited as well as after heating at different temperatures were characterized deploying XPS. The activation temperature was determined based on the shift in the characteristic B.E. peaks of the constituent elements of these films. Microstructures of the prepared films were studied with SEM. Stoichiometry of the coatings were found out using EDX and XRF techniques. The evolution of pressure with time has been shown. Nature of the film was achieved with GIXRD measurements that showed the polycrystalline form of the film with average grain size of 28 - 38 nm.

CHAPTER 2

2.1 Introduction

A brief overview of deposition techniques that have been employed for the preparation of NEG coatings is being described. The design and development of the in-house sputter deposition system and the fundamental principle of its working are also described elaborately. The calculations of different parameters and simulation of the ion electron paths under the influence of magnetic and electric field are included. Role of different steps during the growth of a film is described. Specific details about the substrates are given, e.g., substrate materials, substrate dimensions, cleaning and preparation as well as the expected properties of the deposited film. Targets preparation and cleaning are also discussed. Direct current diode type magnetron sputtering technique which was utilized in preparation of coatings has been discussed. Brief overview of other coating techniques is also mentioned. The advantages of sputtering technique over other techniques have been added.

2.2 Sputter deposition method for preparation of NEG coatings

2.2.1 Physics of Sputtering

The sputter deposition technique has been utilized for the preparation of coatings of NEG materials. The fundamentals of this technique will be discussed in this section.

Bunsen and Glove first observed sputtering over almost 150 years ago in a discharge tube [76]. The process of removal of atoms/molecules from solid surfaces through the irradiation of energetic species is known as *sputtering*. In sputtering, the sputtered individual atoms acquire enough energy (1 – 10 eV) higher than any other deposition (thermal evaporation, chemical decomposition), after escaping from the surface [77]. This process is called sputtering and schematically shown in Fig. 2.1. Unlike thermal evaporation, it does not

require heating [78, 79]. Atoms which are ejected by sputtering from a target are deposited on surrounding surfaces progressively forming a thin film coating after going through all the steps of film deposition such as adsorption, nucleation, island formation etc. on a dedicated substrate. Any energetic atomic particle, in the present case ions of noble gases (Ar, Kr), impinging on a surface can cause sputtering. Since it is easier to accelerate ions than neutral particles, hence only sputtering under ion bombardment is used in practice. The effect of ion bombardment on a material differs from that of electron and photon bombardment because the ion mass is of the same order as the mass of the atoms in the target. This permits an efficient momentum transfer to individual atoms, which is the key feature of ion sputtering.

The minimum energy required to expel an atom from a target is called the *sputtering threshold* [80, 81]. It depends on the material but is quite insensitive to the mass ratio between the impinging ion and the target atoms [80, 81]. In 1962, Stuart and Wehner, measured threshold values by the spectroscopic method [82] in noble gas plasma and the values were in the order of 15-30 eV. The typical sputtering yields were of the order of 10^{-4} to 10^{-5} atoms/ion. The threshold energy also strongly depends on the particular sputtering sequence involved.

2.2.2 Sputtering Yield of different elements (Ti-V-Zr) used in NEG coatings

The role of the sputtering yield of the co-sputtered metal for the deposition of alloy films is important as it provides some kind of qualitative information about the chemical composition.

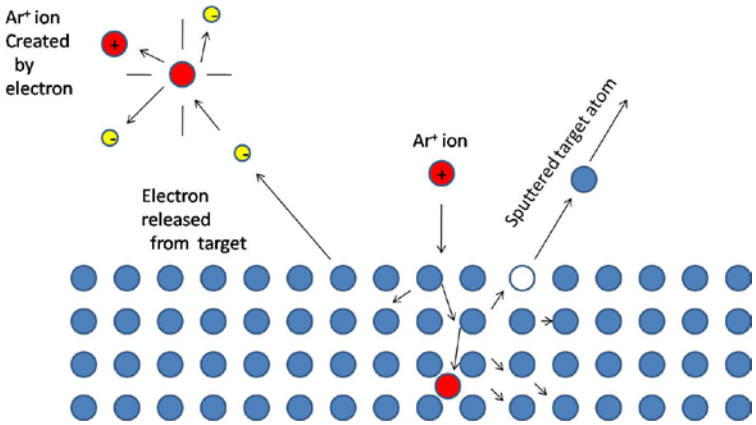

Fig. 2.1: Schematic representation of sputtering method.

It is defined as the ratio of number of sputtered atoms to the number of incident particles. It is a measure of efficiency of sputtering. The sputtering yield S is defined as,

$$Sputtering\ Yield\ (S) = \frac{No.of\ Sputtered\ Atoms}{No.of\ Incident\ particles}$$

Experimental values of S range from 10^{-5} to as high as 10^{3} [83]. However, in a most practical sputtering process, the range of S is narrower from 10^{-1} to 10.

There are a number of factors which affects the sputtering yield. Most important of the factors are given below:

a) Energy of the incident particles

b) Target materials

c) Incident angles of particles

d) Crystal Structure of the target surface

The sputtering yield, S, can be measured by the following methods:

1) Weight Loss of the target

2) Decrease of target thickness

3) Collection of the sputtered materials

4) Detection of sputtered materials in flight

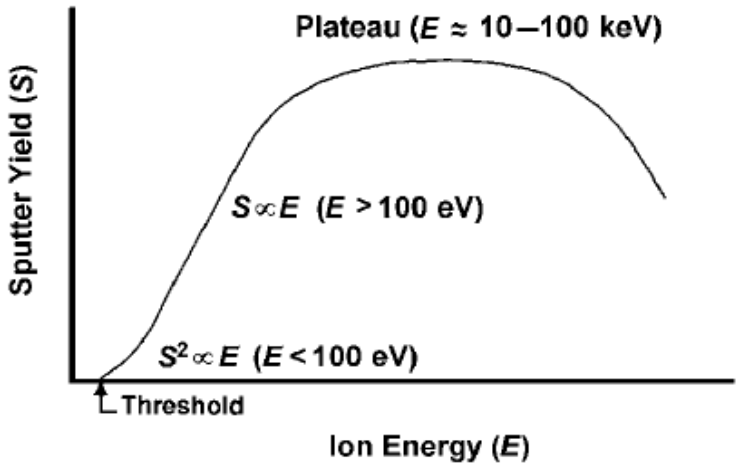

Fig. 2.2: Variations of sputter yield with energy of incident ion.

Fig. 2.2 shows typical variation of the sputtering yield with incident ion energy. From the figure, it can be inferred that:

a) there is a low energy threshold for sputtering. The sputtering yield S is proportional to E^2,

b) at the energy region in the order of 100 eV, the sputtering yield is proportional to E [84, 85] as the incident ions collide with the surface atoms of the target, and the number of displaced atoms will be proportional to incident energy.

c) the sputtering yield is maximum as shown in Fig. 2 as plateau ($E \approx 10 - 100$ keV) in the high energy region as the incident ions travel beneath the surface and the sputtering yield is not governed by the surface scattering.

d) the sputtering yield varies with the angle of incidence of the ions. Metals [Au, Ag, Cu and Pt] which have very sputtering yield, show only slight variation with incident angle. The low sputtering yield metals [Fe, Ta and Mo] show very pronounced angle effect [83, 86]. The yield increases with angle and shows a maximum at angles between 60^o and 70^o.

The sputtering yield of group IVB (Ti, Zr, Hf) and VB (V, Nb, Ta) elements which are used in the preparation of NEG coatings with Ar^+ ions as sputtering species are given in Table 2.1 and more details are given in reference [87]. Typical sputter yields in a low-energy region measured by Stuart and Wehner are shown [87]. Sputter yield vary with the angle of incident ions and for details see the reference [87].

Table 2.1: Sputtering yield of IVB and VB elements for Ar^+.

	Target	Ar^+			
		100eV	200eV	300eV	600eV
IV B	Ti	0.081	0.22	0.33	0.58
	Zi	0.12	0.28	0.41	0.75
	Hf	0.16	0.35	0.48	0.83
VB	V	0.11	0.31	0.41	0.70
	Nb	0.068	0.25	0.40	0.65
	Ta	0.10	0.28	0.41	0.62

2.2.3 Advantages of Sputter deposition over other techniques

Sputter deposition technique has been used to prepare the NEG films of getter materials due to certain benefits over other techniques.

- Sputtering allows the deposition of the film having compositions of target source that also depend upon the sputtering yield of the materials. As in case of ternary alloy deposition on SS304 substrate, the target which was prepared by inter-twisting the wires of Ti, V, Z in (1:1:1). The deposited film had a composition of $Ti_{20}V_{44}Zr_{36}$ following the sputter yields of the individual elements (vanadium has the highest sputter yield, followed by Zr and Ti, See Table 2.1).
- It is reasonably simple and can be used for wide range of materials.
- Suitable for uniform and distributed coating on long, narrow vacuum chambers/pipes. The cylindrical type sputtering system which has been developed is very useful for coating in long and narrow pipes where the substrate in pipe form can be used and target is axially placed in the centre of the system.

- The kinetic energy of the sputtered atoms is large (1 – 10 eV) as compared to other physical vapour deposition techniques so deposited films are mechanically stronger. The deposited film of NEG materials was tested with scratch test.
- Since the magnetron sputtering deposition is a low pressure discharge technique, deposited films are cleaner compared to other techniques.
- Allows co-sputtering using composite targets. In the present work three targets Ti, V and zirconium in elemental form were co-sputtered for the deposition of the alloy thin films of NEG.
- Deposition takes place away from the equilibrium. The highly energetic sputtered species are quenched on the substrate surface and non equilibrium state can lead to formation of exotic materials. Studies revealed that atoms emission reflects the lattice symmetry. In FCC metals, it has been demonstrated that atoms are preferentially ejected along the [110] direction, but ejection in [100] and [111] directions also occurs to lesser extent [88].
- As in the case of evaporation, sputtering also shows the cosine distribution of sputtered atoms with slight deviation and it is energy dependent. At high energy it is extended normal to target and at lower energy it is compressed. Much more material is ejected from the sides than in the direction normal to the target in case of “under cosine”. The distribution approaches a cosine distribution at higher energy which provides the uniform ejection of the material from the target.

2.2.4 Parameters of Sputtering deposition

Deposition parameters are important because they control the morphology of the deposited film. Glow discharge is important in order to get the better idea of sputtering deposition which is a plasma based deposition technique. In a diode gas-discharge tube, the minimum voltage which initiates the discharge is given by [89],

$$V_s(Volt) = a\,\frac{pl}{log\,pl + b} \qquad (1)$$

where p is the gas pressure in mbar, l is the electrode separation in cm, a and b are constants. The relation between spark voltage Vs and the gas pressure p, is called famous Paschen's Law. The typical experimental results shown in Fig. 2.3 exhibit the minimum spark voltage at gas pressure p_m [89].

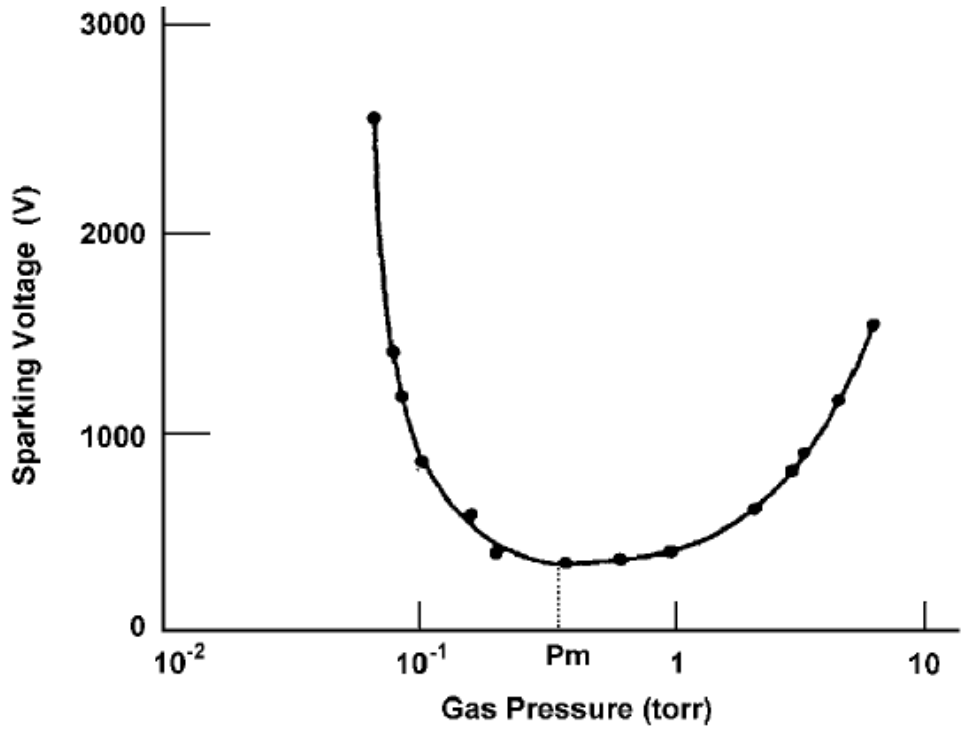

Fig. 2.3: A plot of park voltage as a function of gas pressure measured for Cu electrodes in air (electrode spacing, 5 mm) [89].

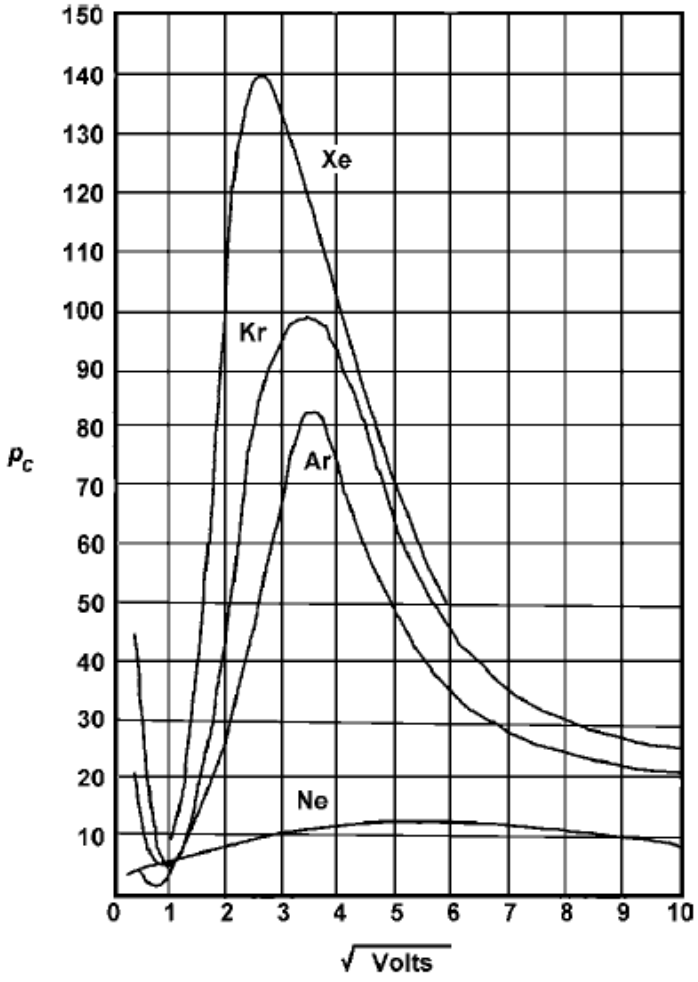

Fig. 2.4: Probability of elastic collision of electron p_c ($cm^{-1} \cdot torr^{-1}$) in Ne, Ar, Kr, and Xe [90].

To initiate a discharge, the gas pressure p_s under a given electrode separation, l, is expressed by,

$$p_s \geq \frac{\lambda_0}{l} \qquad (2)$$

Where λ_0 is the mean free-path of electrons in the discharge given as $\lambda_0 = 1/p_c$, where p_c is the elastic cross section between electrons and gas atoms. P_c values for different noble gases which are used as discharge gases are given in Fig. 2.4 [90, 91]. So for l=10 cm separation, the pressure should be higher than $5x10^{-3}$ Torr to initiate the breakdown and forming discharge. In a diode type discharge, when the discharge is initiated in a low pressure gas, the mode of discharge varies with discharge current.

2.2.5 Cylindrical Type, DC-Magnetron Sputtering system for deposition of NEG coatings

In DC-Magnetron Sputtering system one of the electrodes is a cold cathode and the other is the anode. The cathode is having the target materials to be deposited. The substrates are placed on the anode. The sputtering chamber is filled with sputtering gas, typically argon gas at $4x10^{-3}$ – 12 x 10^{-3} mbar. A magnetic field is superposed on the cathode and glow discharge which is parallel to the cathode surface is created. The electrons in the glow discharge show cycloidal motion, and centre of the orbit drifts in the direction of **E** x **B** with the drift velocity of E/B, where E is the electric in the discharge and B is the superposed on transverse magnetic field, respectively. The magnetic field is oriented such that these drift paths for electrons form a closed loop. This electron-trapping effect increases the collision rate between the electrons and the sputtering gas molecules. This enables one to lower the sputtering gas pressure to as low as 10^{-5} mbar, but more typically 10^{-2} mbar. In the magnetron sputtering system, the magnetic field increases the plasma density which leads to increases in the current density at the cathode target, effectively increasing the sputtering rate at the target. Due to the gas's low working pressure, the sputtered particles traverse the discharge space without collision, which results in a high deposition rate.

In this thesis, a cylindrical magnetron sputtering system has been used to deposit NEG films. The schematic of the cylindrical magnetron is shown in Fig. 2.5. It consists of electrodes arranged in a cylindrical geometry. The target, fabricated as a cylinder, is surrounded in a 2π geometry by anode substrates so that a radial electric field is established between these electrodes. Simultaneously, a uniform magnetic field is applied parallel to the z-direction by means of permanent magnet or electromagnet or via a co-axial solenoid. Electrons emitted radially from the cathode immediately find themselves trapped between perpendicular electric and magnetic fields where they hop around the target circumference in

closed orbits defined by the Lorentz-force geometry. As in the case of the planar magnetron, an intense cylindrical plasma column is created near the cathode by the enhanced gas-ionization efficiency. Cylindrical magnetron sputtering has been commercially employed for many years in coating razor-blade cutting edges with platinum/ chromium. The sputter deposition of diamond like carbon on stainless-steel blades coated with a niobium glue layer is the latest advance in blade technology. This type of magnetron deposition technique is of paramount importance in the coating of NEG materials on large substrate areas. The NEG coating inside the cylindrical pipe is beneficial because the pipe itself is treated as substrate (anode) which is kept at ground potential.

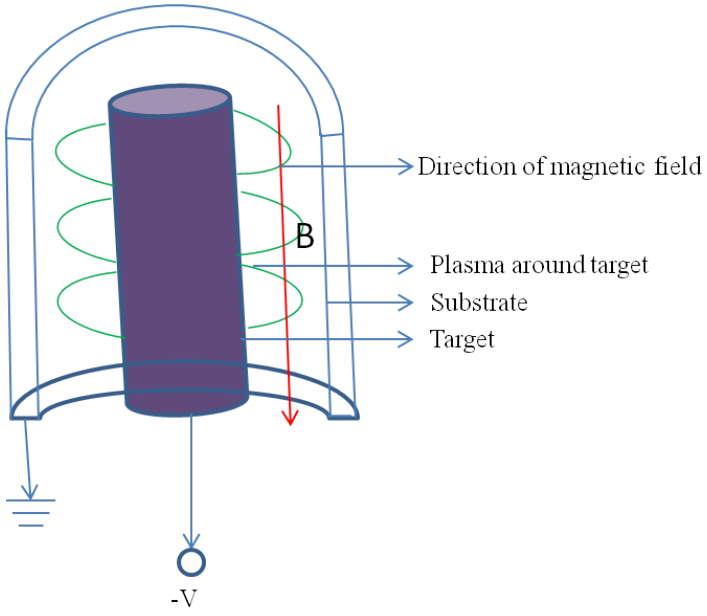

Fig.2.5: Schematic diagram of a cylindrical sputtering set-up.

2.3 Historical View of Sputter deposition

Sputtering or cathode sputtering is used for the deposition of thin films. Several sputtering systems have been proposed for thin-film deposition including DC diode, RF diode, Magnetron and Ion Beam Sputtering. The magnetron sputtering was first proposed by Penning in 1936 [93]. A prototype of the planar was invented by Wasa in 1967 [94].

2.4 Simulation of Cylindrical type DC magnetron sputtering and experimental setup

The simulation of the ion trajectories was done by using SIMION 8.0 software and has been shown in Fig. 2.6 (Magnetic field = 300 Gauss, cathode voltage = 800V(-tive), anode at ground). The electrons move cycloidally with different radii in opposite direction under the influence of both electric field **E** and Magnetic field **B** perpendicular to each other. Ions, being heavy, feel very little affect of magnetic field so their path is almost linear. Confinement in crossed electric and magnetic fields increases the electron path length and thereby enhancing the ionizing efficiency near the cathode that results in a dense plasma and a higher discharge current. In the simulation, three concentric cylindrical lenses were considered; the biggest cylinder is treated as solenoid where magnetic field is applied. The middle cylinder which kept at ground is considered as substrate. The inner most cylinder is treated as target which is kept at a negative potential.

The electronic and ionic radii in the electric and magnetic fields are given by:

$$R_{electron} = 3.37 \text{ X } 10^{-7} E^{1/2}(eV)/ \text{ B (Gauss)}$$

$$R_{ion} = 911 \text{ X } E^{1/2}(eV)/ \text{ B (Gauss)}$$

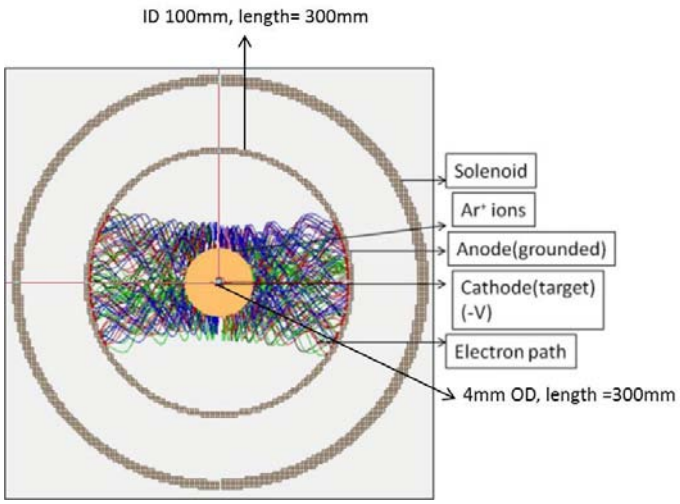

Fig.2.6: Simulated trajectories of ions/electrons in sputtering system (top view)

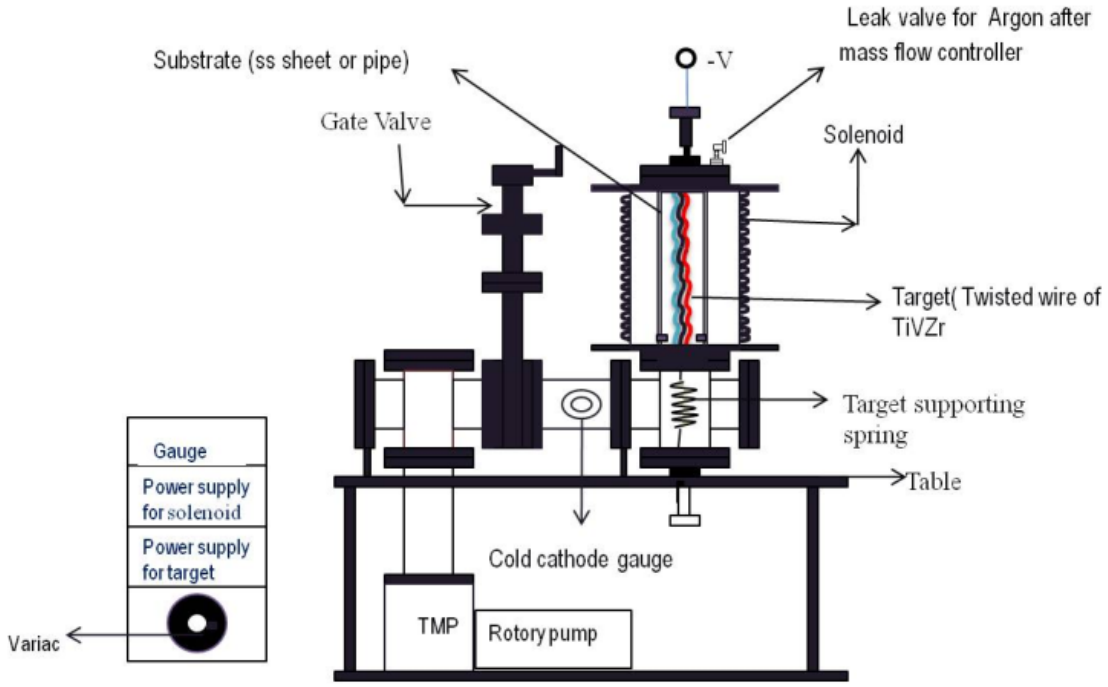

Fig.2.7: Schematic diagram of the cylindrical type DC-magnetron sputtering deposition system.

Fig.2.8: Photograph of the DC-magnetron sputtering system showing pumps and electronic instruments.

Fig. 2.9: Photograph of DC-magnetron sputtering system showing a base pressure of 5.7 x 10^{-8} mbar.

Fig. 2.10: Photograph of a special type of substrate holder with heater.

Experimental setup is an indigenously developed cylindrical type DC-magnetron sputter deposition system schematically shown in Fig. 2.7 and photographs of the system are shown

in Fig. 2.8 and Fig. 2.9. In developing the system, the available literature was surveyed and then simulated to fix up parameters (Magnetic field = 300 Gauss, cathode voltage = 800V(-tive), anode at ground) of the coating system. The system includes a cylindrical type DC-magnetron sputtering system with target holder in the centre of the cylindrical pipe and substrate holder is attached to the same flange as shown in Fig.2.10, parallel to the target with special attachment where 6 substrates can be placed simultaneously. The big size substrate in the form of SS304L sheet can also be held by the welded support inside the cylindrical pipe and also the pipe itself can be used as a substrate, so that different types of substrates can be coated with NEG films using this arrangement. The substrate-to-target distance is about 45 mm. One 1kW arc protected DC power supply was integrated to supply of voltage to the target. The substrate holder was held at ground potential. A dedicated vacuum system consisting of a 500 l/s turbo molecular pump and a high performance rotary backing pump are employed to pump down the chamber from atmosphere. Gas flow control is done via mass flow control valves and a manual high precision leak valves. A solenoid of internal diameter 250 mm φ and length 390 mm, having 500 turns is used to produce the required magnetic field to start the arc discharge at low voltage and low pressure. For a solenoid of fixed number of turns the magnetic field can be controlled by the manipulation of current only as ($B \propto I$). The calculated magnetic field is plotted as a function of distance and current respectively in Fig. 2.11 and in Fig. 2.12.

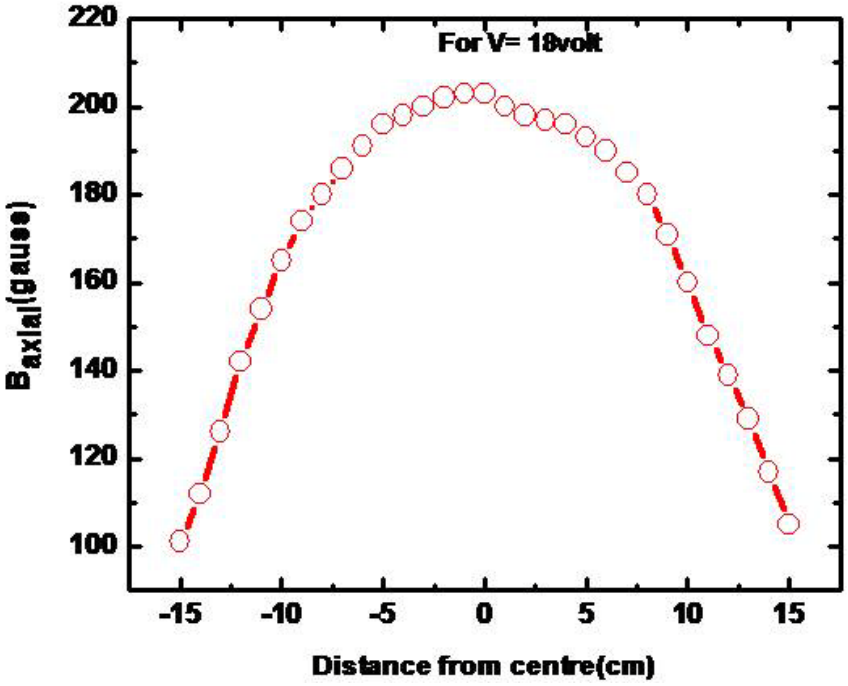

Fig. 2.11: Measured profile of magnetic field as a function of distance.

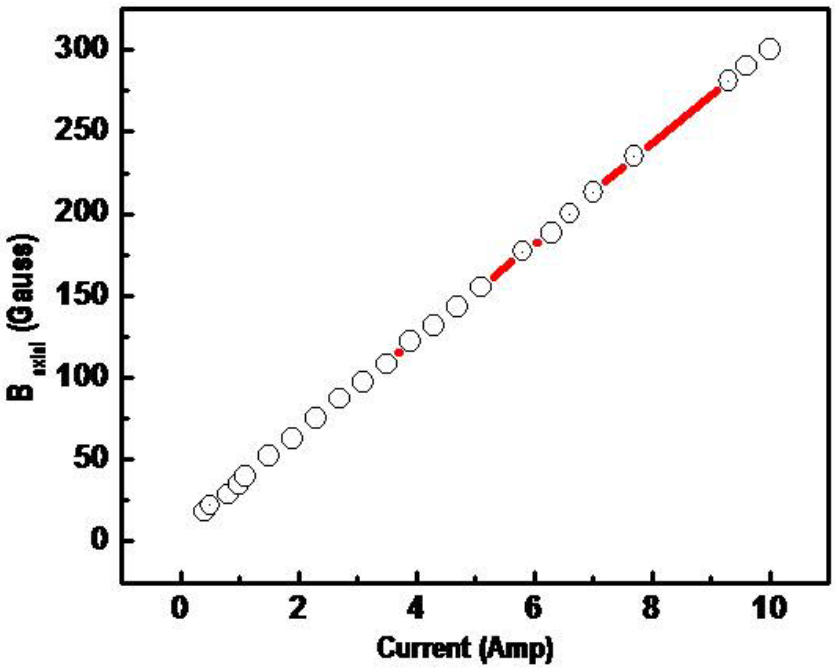

Fig. 2.12: Measured profile of magnetic field as a function of current.

The plot showing the variation of axial magnetic field with distance was measured with the help of Hall probe. The simulation of the ions trajectories was done with the help of SIMION 8.0 software package.

Maximum axial field at the centre

$$B = \mu 0 * n * I * \frac{L}{(4R^2 + L^2)^{1/2}}$$

where $n = N/L$ is no. of turns, in our case 520, L= length of the solenoid, in the present case 390mm, R= Radius of the solenoid and I is the current in A.

2.5 Deposition Conditions and steps in growth of NEG film

The nature of the film is governed by the deposition parameters such as deposition rate, substrate temperature, substrate material and deposition atmosphere [92]. The chemical composition of deposited films is governed by the substrate temperature and/or the deposition atmosphere. Under low substrate temperatures, the chemical composition of deposited films coincides with that of the source materials. Under high substrate temperature, the vapour pressure increases which results in the change of the chemical composition of the deposited film from the source materials due to re-evaporation of the high vapour pressure materials from the film. Gas molecules that are frequently included in the film, also affect the film composition during deposition. The active gas molecules are reacted chemically with the deposited materials and form its compounds.

There are three main steps involved in the growth of thin films;

1) *Production of the proper atomic, molecular, or ionic species,*
2) *Transport them to the substrate through some medium* and
3) *Condensation on the substrate, either directly or via chemical or electrochemical reaction, to form a solid deposit.*

Thin films always start to form via nucleation and growth process. Pictorial representation of the type of growth process is given below:

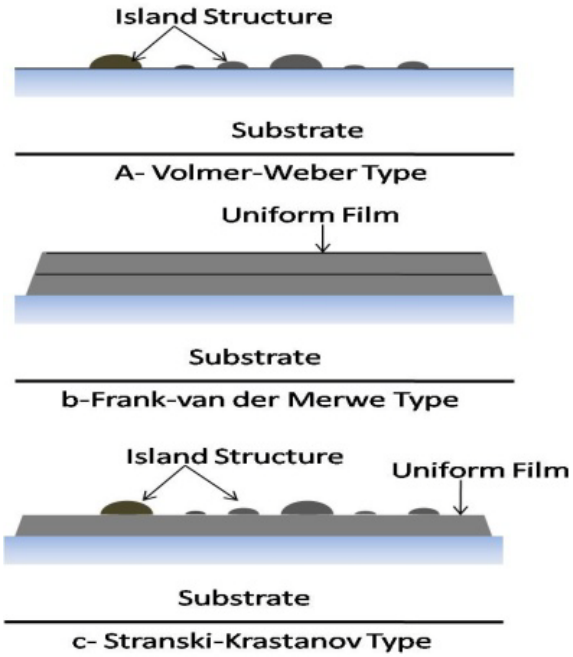

Fig. 2.13: Pictorial representation of the growth process of a thin film.

The general picture of step-by-step growth process is as follows:

a) The units which are coming out from the materials (target), on impacting, lose their velocity component normal to the surface and are physically adsorbed to the surface depending on the sojourn time.

b) At first the absorbed species are not ahead of thermal equilibrium with the substrate and move over the substrate surface which gets them in forming bigger cluster.

c) These clusters are known as nuclei and are thermodynamically unstable. These may tend to desorb in time, depending on the deposition parameter. If the deposition parameter is such that a cluster collides with other adsorbed species before getting absorbed, it starts growing in time and becomes thermodynamically unstable after reaching a critical size (overcoming nucleation barrier). The step involving the formation of stable, chemisorbed, critical sized nuclei is called the nucleation stage.

d) The critical nuclei grow in number as well as in size until a saturation nucleation density is reached. The nucleation density and the average nucleus size depend on a number of parameters such as the energy of the impinging species, the rate of impingement, the activation energies of adsorption, desorption, thermal diffusion, and the temperature, topography, and the chemical nature of the substrate. A nucleus can grow both in lateral and perpendicular growth through surface diffusion or by direct impingement of the incident species. The rate of lateral growth is much higher than the perpendicular growth and grown nuclei are called *islands*.

e) Coalescence stage is the next stage in which small island start coalescing with each other in an attempt to reduce the substrate surface area. This is called *agglomeration* and can be enhanced by surface mobility (increasing substrate temperature) of the adsorbed species.

f) Larger islands grow together, leaving channels and holes of uncovered substrate. The structure of the films at this stage changes from discontinuous type to porous network type. Filling of the channels and holes takes place to form a complete, continuous film.

g) After a continuous film is formed, the anisotropic growth takes place normal to substrate in the form of cylindrical columns. The initial nucleation density determines the lateral grain size or crystallite size. If re-crystallization occurs during the coalescence stage, the lateral grain size is larger than the average separation of the initial nuclei and the average grains per unit area of the film is less than the initial nucleation density. The grain size normal to the substrate is equal to the film thickness. Thicker films are the results of re-nucleation on previously grown grains.

The mechanism of thin film growth has been described in the literature as follows. It is started by the adatoms on the surface of the substrate. The adatoms will be trapped at a

nucleation centre after a Brownian movement. The mean residence time of adatoms, τ_s, is given as,

$$\tau_s = \tau_v e^{(\frac{E_{ad}}{kT})}$$

where τ_υ is the period of vibration perpendicular to the surface assumed to be almost $1/\upsilon$ ($=10^{-13}$s), where υ ($\approx 10^{13}$ Hz) is a frequency of lattice thermal vibration, and E_d is adsorption energy of adatoms on the substrate in the range 0.1 to 1 eV.

The thermal equilibrium time of the adatoms, τ_e is given as,

$$\tau_e = \tau_s e^{-\left(\frac{E_{ad}}{kT}\right)}$$

If E_{ad}>>kT, the adsorbed atom will stay at the surface of the substrate where τ_s>>τ_e. If $E_{ad} \approx$ kT, the adatom will re-evaporate from the substrates. The adatoms will diffuse on the surface showing Brownian movement, the travelling time for diffusion on the surface is given as,

$$\tau_d = \tau_p e(\frac{E_d}{kT})$$

Whereτ_p is a period of vibration parallel to the surface assumed to be almost $1/\upsilon$ ($=10^{-13}$s), where $\upsilon \notin 10^{13}$ Hz) and E_d is the surface diffusion energy for the adatoms against the potential barrier on the substrate surface.

The mean travelling distance of the adatoms, X, is given as,

$$X = (D_s \tau_s)^{1/2}$$

$$D_s = \frac{a_0^2}{\tau_s}$$

where a_0 denotes a lattice spacing of surface atoms of the substrates. Since $\tau_p \approx \tau_\upsilon$, so,

$$X = a_0 e^{\frac{E_{ad} - E_d}{2kT}}$$

Both $E_{ad}$and E_d are crucial for the growth of thin films. The growth of the thin film is also governed by the surface energy of the film, γ_f, surface energy of the substrates γ_s, and the

interfacial energy between thin film and substrates, γ_{fs}. The island growth will be prevalent at $(\gamma_s - \gamma_{fs}) < \gamma_f$ and the layer growth at $(\gamma_s - \gamma_{fs}) > \gamma_f$.

There are three types of growth stages that are described and shown in Fig. 2.13,

(a) Island type or Volmer-Weber,

(b) Layer type or Frank-van der Merwe type,

(c) Mixed type or Stranski-Krastonov Type.

The crystallographic and topographical details of different islands are randomly distributed, so that when they touch each other during growth, grain boundaries and various line and point defects are incorporated into the film due to mismatch of geometrical configurations and crystallographic orientations. If the grains are randomly oriented, the film shows a ring-type diffraction pattern and are said to be polycrystalline in nature.

There are number of parameters that affect the quality of the thin films. Some of these are described below.

2.5.1 Effect of substrate temperature

The substrate at increased temperature enhances the mobility of the adsorbed species at the surface which results in increasing the surface diffusion. The grain size of film is increased by increasing the substrate temperature. Another effect of increasing the temperature of the film is that the post deposition annealing also results in increased grain size. The grains are smaller in post annealing as compared to keep the substrate at higher temperature during deposition. It happens due to involvement of higher activation-energy in the process of thermal diffusion in post annealing. Effects of heat treatments are more pronounced in thick films.

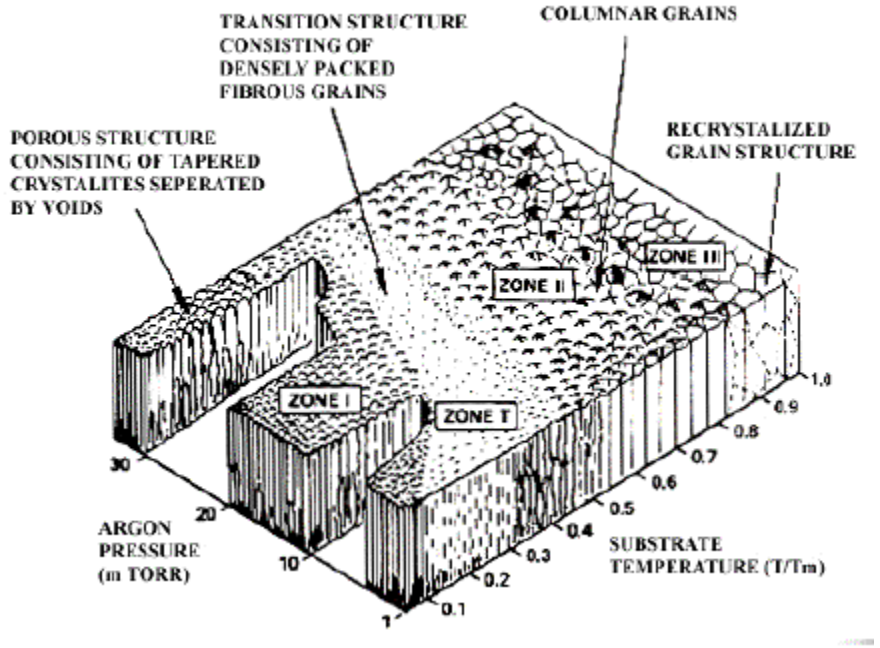

Fig. 2.14: Thronton structure zone model.

The relationship between the substrate temperature, kinetic energy of the ions and deposition rate can be understood by the zone model of Thronton (Fig. 2.14).

2.5.2 Adhesion of the film

The substrate cleaning, chemical nature and micro-topography of the film profoundly affect the adhesion of a film on a substrate and the film starts peeling off with time. The adhesion is better for higher values of kinetic energy of the incident species, adsorption energy of the deposit and initial nucleation density. Loose and porous deposits formed under conditions of high super-saturation and poor vacuum adversely are affected in adhesion. Contaminants present on the substrate surface may increase or decrease the adhesion of the film depending upon the increase or decrease of the adsorption energy.

2.5.3 Different types of targets used for NEG coatings

As the NEG films in the present work are ternary alloy they needed to be co-sputtered from three different metallic targets for the preparation of the film. In a cylindrical type

sputtering system, the target is prepared by inter-twisting of three metallic wires of 1mm diameter and 400 mm length. The wires were 99.7 % pure and procured from Sigma Aldrich Company. Some of the targets are shown in Fig. 2.15.

There are number of targets used to prepare the coatings of NEG materials in different compositions. These targets are Ti(1)Zr(1), Ti(1)Nb(1)Zr(1), Ti(2)V(1)Zr(2), Ti(1)V(1)Zr(1), Ti(1)V(2)Zr(1), Ti(1)V(1)Zr(2) etc.

Fig. 2.15: Different types of inter-twisted ternary targets of (Ti-V-Zr) used in sputtering system.

2.5.4 Types of substrate:

In Fig. 2.16 different types of substrates (UHV pipes of SS304L size CF40 and 350mm, size CF100 length 300 mm and sheet of SS304L of dimension 0.2 X 250 x 300mm^3) have been shown which are coated inside with NEG materials using the cylindrical type magnetron sputter system. NEG coated and uncoated surfaces can be clearly seen in Fig. 2.16. All of these coatings are used and tested to achieve XHV after thermal activation at activation temperature. For the characterization of the film, small portions for the prepared films were cut and used to mount on a specially designed substrate holder as shown in Fig.2.10.

2.6 Other techniques used for NEG coatings

2.6.1 Vacuum Arc deposition

The first sample of ternary coating of NEG material was prepared by a vacuum arc deposition technique as shown in Fig. 2.17 [95]. It is also a physical vapour deposition in which an electric arc is used to vaporize the material from a cathode target. The vaporized material then condenses on a substrate, forming a thin film. The arc evaporation process begins with the striking of a high current, low voltage arc on the surface of a cathode or target that gives rise to a small (usually a few μm wide), highly energetic emitting area known as a cathode spot.

The localized temperature at the cathode spot is extremely high (around 15000 K), which results in a high velocity (10 km/s) jet of vapourised cathode materials. A small ingot of composite material of $Ti_{0.2}V_{0.4}Zr_{0.4}$ about 20 mm in diameter was used as a target in these experiments. Electrodes of size 18 X 8 mm^2 were prepared. A DC dielectric arc was struck between the two electrodes. The pressure was kept 6 X 10^{-5} mbar during the deposition. The SS304L substrates were used to deposit the film.

Fig. 2.16: Diffterent types of substrate on which NEG film have been deposited.

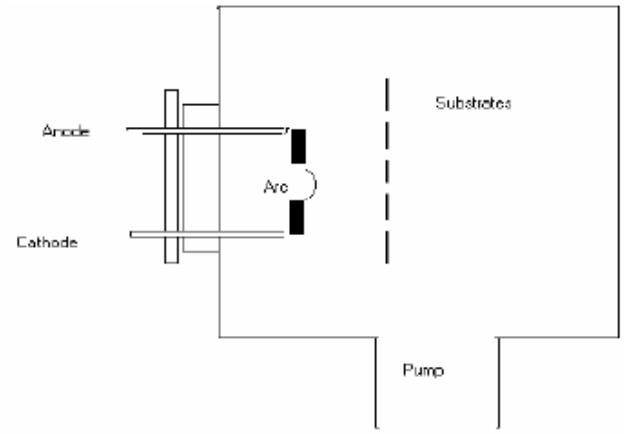

Fig.2.17: Schematics of Vacuum Arc deposition system.

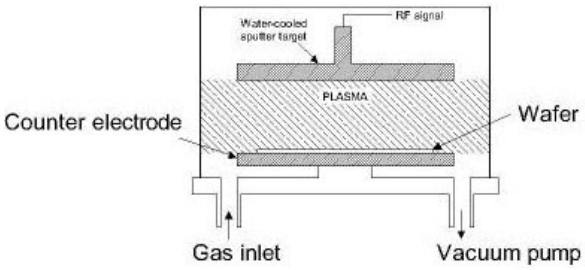

Fig.2.18: Schematics of a planar RF sputtering System.

2.6.2 Planar type RF-sputtering system

This technique is similar to the DC- magnetron sputtering deposition as described in previous section, the only difference is that an RF-power is used in place of DC-power to create the arc discharge. This technique is versatile and can be used to deposit all type of materials such as metallic, insulator and alloy. RF-sputtering has benefitted in depositing the insulated materials where DC-sputtering does not work due to build of positive charge inside the target and deposition stops due to the unavailability of conduction path for the build up of positive charge. The sign of anode cathode bias is varied at a high rate with the RF-frequency. The

very first ternary target of $Ti_{0.3}V_{0.3}Zr_{0.3}$ was prepared by bonding the Ti, and Zr strips on a V 75 mm diameter disk in equal proportion. The RF power of 200 watts at 13.56 MHz was used for this purpose. The SS304L substrates of size 10 x 10 mm^2 were used on which the NEG film was deposited [96]. The base pressure was 5 $x10^{-6}$ mbar and discharge was started in the Ar atmosphere of $5x10^{-3}$ mbar with a deposition time of 4 h. A schematic diagram of the planar RF-sputtering system is shown in Fig. 2.18.

CHAPTER-3

3.1 Introduction

3.1.1 Surface characterization of NEG coatings

NEG films in ternary form were prepared and their surfaces were characterized for activation temperature. The X-ray Photo electron spectroscopic technique was used to study the activation of NEG surfaces. Gettering depends on the available adsorption sites at the surface, hence the morphology of the coatings plays a very essential role. A study was done for the NEG films prepared in different stoichiometry and deposition parameters with help of Scanning Electron Microscopy. The chemical composition of the prepared film was identified by Energy dispersive X-ray Analysis (EDX). All these techniques are relevant and discussed precisely with their references. There are a number of available techniques such as Scanning Electron Microscopy (SEM), Transmission Electron Microscopy(TEM), Atomic Force Microscopy(AFM), Secondary Ion Mass Spectroscopy, X-ray Photoelectron Spectroscopy, X-ray diffraction that provide information about the constituents on the surface, grain sizes and grain boundaries. The techniques which are used for the analysis of the NEG films studied in this thesis will be discussed in this section.

3.1.2 Role of X-ray Photoelectron Spectroscopy in the Characterization of NEG films

X-ray photoelectron spectroscopy (XPS) is an appropriate tool for these studies due to its sensitivity to surface environments [97 - 99]. In solids, the most tightly bound electrons reside in core levels K and L. The outer most levels form a band with certain electron density distribution up to Fermi level E_F. On illumination of a solid with photons of energy greater than the work function of the solid ($E_{vac} - E_F$) (as shown in Fig. 3.1), electrons are ejected from these levels and can be ejected out of the surface. Energy distribution of these

photoelectrons is superimposed as a smooth continuous background by the secondary electrons produced from electron-electron interactions inside the solids. XPS is a very versatile technique for surface characterization of materials. It is based on the well known relation for photoelectric effect given in 1905 by Albert Einstein for which he was later awarded the noble prize in Physics in 1921.

When an incident photon of energy *hv* is incidents on a surface, the ejection of photoelectron from the core level of Binding energy E_B with respect to the Fermi level E_F takes place which has the characteristic of the material in the form of binding energy, momentum, spin etc. The kinetic energy of the ejected electrons is given by the relation:

$$E_k = h\nu - B.E. - \emptyset$$

Where E_k is the K.E. energy of the electron is referenced to the vacuum level of the specimen E_{vac} and F is the work function of the specimen having the value in the range 2 – 5 eV.

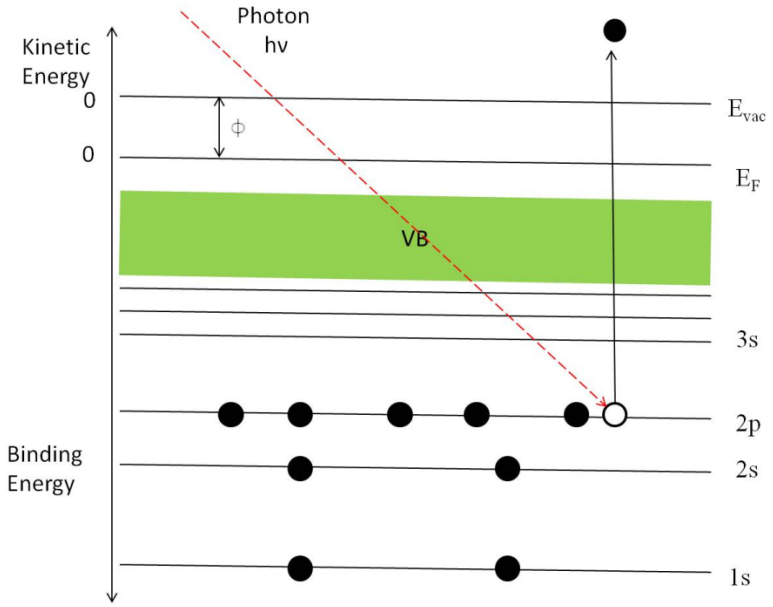

Fig. 3.1: Schematic of XPS process.

The above equation describes the photoemission process in the simplest approximation (the 'frozen orbital' approximation). When an electron leaves an atom by X-

ray absorption of the particular level it leaves a vacancy of positive charge which is later filled by the readjustment of electronic charge around the atom. The ejected electrons present the nature of chemical bonding around the parent atom. Since during bonding valence electrons are shifted towards more electronegative atoms and make the parent atom more positive which results in the shifting of core level B.E. towards higher side. In our case of TiO_2, ZrO_2 and V_2O_5, after heating the B.E. energy peaks of core level of these elements shifted towards lower value of the B.E. energy which showed the change of the oxidation states of the these elements. The shifting of the V(3p) peak is shown in Fig. 3.2.

In our XPS system, the X-ray sources are Al-K_α and Mg-K_α lines. For the studies of the NEG coatings in this thesis, Mg-K_α lines of energy 1253.6 eV has been used. The XPS is surface sensitive technique, the whole system for XPS should be under UHV conditions (in our case the base pressure was 5×10^{-9} mbar). Residual gas species inside the UHV chamber affects the samples in two ways (1) monolayer formation time (2) scattering by gas phase molecules. Also the NEG materials are excellent pumps, therefore, their surfaces are more prone to adsorb residual gases in the system. As a consequence, high pressure may affect the validity of the XPS measurements. The mean free path of electrons of 100 eV is about 1mm at 1 mbar pressure of water vapor. Since the electrons travel many centimeters on their way to detector and the distance, attenuation of the signal under elevated pressure poses a limit on the background pressure in conventional XPS system. Some of the sources which are used in XPS are given in Table 3.1.

Synchrotron radiation of monochromatic wavelength can - also be used for XPS and make it more versatile with properties such as sufficient intensity, energy tunability and polarization etc.. The penetration depth of soft x-ray are about hundreds of nanometers or more, elastic or inelastic interactions of photoelectrons with sample atoms in the sample limit the probe depth to a maximum of few nanometers over a kinetic energy range used in

conventional XPS system. Fig. 3.3 shows the inelastic mean free path as function of their kinetic energy [100,101].

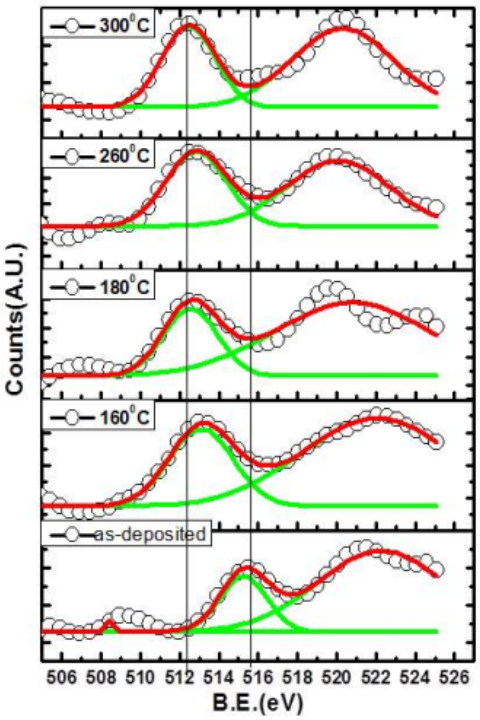

Fig.3.2: XPS spectra of V3*p* of NEG coating showing different oxidation states.

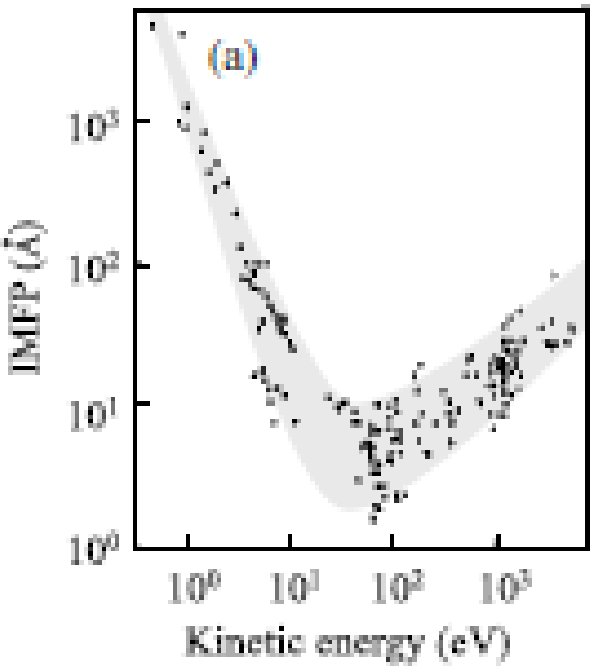

Fig.3.3: Inelastic mean free path (IMFP) as a function of electron kinetic energy in solids.

Table3.1: List of commonly used laboratory X-ray sources.

Photon source	Energy (eV)	Natural width (eV)
Mg K_α	1253.6	0.8
Al K_α	1486.6	0.9
TiK_α	4511	1.4

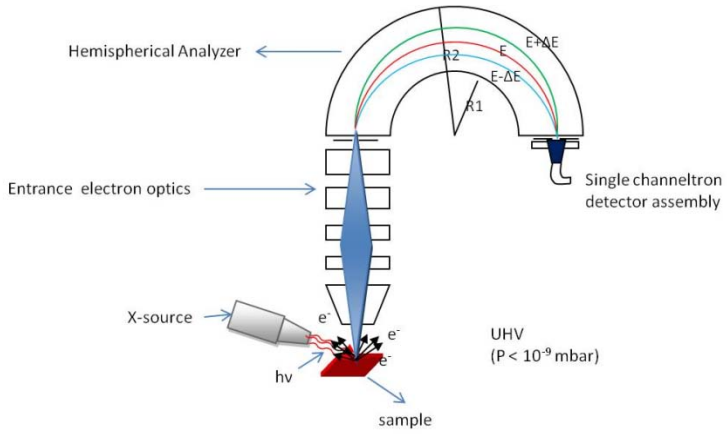

Fig.3.4: Schematic of general XPS system.

Fig.3.5: Photograph of our XPS system.

3.1.3 Description of our XPS system in used in the activation studies of NEG coatings

XPS measurement were carried out with VG Scientific make hemispherical electron spectrometer. The schematic and the actual XPS system are shown in Fig. 3.4 & Fig. 3.5. The analyzer was operated in the fixed pass energy mode (fixed transmission mode). Transmitted electrons are detected with channeltron detector in counting mode connected to a charge sensitive preamplifier assembly. Our aim is to measure the change in the binding energy of core electrons of constituent elements of the thin film of TiVZr which reflects the change in the oxidation state of the elements after heating it to different temperature.

Hemispherical Analyzer with single channel electron multiplier is main detector system in XPS system. Hemispherical analyzer which is used to analyze the ejected electrons from the sample between the energy range E and ΔE. It consists of three parts electrostatic lens system to collect the electrons from the sample with definite acceptance and transfer them to the entrance of the hemispherical analyzer with definite magnification. The electrons then

pass through an entrance slit of width s which is used to transmit the electrons of E±ΔE in dispersive direction and Δα in non-dispersive direction. The transmitted electrons after traversing through the analyzer focused at the exit slit, then reach the detector. At the detector (channel electron multiplier) multiplication (10^5 -10^6) of the electrons take place to increase the signal to a detectable level. The electron bunch then passes through the charge or voltage sensitive preamplifier and the pulses are counted by a counter. The detector works in single electron counting mode. In Fig.3.2, a typical XPS spectra of V3*p* level of ternary alloy coating Ti-V-Zr has been shown.

The resolution R of the hemispherical analyzer depends on the slit width and mean radius of the hemispherical analyzer and is given as

$$R = \frac{\Delta E}{E} = \frac{s}{2R} + \Delta\alpha^2$$

$$s = s_1 + s_2$$

$$Retardation\ factor\ k = \frac{E_k}{E_p}$$

$$R = \frac{\Delta E}{E_p} = \frac{\Delta E}{E/k} = k\frac{R_1.R_2}{(R_2^2 - R_1^2)} = \frac{1}{(R_2 - R_1)(\frac{1}{R_1} + \frac{1}{R_2})} \approx \frac{k}{\Delta R}$$

Where R_1 and R_2 are the inner and outer radii of the hemisphere, s_1 and s_2 are the slit widths of entrance and exit slits, and E_k and E_p are the actual and exit kinetic energies of the photoelectrons.

3.1.4 Benefits of XPS technique

The advantage of XPS for the investigation of the thin films are its surface sensitivity and chemical structure where each elements exhibit a characteristic set of core levels peaks in XPS spectra that directs to get the chemical composition of the surface quantitatively. The binding energy of core and valence electrons show similar changes (of the order of tenth to

several eV) depending on the type of chemical bonding. In this thesis, the ternary alloy coating of NEG materials show the different positions of Z, ZrO_2, Ti, TiO, TiO_2, V, V_2O_3 and $V_2 O_5$, when interpreting these so called 'chemical shifts'. It can be concluded that binding energy is dependent on both on the 'initial state effect' as well as 'final state effect'(when the core hole filled). But there are many cases where the chemical shift is assigned to initial state effects. The sensitivity to the chemical state of the atoms mean that valuable information can be gleaned from XPS measurement such as bonding within the thin films, as well as at the interface to the substrate. XPS can also be used for depth profiling both in etching mode and non destructive mode. In etching mode, surfaces can be etched layer by layer by energetic Ar ions. In this method there is no limitation to depth measurements. In non destructive mode, the collection of electrons of fixed kinetic energy at different take off angle resulting in the depth information of the thin films.

Now the energy tunable sources such as synchrotrons are available, hence the versatility of non destructive depth analysis has improved. When the incident photons of tunable energy fall on the sample, the electrons of different energy from the different depth can be detected which provides the depth profile of the sample.

3.2 Studies of NEG coatings using Scanning electron microscope

The scanning electron microscope (SEM) is the most widely used of all electron beam instruments. It owes its popularity to the versatility of its various modes of imaging, the excellent spatial resolution of its images and easy interpretation of the micrograph it generates and its user friendliness. It can cover the wide range from optical microscope to AFM, TEM. Its resolution can now approach to 0.5nm and it can handle specimens as large as production size silicon wafers. The first modern SEM was described by Zworykin et al [102]. It can be divided into source, electron-optical, the scanning, detector system,

processing and display systems. The sources are thermionic filaments (W, LaB_6) or field emission. Field emission provides a very high beam current so a measurable signal can be achieved at very high magnification which is not possible in thermionic emission SEM. For the studies of NEG coatings, FE-SEM technique is very useful as the alloy film deposited by DC-magnetron sputtering has nano-size grains. The emitted electrons are then accelerated to a typical energy of 500eV to 30 KeV. The electromagnetic optical system does all kinds of required manipulation such as focussing, zooming, magnification and transfer of the electron beam from the filaments to Scanning electron microscopy. A variety of detectors, including an Everhart-Thronley [103] scintillator detector for secondary electrons, some type of detector for backscattered electrons and often a detector for fluorescent X-rays to permit chemical microanalysis with the beam which is called the EDX analysis. The performance of a SEM can be given in terms of the spatial resolution that it can produce. The attainable resolution in SEM is determined by a number of factors including the electron beam diameter d, the current I_b, the magnification of the image and the type of imaging mode that is being used. Over most of the operating energy range (5 – 30 KeV) of the SEM , the probe size and the beam current are related by the expression of the form [104].

$$d = \left(C_s^{\frac{1}{4}}\lambda^{\frac{3}{4}}\right)[1 + \frac{I_b}{\beta\lambda^2}]^{3/8}$$

$$\lambda \approx 1.22\, E_0^{-1/2}\, nm$$

Where λ is the wavelength of the electrons, E_0 is the energy of the electron in eV, β is the brightness of the electron gun in $Acm^{-2}steradian^{-1}$ and C_s is the spherical aberration coefficient of the objective lens. For modern SEM a typical beam size of 1 to 2 nm is available. The pixel size defines the resolution of the image so no information smaller than pixel size can be resolved even though the probe size is significantly smaller than this size.

SEM is a powerful instrument which permits the observation and characterization of heterogeneous organic and inorganic materials and surfaces on such a local scale. The schematic diagram of a SEM is shown in Fig. 3.6. The primary reason for the SEM's usefulness is the high resolution that can be obtained when bulk objects are examined, the resolution of SEM equipment is normally about 3-5 nm. However, in the case of high resolution SEM, the resolution can be up to 1nm [105].

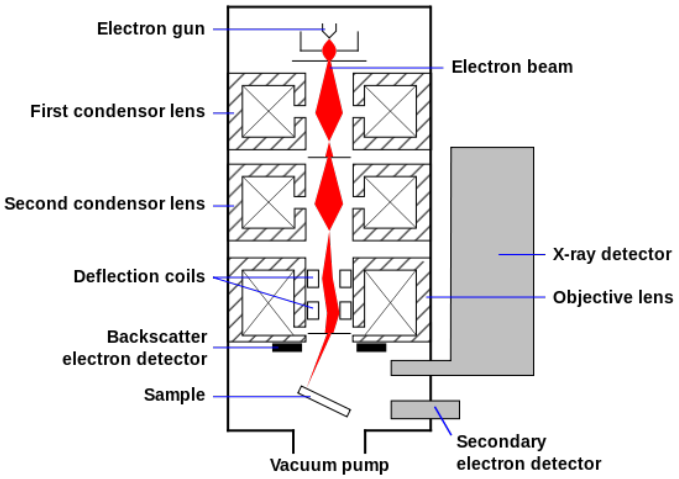

Fig.3.6: Schematic of typical SEM system.

3.2.1 Energy dispersive X-ray spectra

Another important feature of the SEM is the three-dimensional appearance of the sample image. Generally, SEM instrument is combined with Energy dispersive X-ray detector which is used to get stoichiometry of the elements from surface to 1 µm depth inside the material. The EDX can yield both qualitative identification and quantitative compositional information from regions of a sample as small as a micrometer in diameter. In this thesis, the SEM is used to analyze the micro structural properties of the Non evaporable getter coatings on different substrate. Using the back scattered and secondary electrons mode, the multi-segment character of the film was measured.

3.2.2 SEM technique to study the Influence of substrate on NEG film morphology

In Fig. 3.7, Fig.3.8 & Fig. 3.9, the NEG films prepared on the different substrates SS304L, Cu and Si are shown (111). First of two materials are used as construction material for the manufacturing of the vacuum chambers. It is under practical importance to study the effects induced by surface morphology, crystallinity and activation of the NEG coatings of TiVZr.

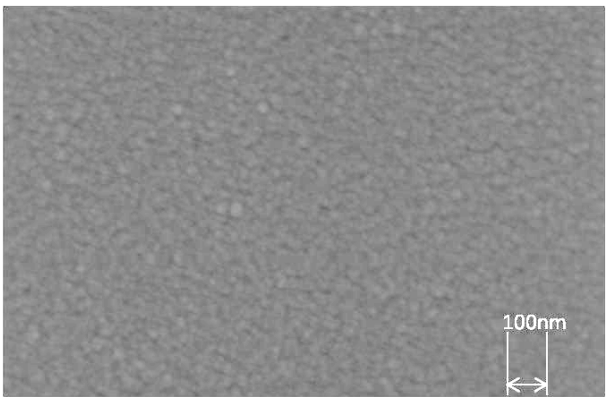

Fig.3.7: FESEM micrograph of TiVZr on Si(111) substrate.

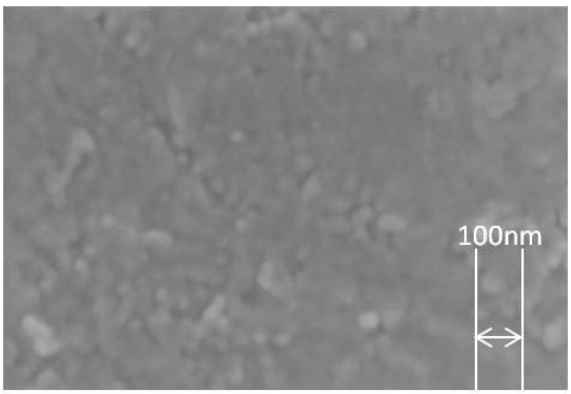

Fig.3.8: FESEM micrograph of TiVZr on Cu substrate.

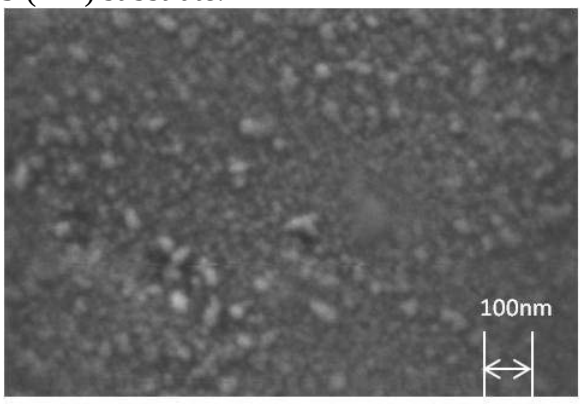

Fig.3.9: FESEM micrograph of TiVZr on SS304L substrate.

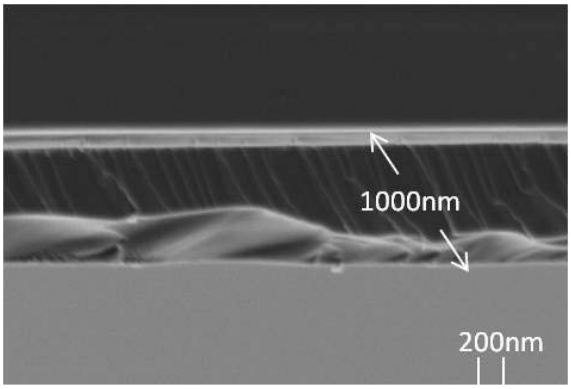

Fig. 3.10: Cross sectional view of the NEG film.

The morphology of the NEG films TiVZr are shown in Figs. 7 – 10. The films were coated on different substrates keeping same deposition parameters. The growth of the film is Volmer-Weber type. The films on all the substrate are nano-crystalline in nature. On Si(111) substrate the grains were smallest, while on SS304L substrate, the grains were comparatively big. In Fig. 3.10**,** the cross sectional view of film has been shown which features the 1μm film

thickness with columnar growth. The roughness of the coating depends upon roughness of the substrate also.

In Fig. 3.11 shows the morphology of other NEG film which was deposited by sputtering a ternary target made by twisting 1mm dia wires of Ti, V and Zr in the ratio (2:1:1) at SS304L substrate at the Ar pressure of 1.2×10^{-2} mbar. Deposition of the film was 4 hrs and substrate was at room temperature only. The stoichiometry of the film obtained from EDX technique was $Ti_{48}V_{31}Zr_{21}$. The grains can be seen clearly of about 10 nm size. There are grain boundaries which help to diffuse the oxygen across the boundaries also. Among the different coating tested till now, the TiVZr films showed the lowest sticking factors and also the smoothest surface [106].

The roughness of a coating may depend not only on the chemical nature of the film, but also on the sputtering parameters and on the nature of the substrate. In Fig.3.7, Fig.3.8, Fig.3.9 and Fig.3.10, the film of TiVZr deposited under similar conditions on various substrate are shown. While Copper and stainless steel favours the very smooth film surface. Aluminium and beryllium produce a “cauliflower” type structure as reported in ref [63].

It was observed that even for very odd combinations of coating and substrate, the roughness of a film may always increased by roughing the surface of the substrate before coating. The method of optimization in this area is under process. Adequate combination of substrate and coating materials with proper surface treatments as well as keeping proper deposition parameters, the surface capacities and sticking coefficient of the these films equal to the alloy St 707 strip of SEAS getters in much smaller thickness of the sputtered coated film.

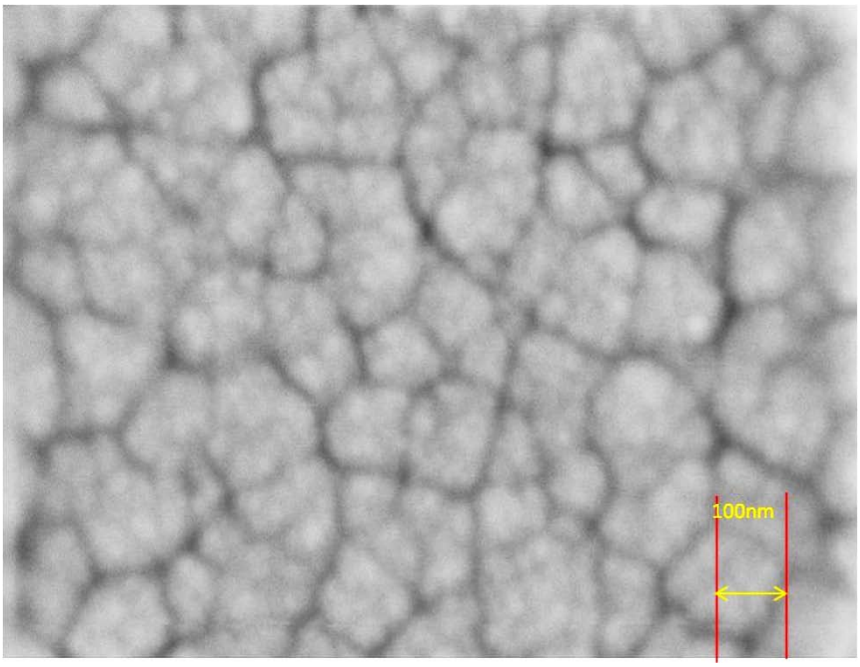

Fig.3.11: FESEM micrograph of $Ti_{48}V_{31}Zr_{21}$ on SS304L substrate.

In Fig. 3.12 & Fig. 3.13 shows the morphology of another NEG film which was deposited by sputtering a twisted ternary target of metals Ti, V and Zr in the ratio of (1:1:1) at SS304L substrate with Ar pressure of 9 mbar. The deposition of the film was 3 hrs. The deposited film was very smooth with grain size of 20nm and many more grain boundaries. This type of film showed very high diffusion across the grain boundaries at elevated temperature. The lateral diffusion of adsorbed atoms on the substrate is normally decreased with the increase of the sputtering gas pressure. It happens due to loss of energy of sputtered atoms in collisions with by discharge gas. It has also reported that the specific surface of the films increases with increasing glancing angle from 0° to 70°. High roughness and porosity induce an increase of both surface gas capacity and sticking probability [66]. High roughness increased the effective surface area and porosity increased the collision of the impinging molecules inside surface pores. The probability of trapping is increased which leads to the breaking of atoms and diffusion inside the bulk such as diffusion of H_2. For coatings with greater roughness was tested in large surface loads, the values of the pumping speed of CO and N_2 are reported

which were expectedly the same for which molecules must penetrate inside the channels of limited conductance [107]. The outer most part of the channels was saturated by CO. An analogous behaviour was also reported for commercially available St101 and St707 NEG strips [108, 109]. A mathematical description of the relation between porosity and pumping speed is given in the refs [66, 107]. However, higher heating temperatures of the substrate increased the activation temperature of the samples. This behaviour could be described due to the appearance of a second phase, either due to its intrinsic diffusion or its large grain size which resulted in the lower density of grain boundaries.

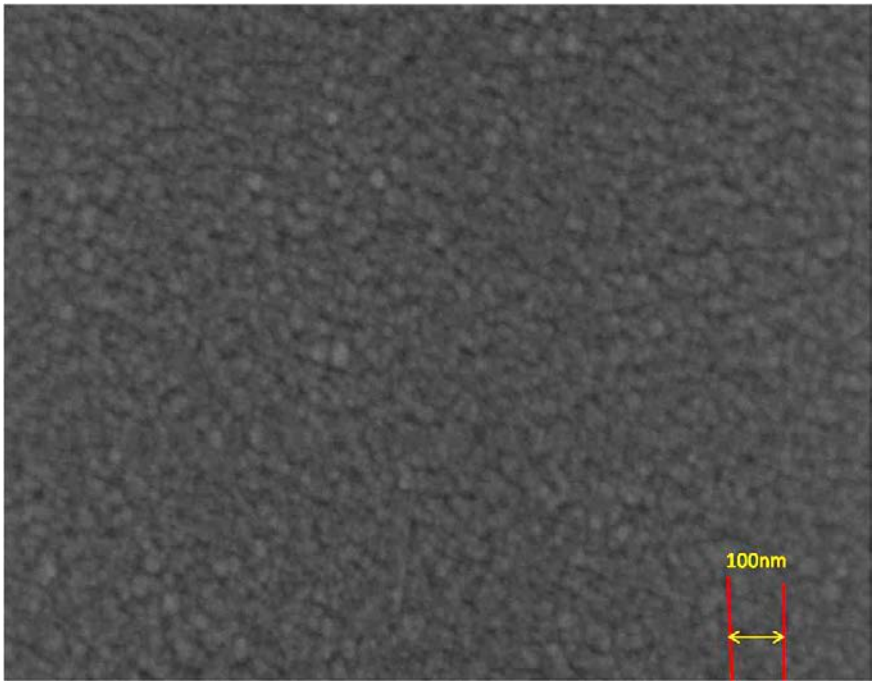

Fig. 3.12: FESEM micrograph of $Ti_{28}V_{44}Zr_{28}$ on SS304L substrate.

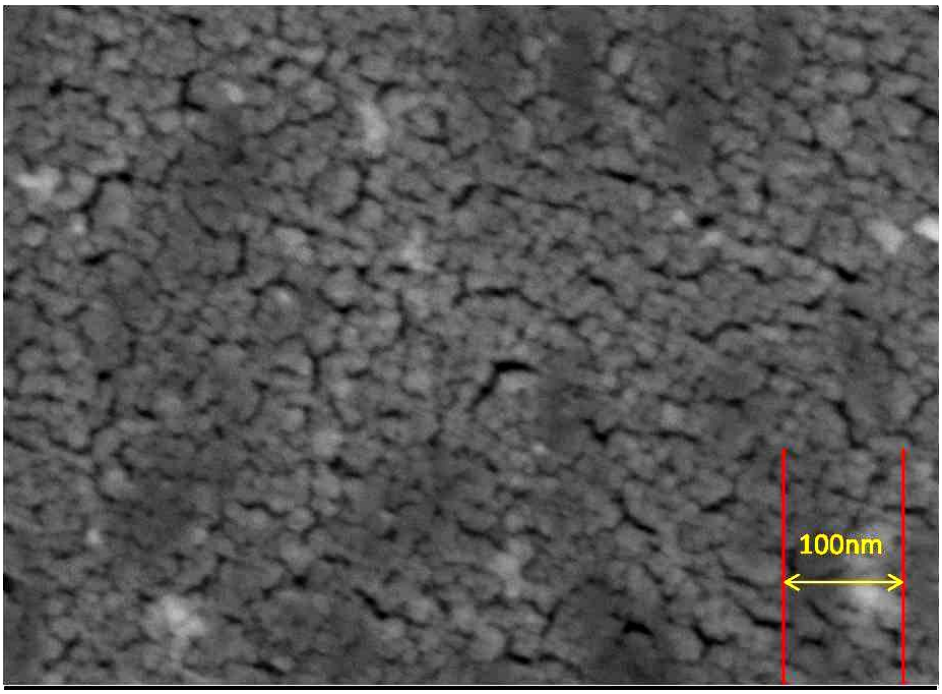

Fig. 3.13: FESEM micrograph of NEG coating on SS304L substrate at high magnification

3.3 Role of diffraction technique in the structural study of NEG coatings

XRD has been very popular tool for characterization of the materials. The crystal structure, lattice constants and texture of the films can be determined effectively and elegantly through the use of X-ray diffraction (XRD) [110 - 112], where one utilizes the interaction between the incoming photon and the electron charge density of atoms. It is a non-destructive and non-contact technique. Because of this it has been essential technique for structural characterization. When an X-ray beam is incident on a particular set of parallel (*hkl*) lattice planes spaced apart, specularly reflected beams from two adjacent planes will have a path difference which is $2d \sin \theta$, where θ is the angle between the planes and the incident beam. The schematic is shown in Fig. 3.14**.** The constructive interference of reflected beam from successive planes occurs when the path difference is an integral number '*n*' of the wavelength λ, so that $2d \sin \theta = n\lambda$.

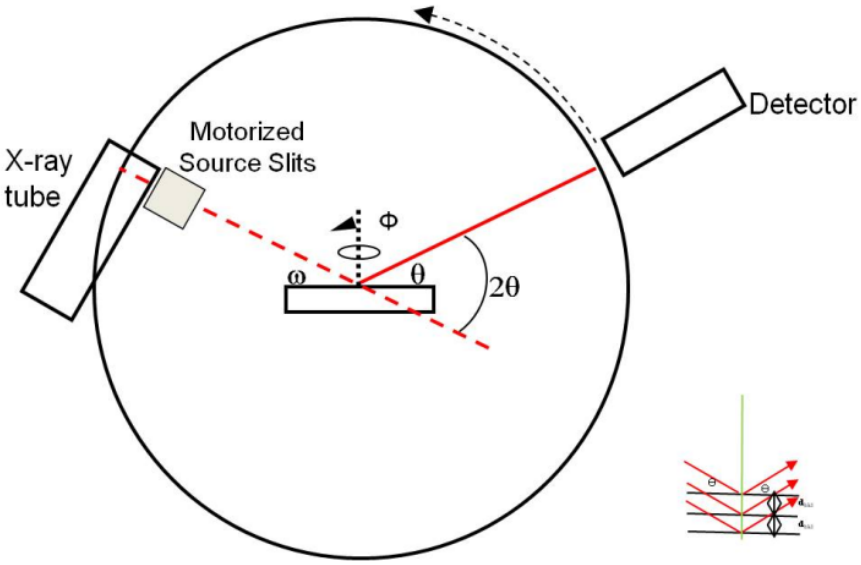

Fig. 3.14: Schematic of X-ray Diffractometer.

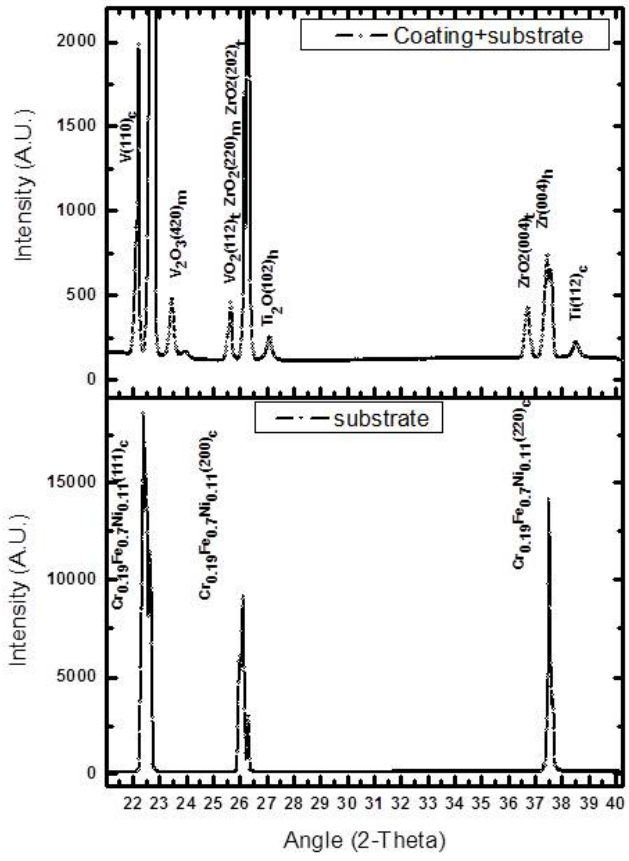

Fig. 3.15: Typical XRD pattern of NEG film & substrate by XRD beam line.

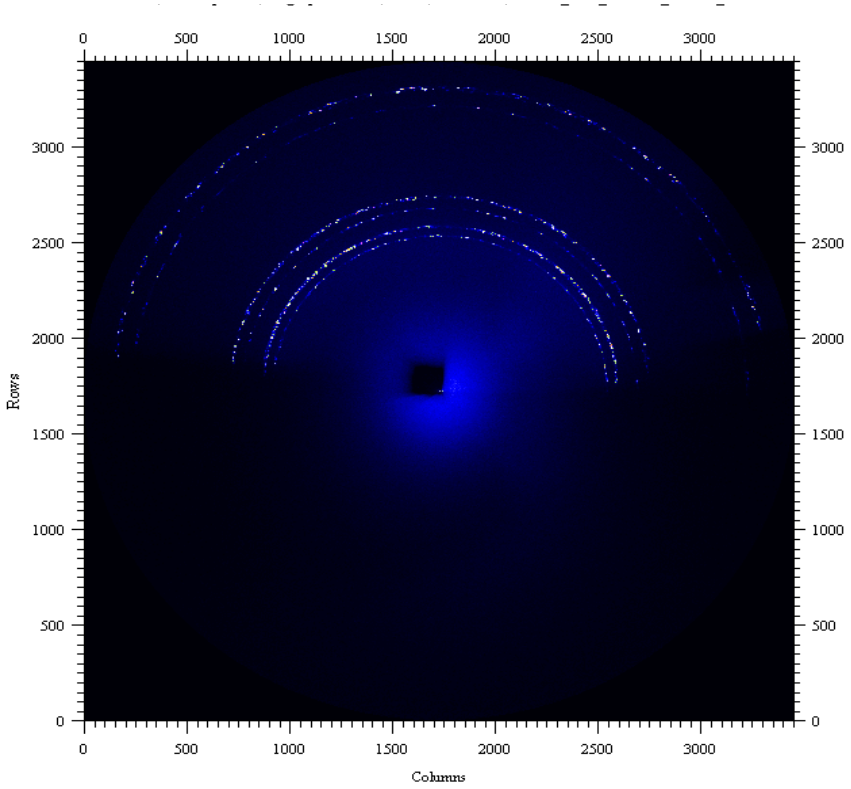

Fig.3.16: Powder diffraction pattern of the NEG film by XRD beam line at Indus-2 source.

In the studies of NEG thin films, the grazing incidence x-ray diffraction was more prominent due to minimum contribution from the substrate. In conventional X-ray diffraction and fluorescence with large incident angles, an incident x-ray beam penetrates deep into a material. The XRD peaks and powder diffraction pattern which were achieved on XRD beam line at RRCAT, Indore has been shown in Fig. 3.15 & Fig. 3.16. To limit the incident X-ray beam to the surface, grazing-incidence x-rays are needed.

In grazing-incidence experiment, the detector is placed in a horizontal plane parallel to the film surface to record diffraction from lattice planes which are perpendicular to the surface. At incident angles near to the critical angle, X-rays are enhanced by 2-4 times the surface over the intensities in the bulk [111]. Small penetration depths and intensity enhancement make possible the use of X-rays for the characterization of surfaces, buried interfaces and thin films. GIXRD has been successfully applied to studies of surface treatment, oxidation and ion implantation. In GIXRD, X-rays pass through a suitable slit system and are made to

fall on the sample at a glancing angle (α) while the detector on the 2Θ axis scans the XRD pattern. The diffracted beam optics is modified to a parallel beam optics and a flat plate monochromator is incorporated in the diffracted beam. This technique has immense potential in characterizing graded and multilayer thin film structures. X-ray beam irradiates the sample surface. Conventional Θ -2Θ scan and radial scan provides information about the epitaxial relation, orientational spread, crystallite size and lattice grain.

Diffraction pattern of NEG thin films was taken on XRD beamline installed at third generation synchrotron source Indus-2 at RRCAT, Indore. The monochromatic beam x-ray of energy 15 KeV was used for the diffraction peaks of NEG thin film coated on SS304L substrate. The x-ray beam was made to fall at the grazing incidence of 3° from the sample surface. Powder diffraction pattern of the NEG film in Fig. 3.15 showed the presence of substrate as well as NEG films peak. The Ti ,Zr and V which are constituents of the NEG film found in metallic phase and a small quantity of oxides are also available in the film.

3.4 Morphological study of NEG thin film using Atomic force microscopy

The Atomic force microscopy provides the morphological information of a surface with very high spatial resolution on the order of sub nanometer scale. The quantification of the surface roughness can be also achieved using AFM.

The AFM consists of a micro size cantilever with a sharp tip (probe) at its end, which is used to scan the specimen surface. The cantilever is made up of typically a silicon or silicon nitride with a tip radius of curvature on the order of nanometers. When the tip is brought into proximity of a sample surface, atomic forces between the tip and the sample lead to a deflection of the cantilever according to Hooke's law. Depending on the situation, forces that are measured in AFM include mechanical contact force, Vander Waals forces, capillary forces, chemical bonding, electrostatic forces, magnetic forces, salvation forces etc.

Typically, the deflection is measured by using a laser spot reflected from the top of the cantilever into an array of photodiodes. Other methods that are used include optical interferometry capacitive sensing or piezo-resistive elements that act as a strain gauge. Using a Wheatstone bridge, strain in the AFM probe due to the deflection can be measured, but this method is not as sensitive as laser deflection or interferometry. The morphology of NEG samples were studied in this thesis by atomic force microscopy. The schematic is shown in Fig. 3.17.

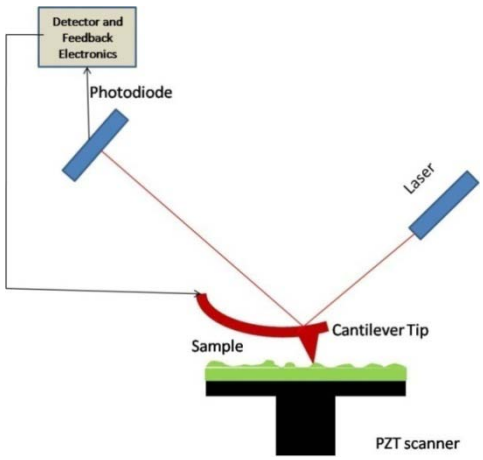

Fig. 3.17: Schematic of Atomic force microscopy.

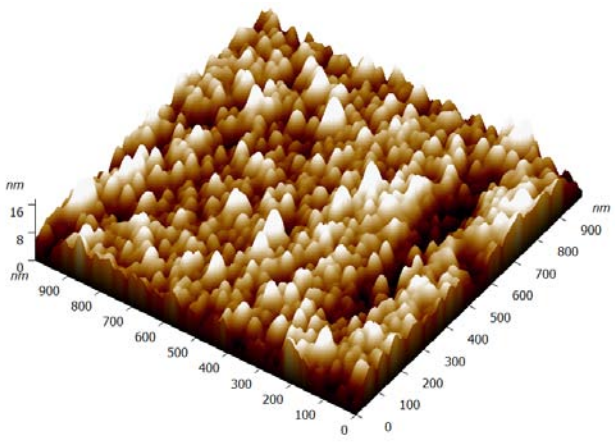

1 (a)

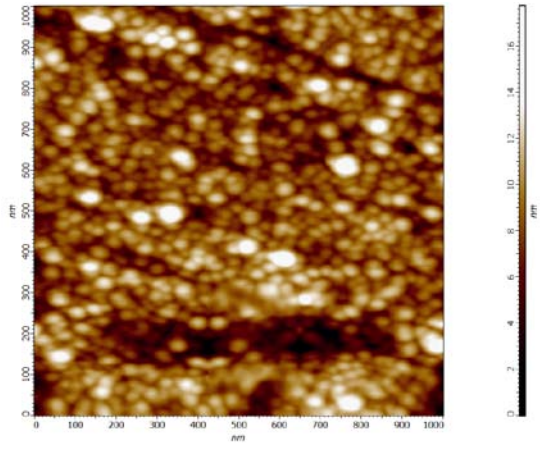

1 (b)

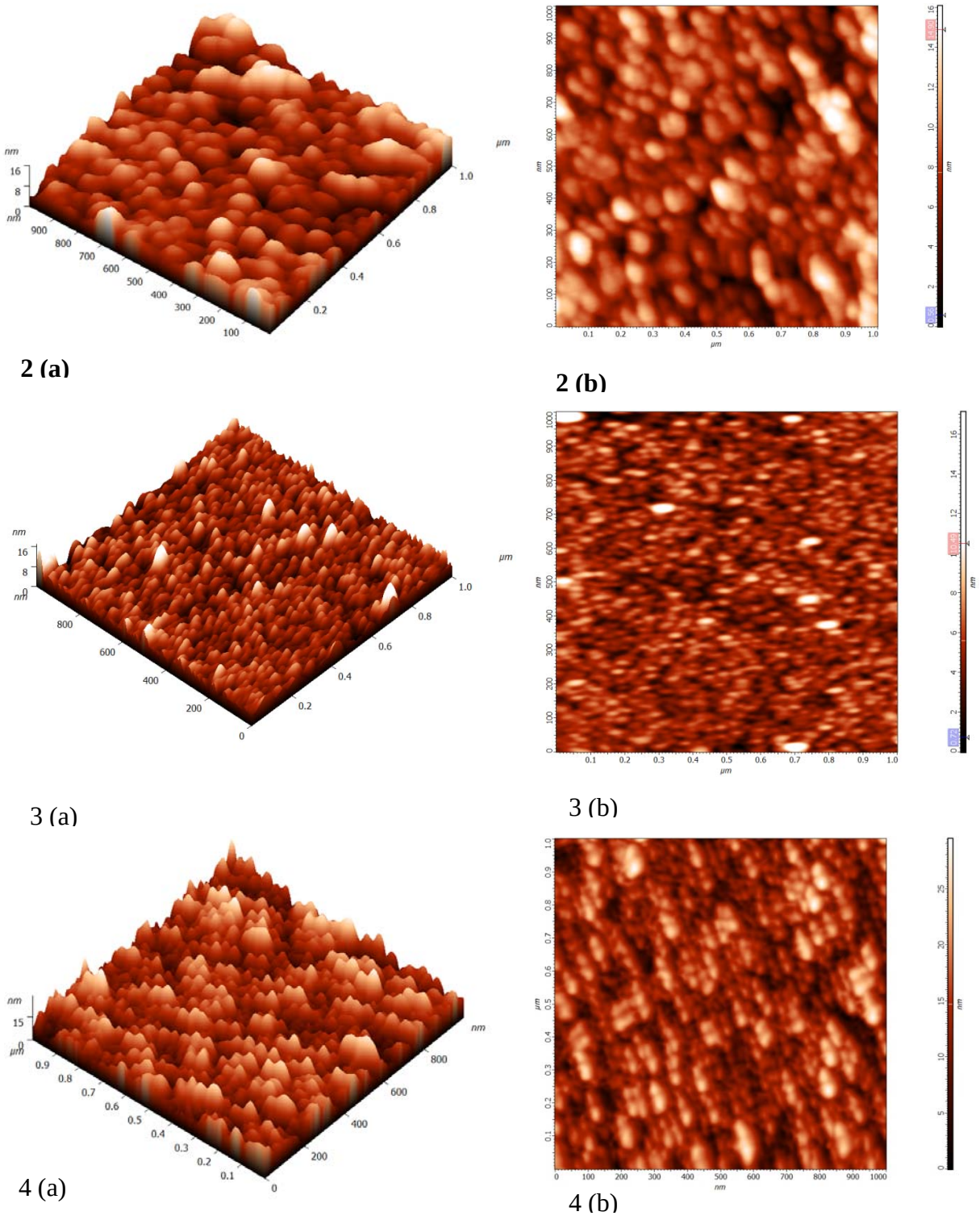

Fig. 3.18: AFM micrograph of four sample in both 3d and 2d form is given in 1 (a) & 1(b), 2 (a) & 2(b), 3 (a) & 3 (b), 4(a) & 4 (b).

Table 3.2 Surface roughness of different deposited NEG films achieved by AFM.

Elements	Average Surface roughness (nm)	RMS roughness (nm)	Peak to peak roughness (nm)
Sample-1	1.91	2.95	36.7
Sample-2	7.69	2.41	16.0
Sample-3	1.075	1.43	17.1
Sample-4	3.50	4.36	29.43

Surface roughness is an important parameter in promoting gettering action of the NEG film. The rougher is the surface, larger is the actual area available for adsorption of the gaseous molecules which enhances the pumping speed of the NEG film. It also cause the gaseous species for multiple reflections so molecules or atoms become more probable to be trapped and finally sorbed inside the bulk of the NEG. Fig. 3.18 showed the 3D and 2D images of the NEG films of four samples prepared on SS304L substrates. Details of the surface roughness of all the four samples are given in Table. 3.2.

3.5 Summary and Conclusions

The different techniques which are used in the characterization and activation studies of NEG thin films are described. These are XPS, SEM, EDX, XRD and AFM techniques. NEG film of ternary materials on SS304L, Cu, Si substrates were prepared using ternary targets of TiVZr and TiNbZr in different ratios. The morphological features of these films were studied by the SEM technique. The surface roughness of these films was studied by AFM technique. The SEM micrograph of these samples shows the nano-crystalline type of grains. The grain sizes of the film on Si(111) were smallest as compared to Cu, SS304L substrate. Smaller grain sizes provides more number of grain boundaries which enhances the surface diffusion. The AFM micrograph provide the quantification of surface roughness of the films which comes out average valve of 24 nm peak to peak roughness.

CHAPTER 4

4.1 Introduction

Coatings or bulk of NEG materials essentially act as a sorption vacuum pump due to their gettering action when activated by elevating the ambient temperature of these coatings in a sealed-off vacuum chamber. The gettering action of these coatings is due to their large solubility, and high diffusivity towards the adsorbed gases [63, 113– 116]. These coatings can be used for efficiently pumping the low-aperture and micro miniature vacuum sealed devices or to construct getter pumps to complement conventional pumping devices. In addition to that, an important application of NEG materials is in large vacuum systems such as synchrotrons, particle accelerators, and colliders [113, 114, 116]. The NEG coatings on SS304L substrate were deposited using a cylindrical type DC-magnetron sputtering technique at different argon gas pressures using different targets for achieving better pumping results. As discussed earlier, an oxide layer forms on the fresh metallic surface when they are exposed to atmosphere after deposition. These coatings or thin films show their passive behaviour towards active gases unless their passive oxide is removed partially or fully in the process of activation. One method of NEG pumping is to evaporate NEG materials in both thin film and bulk form at very high temperatures make fresh film which deposited on the walls of the chamber and the fresh film starts gettering action. The other method which has been described in this chapter is the activation of the NEG films at low temperatures. In this method we sequentially test the film by heating it at different temperatures and characterize its surfaces using the XPS technique. The reduction of surface oxides shows the film is getting activated. A full reduction of the surface oxide shows the active metallic surface which is ready to chemically pump the residual gases present in an isolated chamber. The whole experiment is done under ultra high conditions. The XPS technique has been

efficiently used for this type of study. It is a sequential study which has involved a number of steps such as raising temperature of the sample at the desired level at constant rate and soaking it at this temperature for 2 – 3 hrs. After switching off the heater, it is required to achieve the required level of UHV in the chamber and allow the sample to achieve the equilibrium.

4.2 Activation studies of ternary Coating of NEG material (Ti-V-Zr) prepared by plasma arc deposition.

Before discussing the activation studies of ternary form of coating, the coating of Zr metal and binary Ti-Zr were prepared on SS304L substrate by a planer type DC-magnetron sputtering system and studies by the XPS technique. The details of the sample preparation and characterization can be found in the reference [117]. The activation temperatures of these coatings were found to be in the range from 350°C to 400°C.

The first coating of NEG materials in ternary alloy form was deposited by using a composite target of $Ti_{0.2}V_{0.4}Zr_{0.4}$ by vacuum arc evaporation at a pressure of 6 X 10^{-5} mbar [118]. The target was in ingot form which was prepared by a non-consumable arc melting using a tungsten electrode in a water-cooled copper hearth, in vacuum of < 10^{-3} mbar using three metals (Ti,V, Zr). The details of the preparation of the target are given in ref [118].

To study the activation process of coating of Ti-V-Zr, XPS measurements were performed in an ultra high vacuum chamber equipped with VG Scienta make sample manipulator facilitated with Tantalum heater and VG Scienta hemispherical energy analyzer facilitated with single channel analyzer detector. The analyzer worked in a constant pass energy mode with the energy resolution of about 100 meV. The excitation source MgK_{α} (1253.6 eV) was used in this experiments and take-off angle of the photoelectrons was 54.5º. The depth of the sampling was about 2 – 3 nm and the base pressure was 2 X 10^{-9} mbar. The

samples were mounted on a copper holder that could be heated by a Tantalum heater. A K-type (chromel – alumel) thermocouple was attached to the sample surface to measure the sample temperature. The heating rate was kept as 5ºC/min. The samples were kept at the indicated temperature for 2 hrs and then cooled down to room temperature. While during the sample was being heated, the pressure of the chamber increased with increasing temperature. The chamber pressure did not exceed 3 X 10^{-7} mbar even after the sample was heated to 250ºC for 2 hrs. The binding energy scale was calibrated by measuring the carbon 1s peak (284.6 eV) and the core level signal of the copper holder reference before/after measuring the sample. All the spectra were normalized in intensity by using the same background-to-peak.

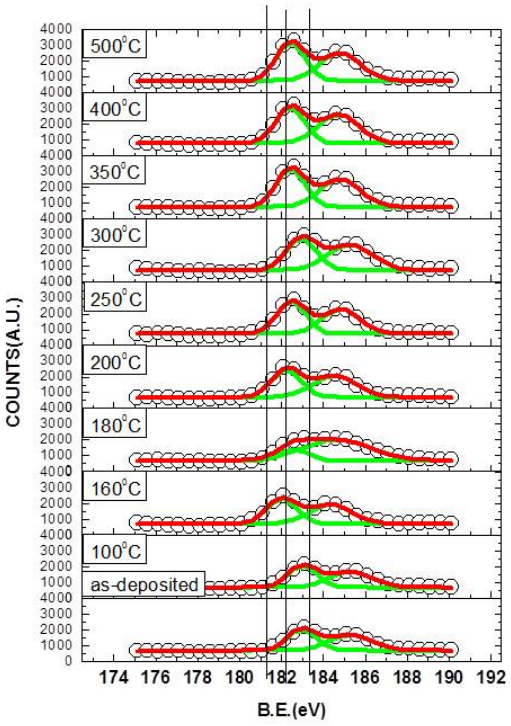

Fig. 4.1: XPS peak of Zr3d after treating at different temperatures under UHV conditions.

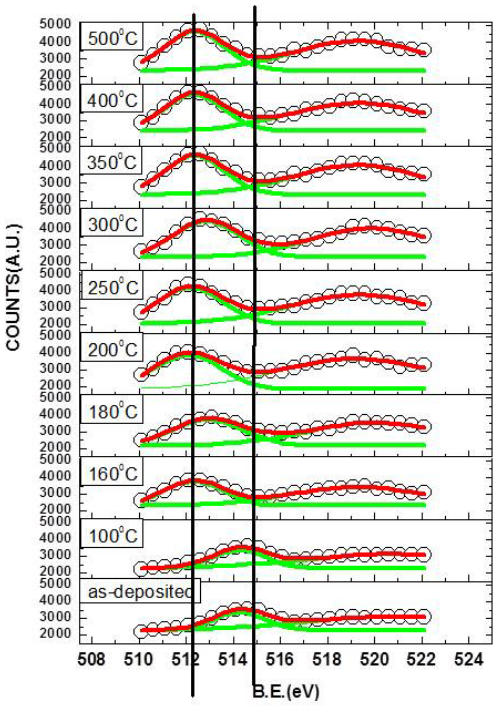

Fig. 4.2: XPS peak of V3p after treating at different temperatures under UHV conditions.

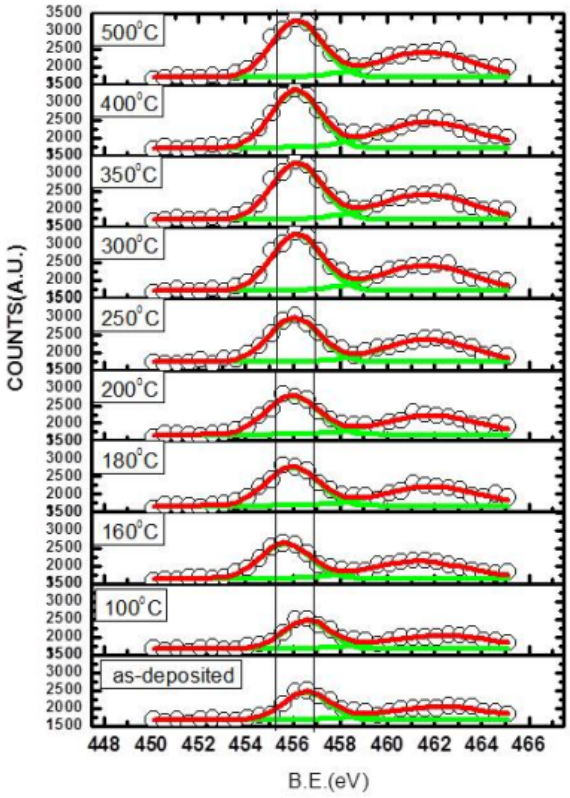

Fig. 4.3: XPS peak of Ti3p after treating at different temperatures under UHV conditions.

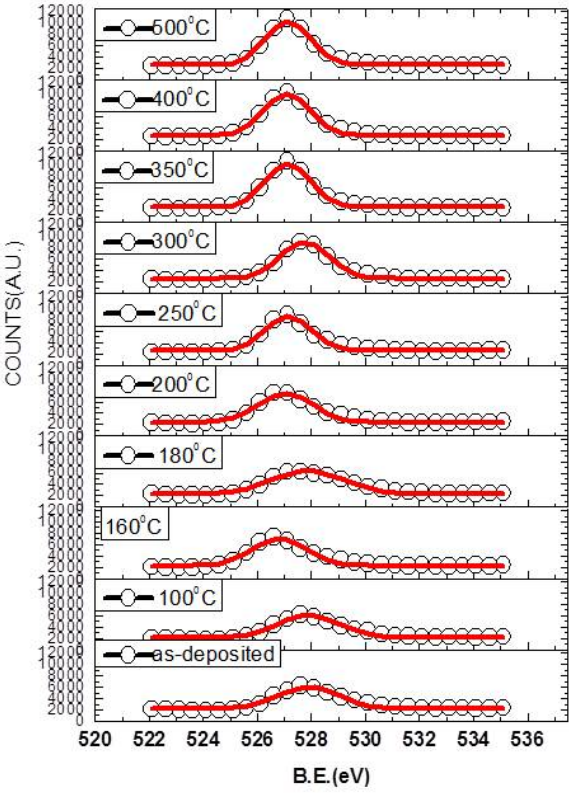

Fig. 4.4: XPS peak of O1s after treating at different temperatures under UHV conditions.

The Zr3d in oxide exhibits several peaks which can be attributed to different oxidation states of zirconium represented as Zr^{n+}(where n=0 to 4), as shown in Fig. 4.1. The Z^{0+} corresponds to metallic zirconium which can be achieved after full activation of the film. The peak at 183.2 eV corresponds to ZrO_2 in as-deposited samples correspond to Zr^{4+}, i.e. zirconium is fully oxidized. On heating it losses oxygen which diffuses inside the bulk and lead to the conversion of lower oxides of Zr and then to metallic oxide Zr^{0+} and metallic carbide (ZC).

The V3p exhibit several peaks which can be attributed to different oxidation states of vanadium represented as V^{n+} (where n = 0 to 5), as shown in Fig. 4.2. The V^{0+} corresponds to metallic vanadium which can be achieved after full activation of the film. The peak at 515 eV of as-deposited samples corresponds to V_2O_4, i.e. vanadium was not fully oxidized. On

heating it losses oxygen which diffuses inside the bulk and lead to the conversion of lower oxidation states and finally to metallic vanadium. The peak at 512.1eV after 2 hrs of heating at 160ºC corresponds to metallic vanadium mixed with VC.

The different oxidation states of Ti3p are shown in Fig. 4.3 corresponding to Ti^{n+} (where n = 0 to 4). The Ti^{0+} corresponds to metallic titanium which can exist after full activation of the film. On the other hand, the Ti3p peak at 457 eV corresponds to Ti^{4+} (TiO_2) i.e. fully oxidized state of Ti. On heating the film at 160ºC its peak shifts to broad peak centred at 455 eV which corresponds to mixed value metallic Ti^{0+}, TiC and TiO as oxygen of superficial TiO_2 diffuses inside the bulk at elevated temperature. In Fig. 4.4, the shift in B.E. after heating at different temperature of the O1s peak has been shown.

In Fig. 4.5, Fig. 4.6 and Fig. 4.7, the shifting of the peak values of V3p, Ti3p and Zr 3d on account of heating has been shown which provide quantitatively the change in the B.E. of these elements in different oxide forms.

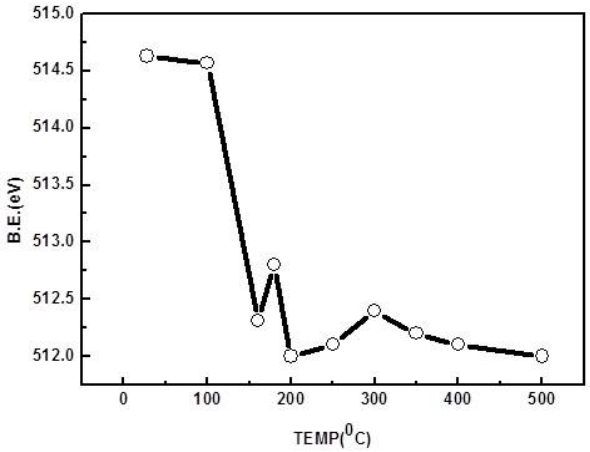

Fig. 4.5: Shift in the B.E. of V3p after treating at different temperatures under UHV conditions.

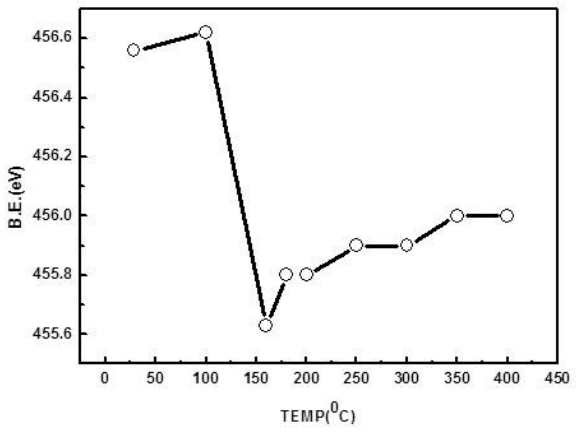

Fig. 4.6: Shift in B.E. of Ti3p after treating at different temperatures under UHV conditions.

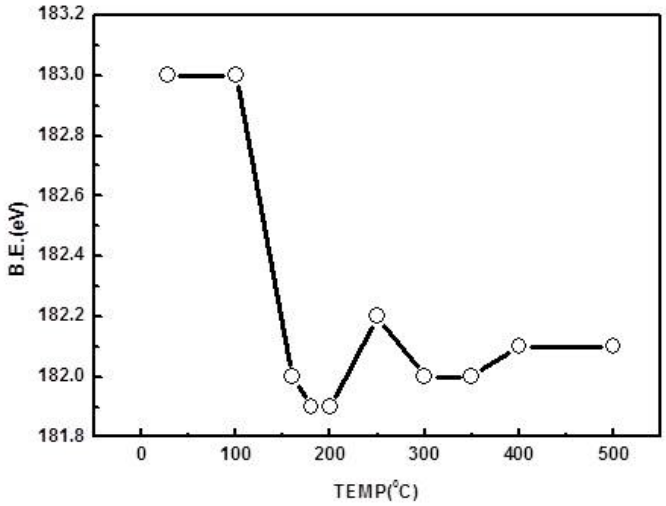

Fig. 4.7: Shift in B.E. of Zr3d after treating at different temperatures under UHV conditions.

4.3 Activation studies on ternary coatings of NEG material (Ti-V-Zr) prepared by DC-magnetron sputtering deposition (Ar pressure of 8 X10^{-3} mbar)

Thin films were deposited using a ternary target of Ti-V-Z on SS304L substrate using the cylindrical type DC-magnetron sputtering system. During the deposition, Ar pressure of 8 X10^{-3} mbar was maintained after achieving the base pressure of 2 X 10^{-6} mbar. The target was made by twisting three wires of Ti/V/Zr (purity: 99.7%) of diameter (1mm) and kept at a voltage of -500V with a deposition time of 3 hrs. A magnetic field of 250 Gauss was applied using an external solenoid to increase the mean free-path of the electrons.

In Fig. 4.8, changes in the B.E. energy of the oxygen 1s peak have been shown. The peak at 530.5eV corresponds to oxygen in Zr oxide and its suboxides, and the broad peak at 530.2 eV is due to oxygen in (Ti, V) oxides and their suboxidesTiO, TiO_2, VO, V_2O_3, V_2O_5 etc. [119]. The oxygen peaks shifts to higher energy after heating the film which corresponds to lower metallic oxide peaks. The peak with binding energy 531.6 eV corresponds to the OH group. The surface layer of NEG film consists of all the constituent metallic oxides and hydroxides. The OH peak of air exposed films disappears in the activation of the NEG

coatings. When the films exposed to atmosphere were thermally activated the oxygen 1s peak shifts from oxides of Ti, V and their lower oxides to O peak of Zr oxide and its sub-oxides. This intends that the most oxidized films are preferentially reduced to a metallic state during the activation at 180ºC for 2 hrs.

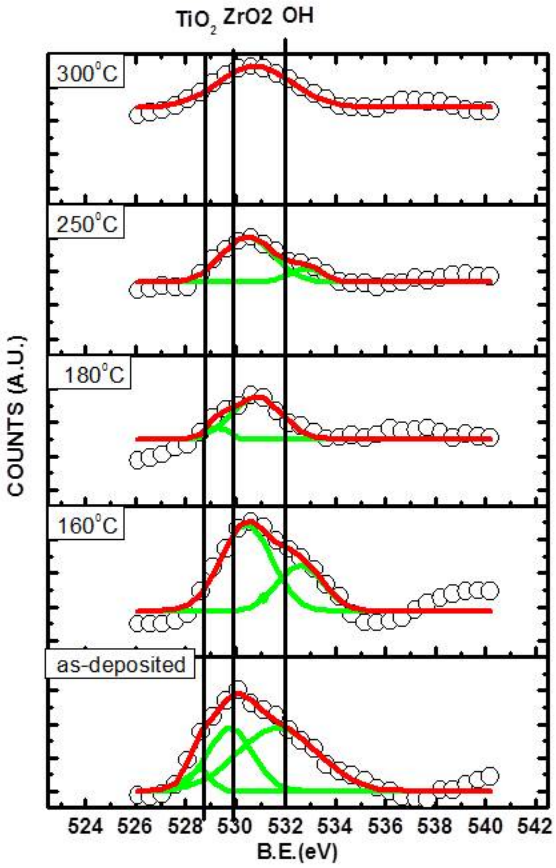

Fig. 4.8: XPS peak of O1s after heating at different temperatures.

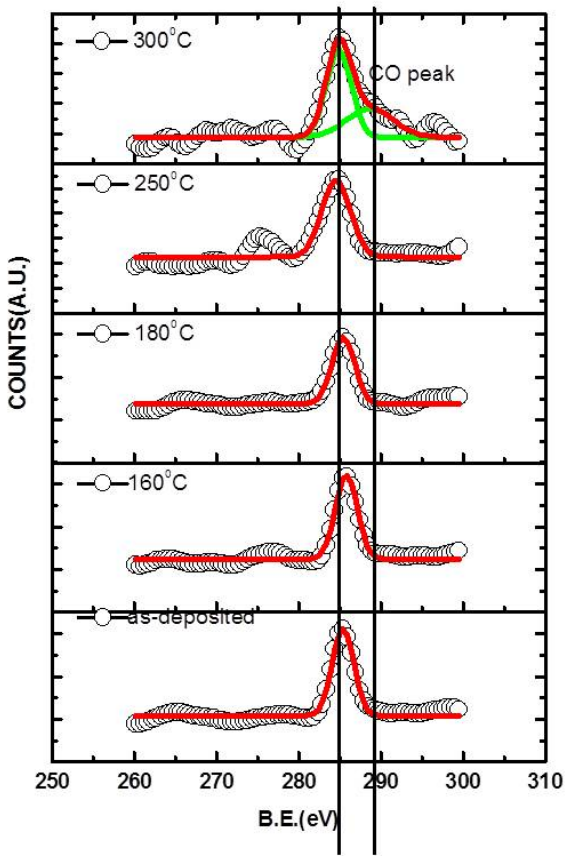

Fig. 4.9: XPS peak of C1s after heating at different temperatures.

Fig. 4.9 shows the series of C1s spectra of the NEG film of Ti-V-Zr after being exposed to air and then heated under UHV conditions. The spectrum of the film shows that the film is composed of C-C and C-O bonds, after the film was activated at 180°C for 2 hrs. However, carbides of Ti, V and Zr which are TiC, VC and ZrC, were found in the TiVZr film after the activation due to contamination of the samples during activation by CO, CO_2. The C-C bound was also found in the activated film and remains in the further air-exposure/activation cycle

[120]. It has been already shown that the carbides form in the subsurface region of the ZrV getter after a thermal activation of the film at 200°C [114, 115]. The formation of these metal carbides may be attributed to the low solubility (<2 at%.%) of carbon in Ti, V, Zr [121]. C. C. Li et. al. also confirmed the presence of metal-oxide in the film with Raman spectroscopy technique [120].

Fig. 4.10 shows a series of Zr 3d spectra of Ti-V-Zr film after heating it at different temperatures. For the air-exposed film, the B.E. of the Zr $3d_{5/2}$ peak is 183.2eV, corresponding to oxidized Zr (Zr^{4+}) [118]. However, the broad peak in the Zr3d spectra after heating to 180°C corresponds to metallic Zr^0 and mixed lower oxides Zr^{n+} (n<4). This increase in binding energy is due to the presence of a larger amount of Zr oxides on the surface of the Ti-V-Zr film.

In Fig. 4.11, $Ti2p_{3/2}$ and $Ti2p_{1/2}$ peaks of Ti-V-Zr shown with one air-exposure/activation cycles, are at 458.0 eV and 463.2eV, respectively corresponding to those of fully oxidized Ti^{4+}[124]. After the heating cycle at different temperatures, the peaks shifted to 454.5 eV corresponding to metallic state Ti^0 and also some reduced oxides of Ti^{n+}(n<4). The TiC was observed at a higher energy of 454.7eV.

Fig. 4.12 shows a series of V2p spectra of Ti-V-Zr film with air exposed/activation cycles. The air exposed films shows broad V2p spectra with centre at 516.2 eV, and composed of V_2O_5 and its sub oxides V^{+n} ($n \leq 5$). Compared to the V 2p broad peak of the air-exposed film, the sharp peak of the activated film has a lower binding energy of 512.5eV after heating to 180°C. It showed the residual presence of V carbides after the activation due to CO_2 and CO [118]. O1s and C1s spectra suggest that the VC will be found in the film after the activation also.

In Fig. 4.13**,** the activation study of the NEG coatings exhibit a decrease in the oxygen 1s peak intensity during the activation due to a reduction of the quantity of oxygen on the

surface in the form of surface oxides. The oxygen diffuses inside the bulk of the TiZrV filmat low temperature of 150ºCto180ºC due to a high diffusivity for oxygen of TiZrV produced by DC magnetron sputtering.

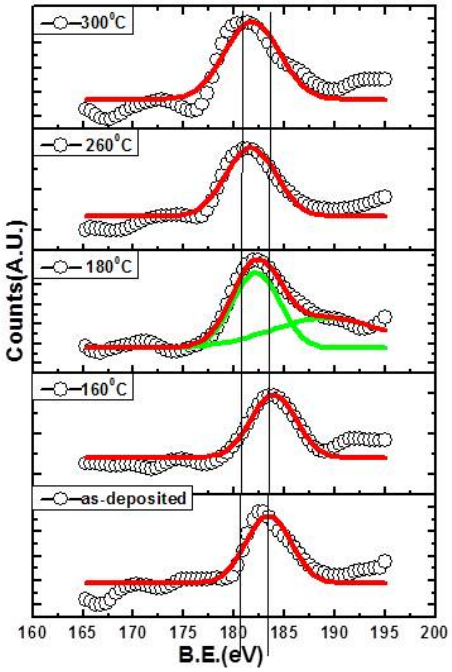

Fig. 4.10: XPS peak of Zr 3dshifted by almost 2.5eV.

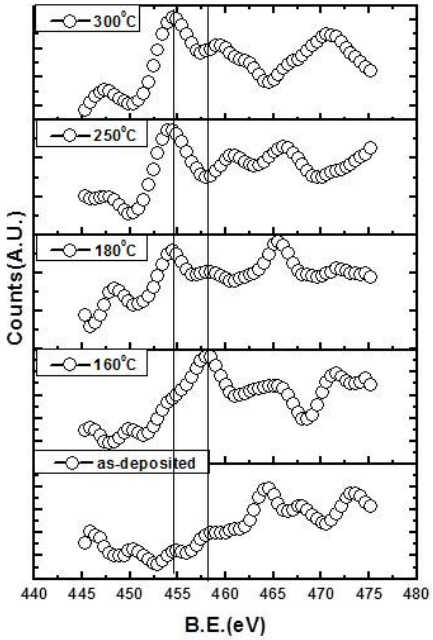

Fig. 4.11: XPS peak of Ti 3pshifted by almost 3.49 eV.

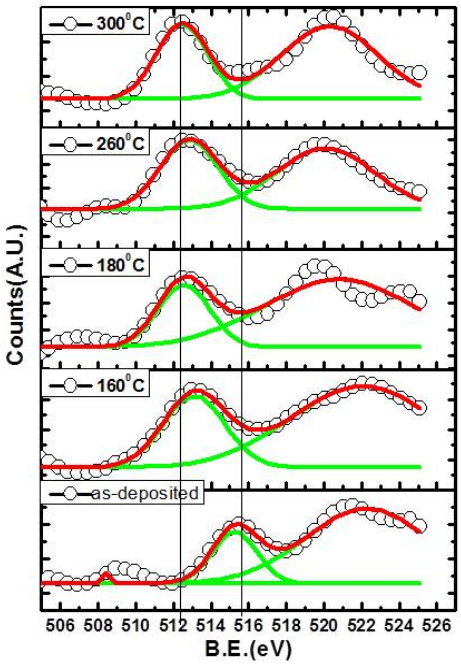

Fig. 4.12: XPS peak of V 3p shifted by almost 3.0 eV.

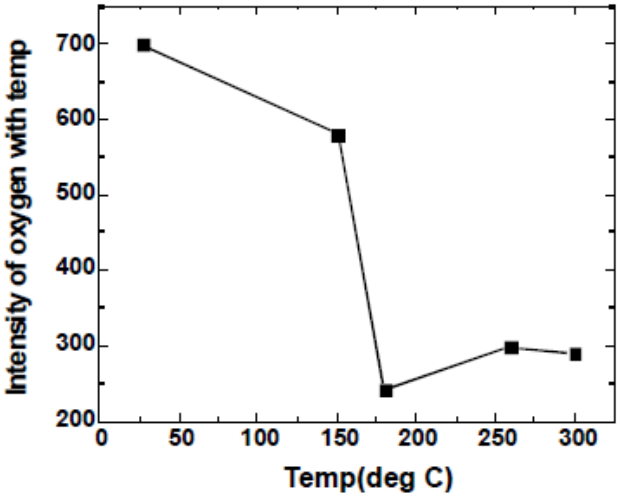

Fig. 4.13: Change in the intensity of oxygen on the NEG surface during activation.

4.4 Activation Studies of ternary alloy coating of NEG materials (Ti-Zr-Nb)

The thin films of NEG materials in ternary alloy form were prepared on SS304L substrate. The different combinations of group IVB (Ti, Zr, Hf) and V(V, Nb, Ta) were prepared on 300 x 250 x 0.2 mm^3 SS substrates using the cylindrical magnetron sputtering system in Ar environment. The target was made by twisting wires (400mm long and 1mm diameter) of three metals Ti, Nb and Zr in the ratio of 1:2:1. The target and substrate were cleaned thoroughly in an ultrasonic bath with soap solution, acetone and methanol. After the ultrasonic bath, both were dried by purging high speed dry nitrogen from the air gun. The sample cleaning is essential for good adhesion and purity of the deposited film. A base pressure of about $2x10^{-7}$mbar was achieved before the deposition and Ar pressure of 1.2 $x10^{-2}$ mbar was kept during deposition. The deposition time was 3 hrs with the deposition rate of about 3 Å/s. After the deposition, the film was exposed to air and then placed inside the XPS chamber with a load lock arrangement. The VG Scienta make sample manipulator facilitated with heating arrangement was used for the sequential study of activation. The sample was heated between 100°C and 300°C at rate of 5°C/min for two hours. During heating the pressure of the UHV chamber was increased from 10^{-9} mbar to 10^{-7} mbar. The sample was then cooled to the room temperature. XPS spectra of the sample were recorded using MgK_{α} X-ray source after heating at each temperature.

Fig. 4.14 shows the reduction of Zr3d peak that started from the oxide peak Zr^{4+} at 183 eV to Zr^{n+} ($n < 4$) after heating the sample to 250°C as the peak was broaden. After 300°C, the Zr3d peak was clearly reduced to 179 eV which is a metallic peak of Zr^0 of zirconium.

Fig. 4.15 shows the reduction of Nb3d peak from the oxide Nb^{5+} at 208eV to Nb^{n+}(n< 5) after heating to 250°C as the peak clearly shifted to 204 eV corresponding to metallic Nb^{0}. After 300°C the Nb3d peak clearly shows a split in to $3d_{5/2}$ and $3d_{3/2}$.

In Fig. 4.16 oxygen 1s peak is shown after heating the sample at different temperatures from 100°C to 300°C. The air exposed film showed a broad 1s peak of oxygen in the oxide form at 529.5 eV and 530 eV corresponding to oxides of Ti, Nb and oxide of Zr. The small peak at 532 eV corresponds to CO. After heating the sample the CO peak grows indicating the formation of carbon monoxide at the surface. This CO peak disappears after heating to 250°C and a single peak of oxygen remains. In Fig. 4.18, the intensity of the oxygen 1s peak in oxides also goes down after activation which reflects the dissolution of superficial surface oxides inside the bulk. To monitor the oxygen intensity, each curve is normalized. The activation temperature of this NEG coating (Ti-Nb-Zr) was found to be about 250°C. The full activation has been achieved at 300°C for 2 hrs of activation, as shown in Fig. 4.17.

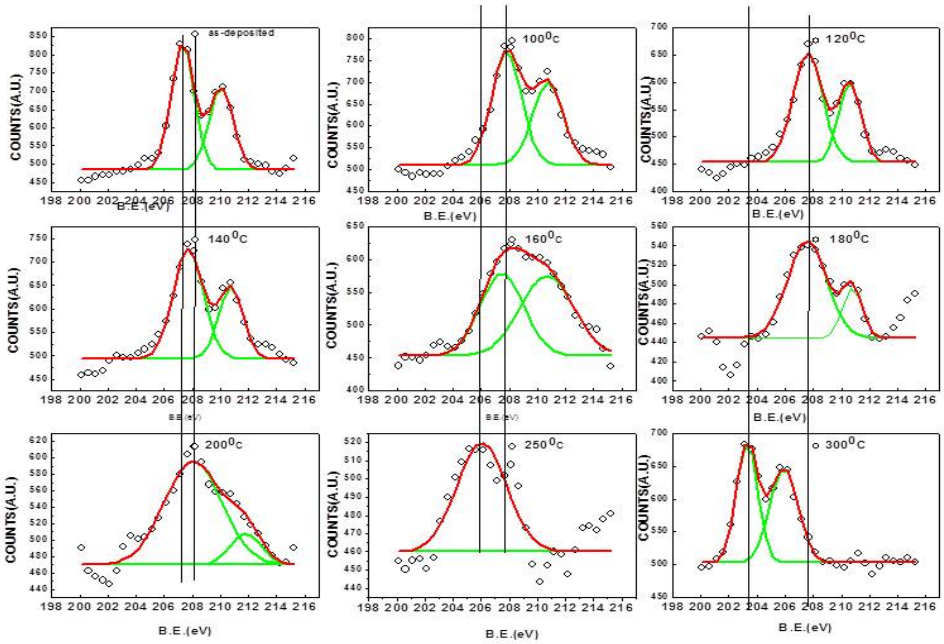

Fig. 4.14: XPS peak of $Nb3d_{5/2}$ after heating the Ti-Nb-Zr film at different temperatures.

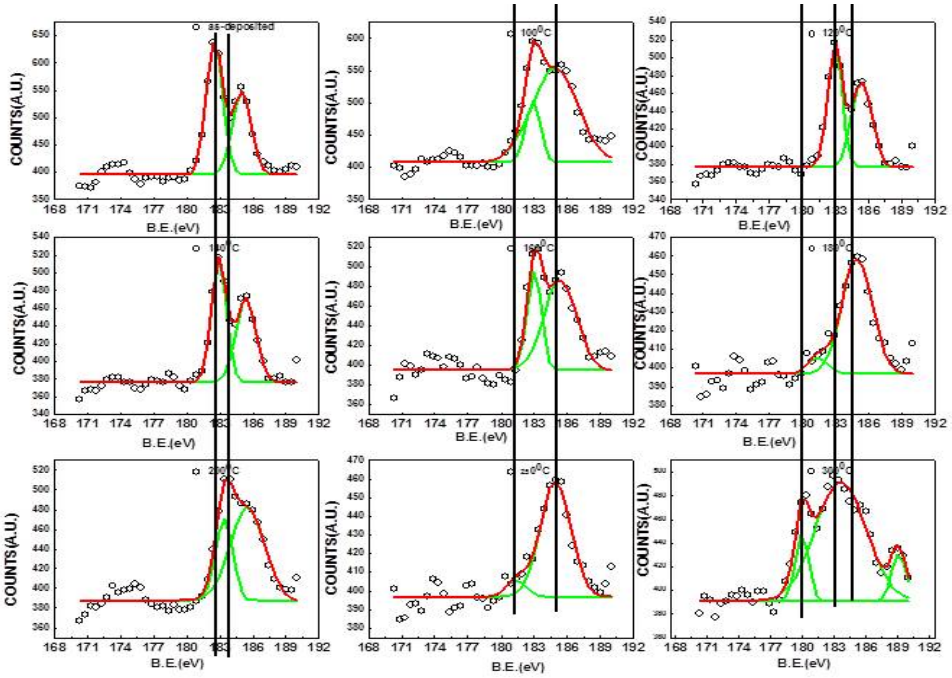

Fig. 4.15: XPS peak of $Zr3d_{5/2}$ after heating Ti-Nb-Zr film at different temperatures.

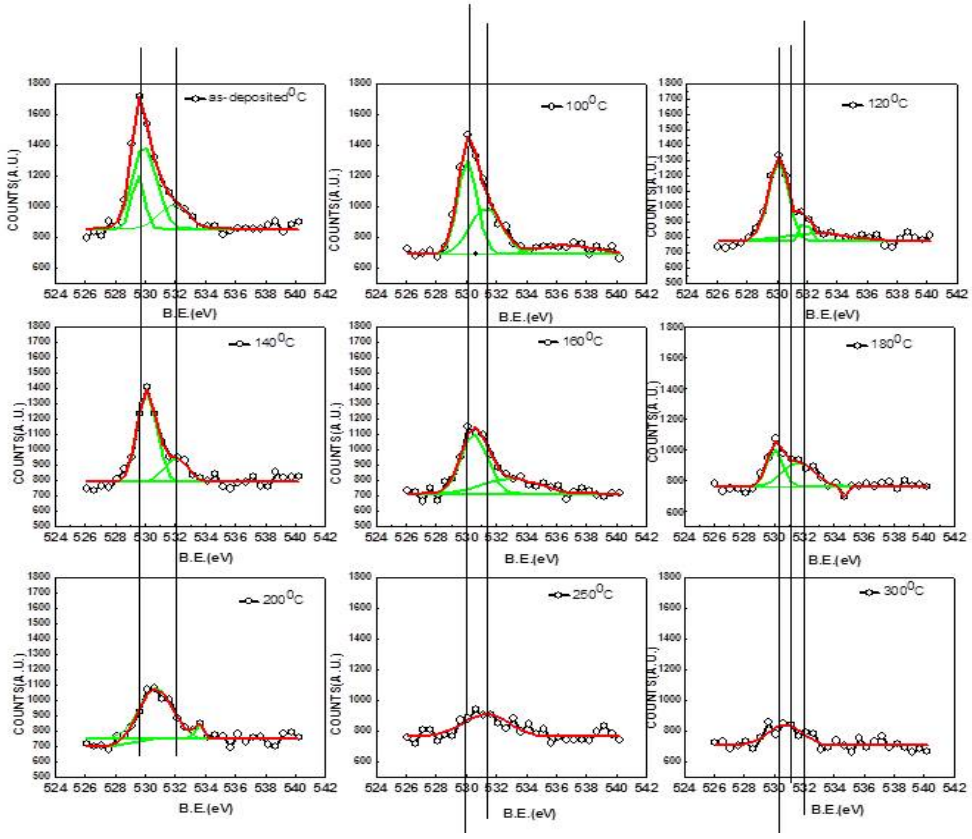

Fig. 4.16: XPS peak of O1safter heating the Ti-Nb-Zr film at different temperatures.

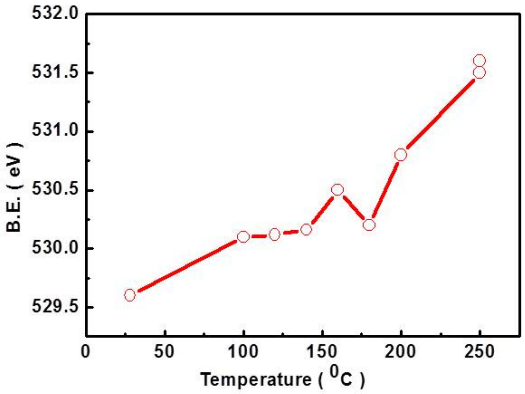

Fig. 4.17: B.E. Shift in 1S level of oxygen as a function of temperature.

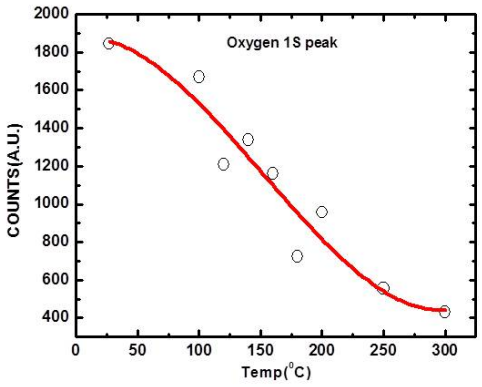

Fig. 4.18: Reduction in surface oxide peak after heating the film at different temperatures.

The surface plays an effective role for the adsorption of the residual reactive gases and adsorption sites are depended on the quality of the film surface. Presence of the more number of grain boundary leads to the bulk as well as surface diffusion. The columnar growth is preferable as it leads to increased number of adsorption sites. The ternary coating of Ti-Nb-Zr was studied by secondary ion mass spectra (SIMS) results are shown in Fig. 4.19, Fig. 4.20 and Fig. 4.21. The SIMS can also be used for the activation studies of the NEG coatings [122]. The spectra reflect the presence of all the constituents elements and their oxides in almost same chemical composition as revealed by EDAX measurements that are given in Table 4.1.

Table 4. 1. Atomic fractions of the Ti-Zr-Nb film deposited on SS304L.

	Atomic fraction(EDX)
Ti	20%
Nb	55 %
Zr	25%

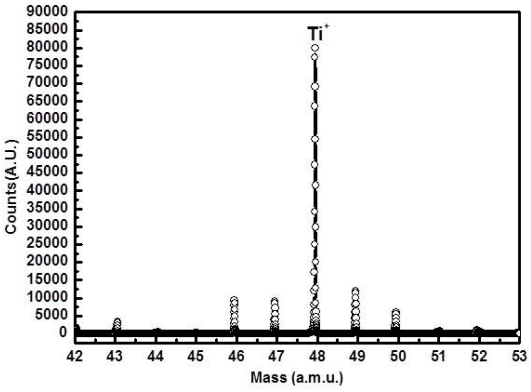

Fig. 4.19: SIMS spectrum of Ti^{+}.

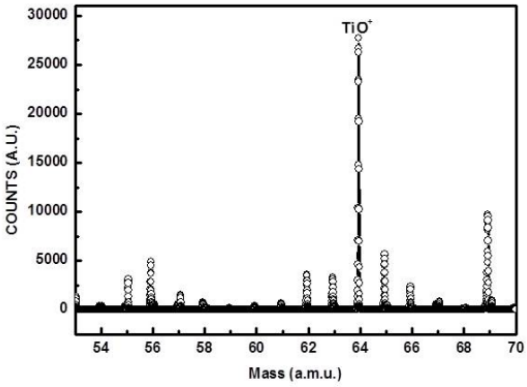

Fig. 4.20: SIMS spectrum of TiO^{+}.

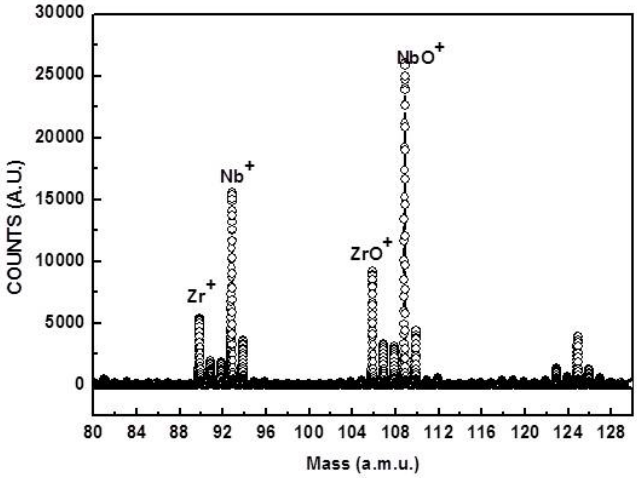

Fig.4.21: SIMS spectrum of Zr^{+} and Nb^{+} and their oxides.

4.5 Activation studies of different ternary Coatings of Ti-V-Zr prepared by DC-magnetron sputtering deposition (Ar pressure of 1.1 $X10^{-2}$ mbar)

Coatings of NEG of ternary alloy Ti-Zr-V were deposited using the DC magnetron sputtering technique at Ar pressure of 1.1 $X10^{-2}$ mbar. The activation studies of the coating were carried out using the XPS technique under UHV environment. The sample was heated in-situ to desired temperatures in the range from 140°C to 200°C for 3 hrs at a constant rate. The XPS spectra were recorded after every heating.

All elementary XPS peaks are shifted by about 2 eV to lower BE for Zr($3d_{5/2}$) as shown in Fig. 4.22.These lower B.E. peaks correspond to reduction of higher to lower Zr oxide states due to diffusion of oxygen present in the form of oxide from the surface in to the bulk during activation.

In Fig. 4.23, Ti ($2p_{3/2}$) peak of an as-deposited sample shifted by about 2 eV to a lower B.E. after heating the sample to 180°C. It corresponds to the lower oxide state of Ti on the surface that forms after the reduction of surface oxide due to the diffusion of oxygen atoms into the bulk during activation.

In Fig. 4.24 , vanadium($V2p_{3/2}$), B.E. peak shifted by about 4 eV to lower B.E. after heating at 180°C which is a metallic state of V. The vanadium is completely converted to metallic state after the diffusion of the all oxygen atoms in to the bulk.

The activation of the ternary Ti-V-Zr film was seen to proceed by the subsequent transition of oxides (TiO_2, ZrO_2 and V_2O_3) to lower suboxides of Ti, Zr and V mixed with metallic Ti, Zr and V phases after 180°C. This oxide reduction leads to the formation of active surface for CO and CO_2 to form carbides and oxide. H_2 dissociated over the active NEG surface and dissolved in the bulk as solid solution. These effects result in to the lowering of the pressure inside the chambers.

The XPS studies exhibited the lowest achievable activation temperature that lies in the range from160°C to 180°C for 3 hrs of heating of Ti-Zr-V films. The Ti-V-Zr films can be used as NEG to achieve lower pressures in extreme high vacuum applications.

In Fig. 4.25, the XPS of C1s peak shows that the film is composed of C-C and C-O bonds, after the film was activated at 180°C for 2 hrs. However, a residual presence of carbides of Ti, V and Zr were found in the TiVZr film after the activation. In Fig. 4.26 and Fig. 4.27**,** the SIMS spectra of as-deposited NEG film are given which show the presence of Ti^+, V^+. Zirconium is present in the form of both Zr^+ as well as ZrO^+ oxide.

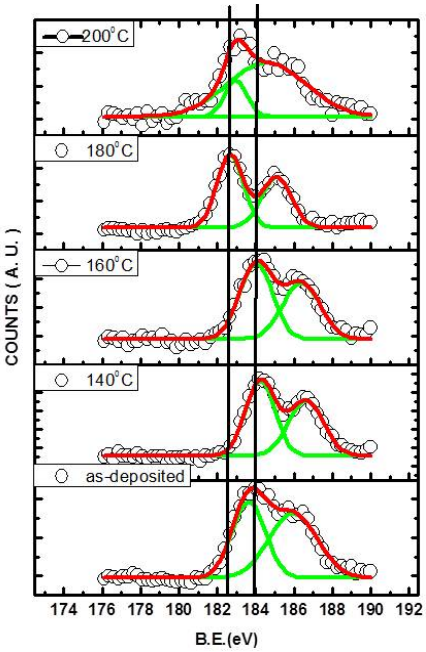

Fig. 4.22: XPS peak of Zr3d afterheating it at different temperatures.

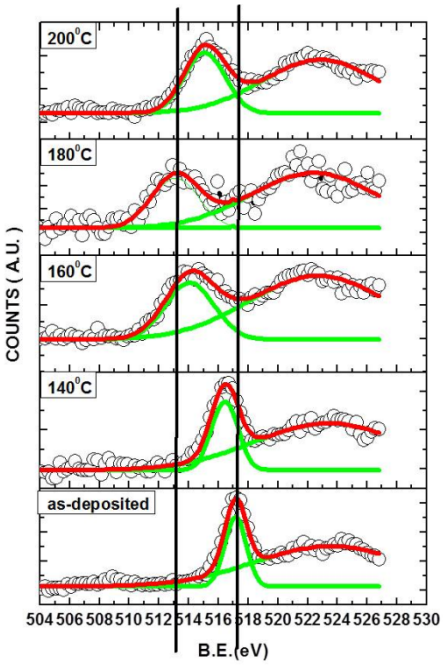

Fig. 4.23: XPS peak of Zr3d after heating it at different temperatures.

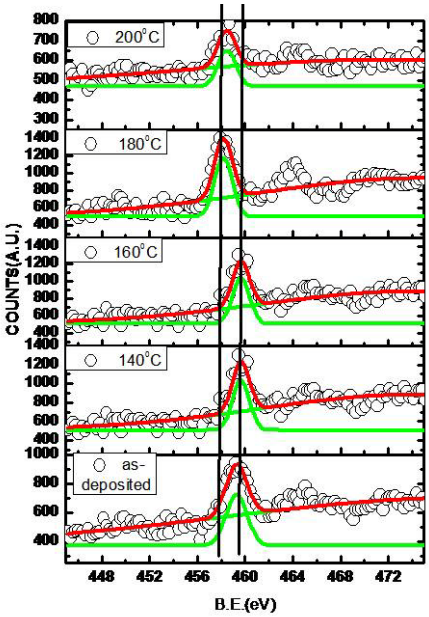

Fig. 4.24: XPS peak of Ti3p after heating it at different temperatures.

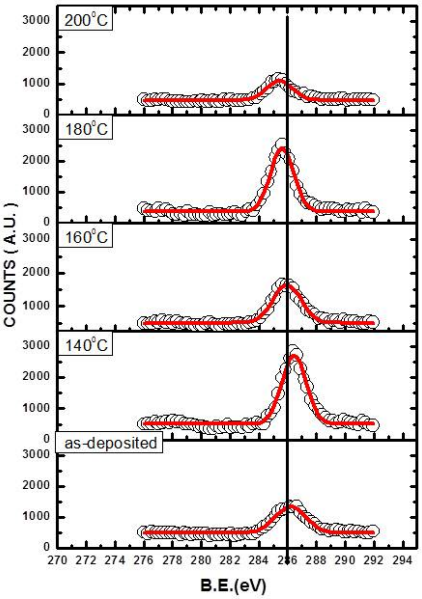

Fig. 4.25: XPS peak of C1s after heating it at different temperatures.

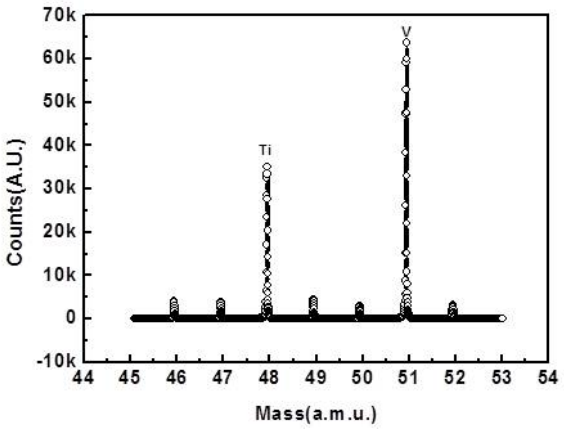

Fig. 4.26: SIMS spectra of as deposited film showing Ti^+ and V^+.

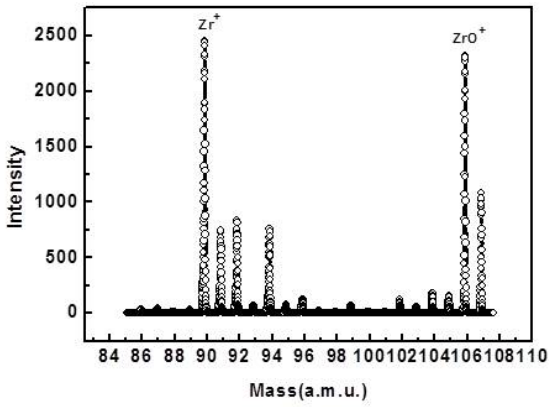

Fig. 4.27: SIMS spectra of as-deposited film showing Zr^+ and ZrO^+.

Fig. 4.28 shows the change in the B.E. energy of the oxygen 1s peak. The peak at 530.5 eV corresponds to oxygen in Zr oxide and its suboxides, and the broad peak at 530.2 eV is due to oxygen in oxides of Ti, V and their suboxides TiO, TiO_2, VO, V_2O_3, V_2O_5 etc. [119]. The oxygen peaks shift to higher energy after heating the film which correspond to lower oxide states of metals. The peak with binding energy 531.6 eV corresponds to the OH group. The surface layer of NEG film is constituted with metallic oxides and hydroxides. The OH peak of air exposed films disappears in the activation of the NEG coatings. When the films exposed to atmosphere were thermally activated the oxygen 1s peak shifts from oxides of Ti, V and their lower oxides states to O peak of Zr oxide and its sub-oxides. This indicates that most of the oxidized on the air-exposed films are preferentially reduced to a metallic state during the activation at 180ºC for 3 hrs.

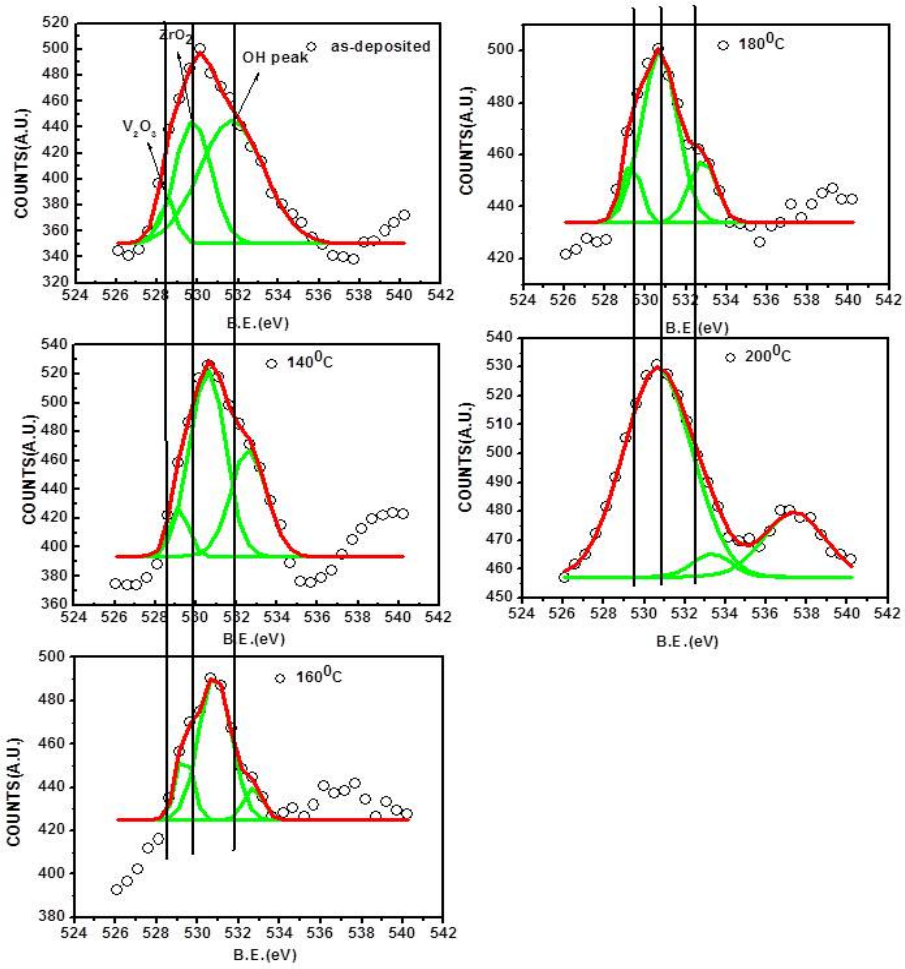

Fig. 4.28: XPS of O1s peak after heating at different temperatures.

4.6 Crystallographic structure of NEG coating of Ti-V-Zr

Crystalline structure information of the NEG coating was studiedusing the grazing incident X-ray diffraction. Samples of NEG films on SS304L were studied on an XRD beam line at Indus-2 synchrotron radiation source. This technique works on the Bragg's law as described in Chapter-3 [110, 123- 128]. For this purpose, a monochromatic beam of X-rays of 17 keV was used as a source. The beam of X-rays was made to incident at a grazing angle of 3º for maximum absorption by the thin film. The diffraction pattern shown in Fig. 4.29 revealed the peaks due to the film as well as those from the substrate. Using the JCPDF software, it was

found that the film had polycrystalline grains and all the constituent elements of the film were present in metallic as well as metal-oxide phases.

4.6.1 Calculation of crystallite size

Under the assumption of homogeneous single phase and of equiaxed crystal grains, Debye Scherrer formula can be applied to calculate the average crystallite size of the polycrystalline film [111, 130,131]. The formula is given as:

$$\omega = \frac{k.\lambda}{\Delta_c(2\Theta).\cos\Theta}$$

where, λ is the wavelength of the source, 2Θ is the angular position of the recorded peak in radians; and $\Delta_c(2\Theta)$ is the full width at half maximum of the peak at position 2Θ in radians, k is the shape factor which is (k = 0.94) for cubic crystalline and cubic geometry shape. The constant k has been determined that varies between 0.89 and 1.42 [131]. The calculated crystallite size is found to be 35 nm for a film with an average composition of $Ti_{21}V_{55}Zr_{24}$.

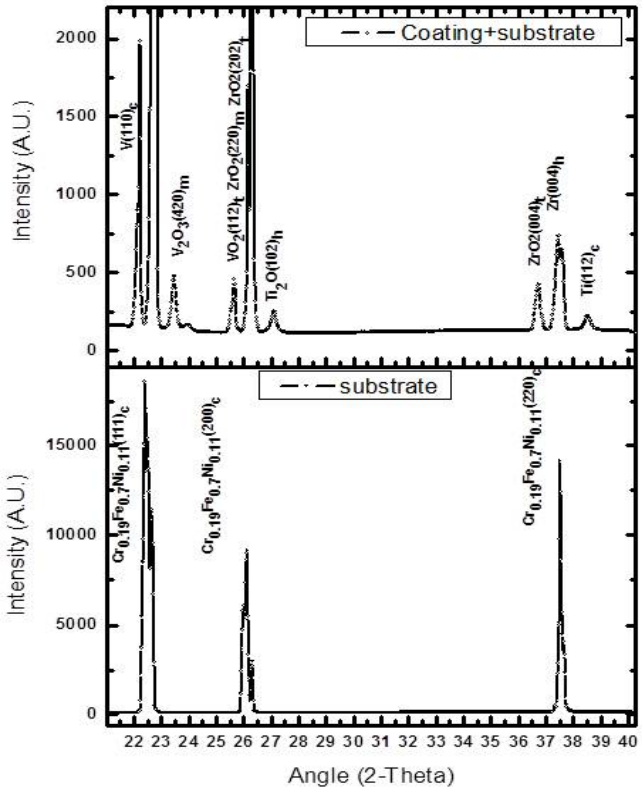

Fig. 4.29: XRD pattern of NEG thin film of Ti-Zr-V recorded using an XRD beamline on Indus-2 synchrotron radiation source.

4.7 Elemental composition of NEG thin films

4.7.1 Energy Dispersive X-ray spectroscopy (EDX)

In-depth stoichiometry of the NEG coatings was measured by EDX spectroscopy which works on the principle of the emission of characteristic X-ray radiation from the sample as a result of the bombardment of the primary beam of electrons on the samples. It is elaborately described in the references [123, 124]. The constituent elements are identified with the help of well known Mosley's law that relates the wavelength of the each observed spectral line to a specific element through the relationship:

$$\frac{1}{\lambda} = k.(Z - \sigma)^{\frac{1}{2}}$$

where, Z is the atomic number of the material, σ is the screening constant and k is the for each spectral line series, λ is the x-ray wavelength [125]. This technique is good for high Z materials and light elements are poorly detected due to their low fluorescent yield as well as their low energy of characteristic X-ray which is reabsorbed by the sample itself.

EDX measurement were performed in a Tescan Vega make Scanning Electron Microscope. The analyzed depth of the film is the order of 1000 nm. The evaluated thin film compositions of different NEG films which were studied in the present work are given in Table 4.2.

Table 4.2: Chemical composition of different NEG films by EDX spectra.

Preparation Technique	**NEG film**	**Stoichiometry**	**Activation temperature**
Vacuum Plasma Arc deposition	TiVZr	$Ti_{23}V_{47}Zr_{30}$	160ºC
DC-magnetron Sputtering	TiVZr	$Ti_{21}V_{55}Zr_{24}$	180ºC
DC-magnetron Sputtering	TiNbZr	$Ti_{20}Nb_{55}Zr_{25}$	250ºC
DC-magnetron Sputtering	TiVZr	$Ti_{28}V_{45}Zr_{27}$	180ºC
RF-magnetron Sputtering	TiVZr	$Ti_{48}V_{20}Zr_{32}$	200ºC

4.8 Summary and Conclusions

To summaries, the activation studies were carried out on different NEG coatings prepared by vacuum plasma arc deposition and DC-magnetron sputtering technique. The EDX measurements provided the chemical composition of the deposited films. The activation studies are done using in-situ XPS techniques under UHV conditions. The results revealed the activation temperatures of these NEG films range from 160ºC to 250ºC. The NEG film of chemical composition $Ti_{23}V_{47}Zr_{30}$ which was deposited by the vacuum plasma arc deposition using a composite target of Ti-V-Zr exhibited an activation temperature of 160ºC after 2 hrs of heating. The second NEG film of chemical composition $Ti_{20}Nb_{55}Zr_{25,}$ prepared by the DC-magnetron sputtering showed the activation temperature of 250ºC after 2 hrs of heating. The other NEG film of chemical composition $Ti_{28}V_{45}Zr_{27,}$ prepared by the DC-magnetron sputtering showed the activation temperature of 180ºC after 2 hrs of heating. The NEG film prepared by RF-sputtering and chemical composition $T_{48}V_{20}Zr_{32}$ showed the activation temperature of 200ºC. The GIXRD of the NEG film on SS304L substrate showed the polycrystalline nature of the film with an average grain size of 35 nm. The activation studies of the film using the XPS showed that the reduction of higher oxides of Ti, Zr and V into lower oxide and then to metallic, revealed the activation starts at 160ºC for this film.

CHAPTER 5

5.1 Production of XHV using NEG coated pipes

In this chapter we present the method of achieving extreme high vacuum (XHV, pressures below 10^{-11} mbar) and its measurement. Achievement of extreme high vacuum in a sealed off vacuum chamber require systematic efforts. The NEG films when coated on the inner walls of a chamber help in achieving XHV in a sealed off UHV system after activation at elevated temperatures. Pumping of a sealed-off UHV system with NEG coatings has a number of benefits over other methods, such as it does not require a continuous source of power, vibration free operation, absence of magnetic field, distributed pumping in longer and narrow pipes, etc.

Several coatings of NEG were prepared on SS304L substrate using the cylindrical type DC- magnetron sputtering system to study the pumping characteristics. In this chapter a few of these will be discussed. The NEG coatings were prepared on thoroughly cleaned SS304L substrate of size 300 mm x 250 mm x 200 μm which was folded cylindrically and placed inside the cylindrical chamber. The method of preparation of the film is given in Chapter 2. The Inner surface of SS304L vacuum pipes were also coated by the same method as discussed in detail in chapter 2. The deposition time was kept 4 hrs in each case.

5.1.1 Materials for XHV

The systems being utilized in XHV allocation need to take special care and very few materials are qualified for XHV such as stainless steel, aluminium, copper and glass in early demonstrations. These materials should have been properly conditioned and achieved from highly purified form of raw materials. These materials need to be pre-baked under vacuum environment and in-situ baked. For this type of application, it is needed to prepare highly cleaned and modified surfaces. Cleaning leads to reducing the contamination levels on the

surface to an acceptable level for applications in the vacuum environment. Surface modification can involve changing the surface morphology to be more rough or smooth, changing the chemical composition of the surfaces, changing the outgassing or outdiffusion properties of the material, or changing the mechanical properties of the surface. The material needs to take special care during welding and should be free from any gas trapping regions. The materials should be free from any kinds of permeation or pumping barriers on the vacuum systems.

5.1.2 Setup for XHV measurement

Fig. 5.1shows the schematic of the XHV set and Fig. 5.2 shows the photograph of the test set-up. In the XHV test set-up, all the vacuum pipes used were thoroughly degreased in an ultrasonic bath and later degassed in a vacuum furnace. To evacuate the chamber a Pfeiffer make turbo molecular pump combined with a dry root pump was connected via a right angle valve of size DN40. An indigenously developed triode sputter ion pump was connected to the NEG coated vacuum tube of size DN100 via a gate valve of size DN100. A vacuum tube of flange size DN100 and 300 mm long was sputtered coated using the cylindrical type magnetron sputtering with a ternary target of Ti/V/Zr in the ratio of (1:2:1). The deposition time of the film was 4 hrs and film thickness was approximately 1.5 μm which was achieved by measuring the thickness of small samples placed within the pipe at different locations. The other side of the NEG coated pipe was connected with a 6-way cross of size DN40. For measuring the 1000 mbar to 10^{-9} mbar pressure, a full range Pfeiffer make PBR type cold cathode gauge was connected. A Pfeiffer make Prisma residual gas analyzer was connected to the system for the measurement of partial pressures of gases. A Pfeiffer make Bayard Alpert (BA) PBR 260 gauge was all also connected to measure the pressure. Heating tape is wrapped around the surface to bake the system. During the baking of the test set up, NEG coated pipes were maintained at 100°C by air cooling of the pipe.

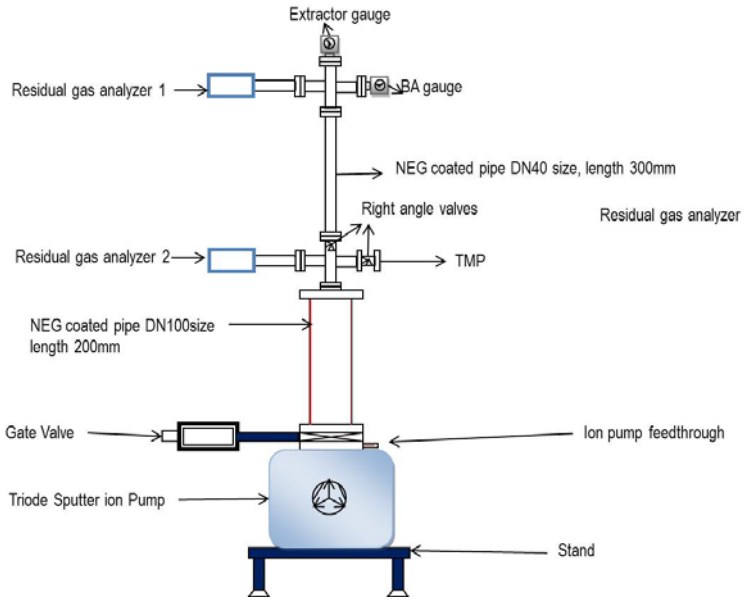

Fig. 5.1: Schematic of XHV test set-up showing the NEG coated pipe.

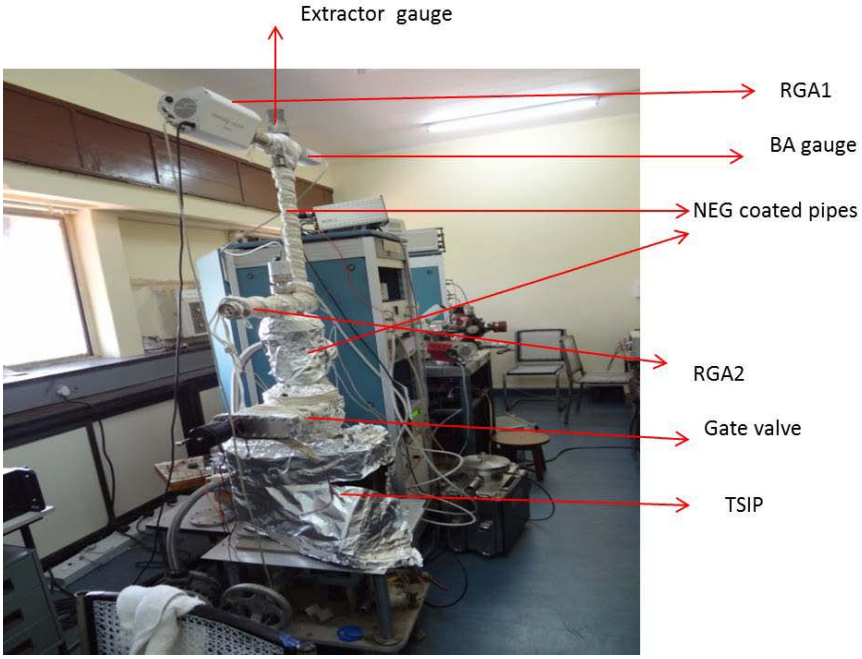

Fig. 5.2: Photograph of the XHV test set-up.

Temperature was controlled by a temperature controller and K-type thermocouple. A pressure of the order of $1x10^{-8}$ mbar was achieved without baking the system. The set-up was then baked continuously for 36 hrs and a total pressure of $1.6\ x10^{-10}$ mbar was achieved and measured using a residual gas analyzer (RGA) in SEM mode (1.5 kV) as shown in Fig. 5.3. The BA gauge was also in the range of lower 10^{-10} mbar. The measured pressure did not

reduce even after a continuous pumping with the TSIP for 3 days. The temperature of the NEG coated pipe was then raised to 180ºC at a rate of 5ºC/min. The temperature was kept 180ºC for 24 hrs and then the heater was switched off. During activation of the NEG pipe the pressure inside the chamber increased to 5 X 10^{-9} mbar (approx.) range. The BA gauge was turned off after the activation to avoid the extra heat source. After switching off the heater the pressure of the test set-up started to decrease and goes down to less than 5 X 10^{-12} after 10 hrs as shown in Fig. 5.4.

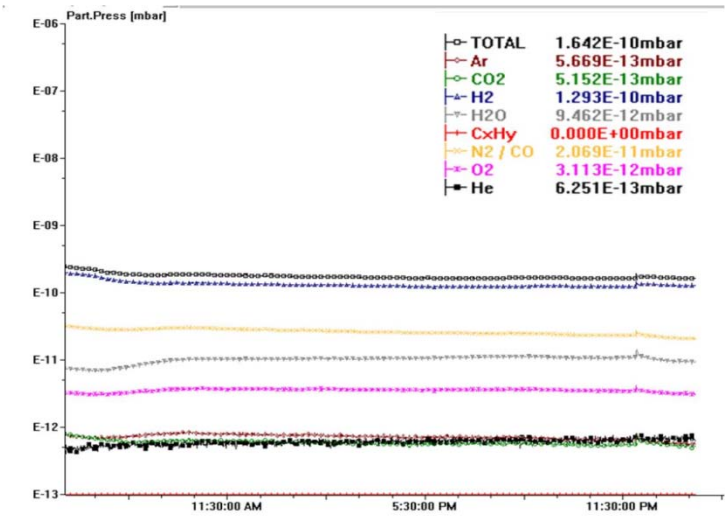

Fig. 5.3: RGA measurement showing an ultimate pressure without the activation of the NEG film.

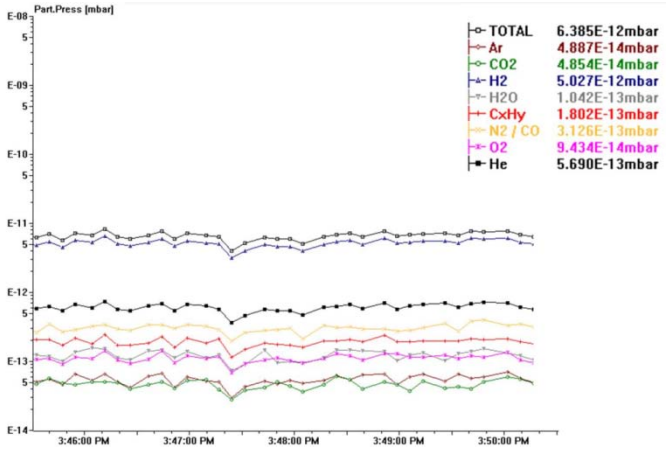

Fig. 5.4: Ultimate partial pressures measured after 24 hrs using the RGA after the activation of the NEG films.

5.2 Development of NEG pump with heating elements

An NEG pump was developed consisting of a strip of SS304L sputtered coated with a target of Ti-V-Zr. The size of the strip was 1200mm X 30mm X 200 µm and thickness of the coating was measured to be about 1.5µm. The photograph of the NEG pump is shown in Fig. 5.5. The strip was wound on ceramics tubes which were tightened with long bolts on a DN100 size flange. The strip was heated by passing a DC current of 10 A through a UHV compatible electrical feed-through. A K-type thermocouple was attached to the strip. An Allectra make UHV compatible feed-through was used for measuring the temperature of the strip as well as passing high current through it during the activation process. A high current/low voltage power supply was used for the resistive heating of the NEG strip.

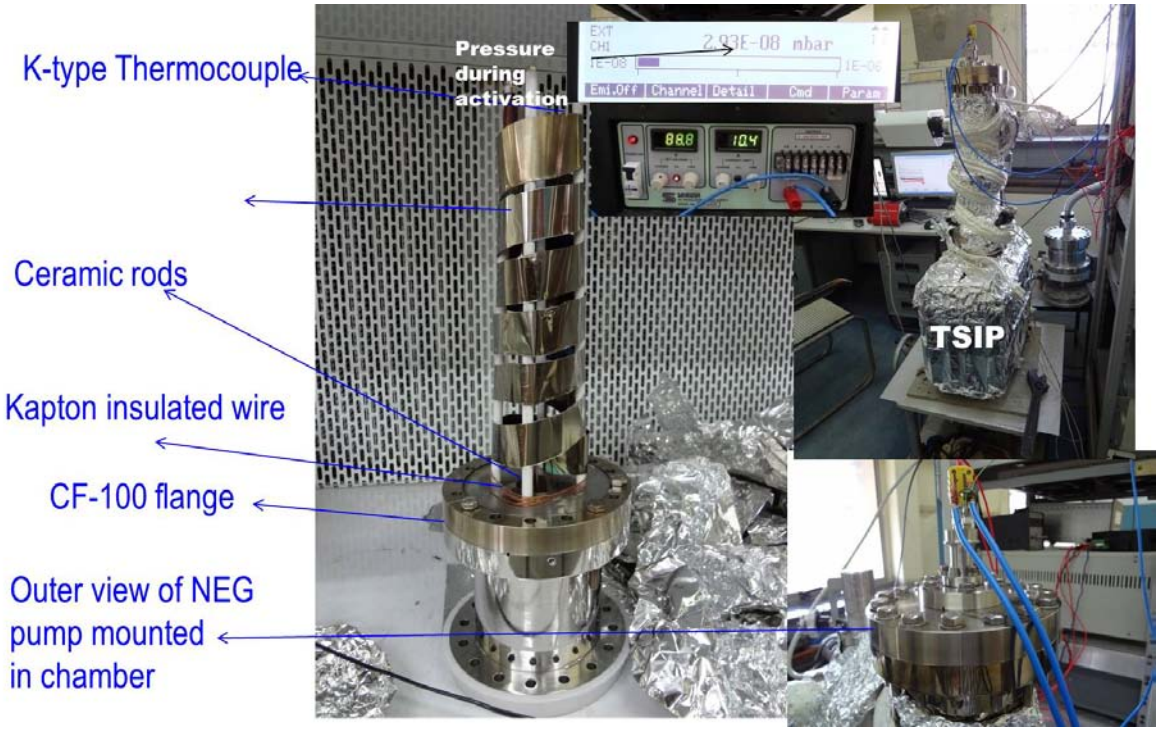

Fig. 5.5: NEG pump developed by using coating of Ti-Zr-V films coated on SS304L substrate.

5.2.1 Activation studies of NEG pump

The NEG pump was developed and tested by mounting in a specially designed NEG test set-up Fig 5.5. The activation of the NEG strip was achieved by passing a current of 10A from a dc-power supply directly through the strip. The current was slowly increased to 10 A to elevate the temperature up to 180ºC. The strip was kept at this temperature for 24 hrs. The evolution of partial pressure of $H_2$and total pressure in the XHV test set-up after activation of the NEG strip are shown in Fig. 5.6. The partial pressure of the H_2 as measured with the RGA was reduced to less than 10^{-13} mbar after 10 hours of activation of the NEG film at 180ºC. The total pressure inside the set up was less than 10^{-12} mbar. The partial pressure of CO_2 as measured by the RGA is been shown in Fig. 5.7. The partial pressure of CO_2 also decreased from 10^{-10} mbar to 10^{-14} mbar due to pumping action of the NEG strip after the activation.

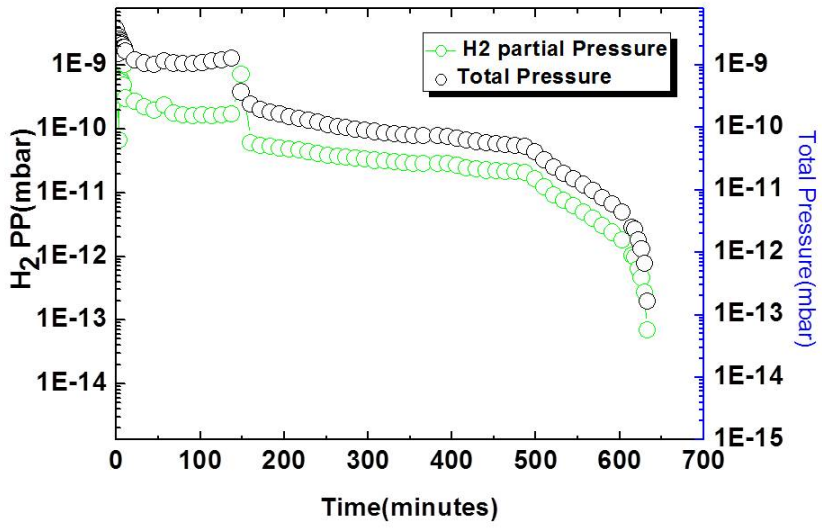

Fig. 5.6: Evolution of partial pressure of CO_2 and total pressure with time after activation.

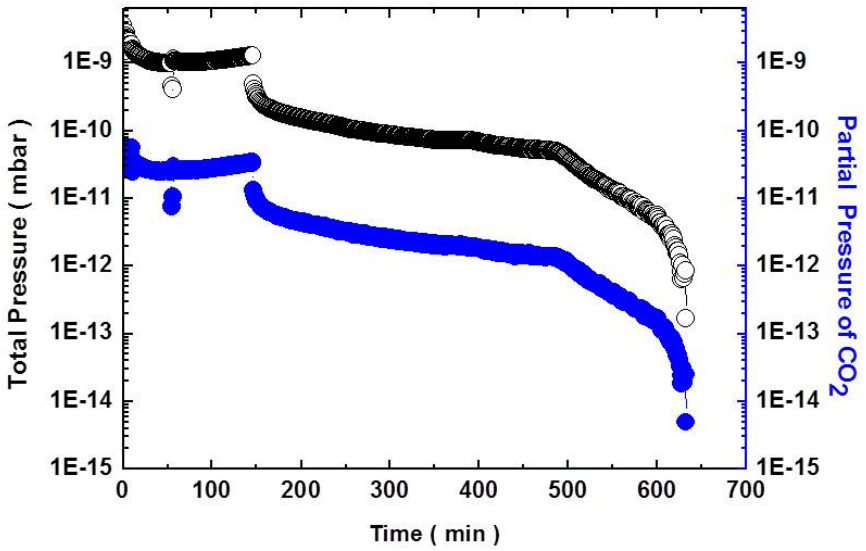

Fig. 5.7: Evolution of partial pressure of CO_2 and total pressure with time after activation.

5.2.2 Measurement of XHV

The NEG coated surfaces under the UHV conditions need to be activated. Oxygen present in the form of superficial oxide over the films which is formed after exposing it to atmosphere is progressively reduced due to diffusion inside the bulk during the activation and the surface starts gettering/sorbing the residual gas species which is referred as the pumping action of the getter materials. During the activation of the NEG, it needs to be heated either externally or internally. Activation is completed when the oxygen surface content reaches a minimum and pumping speed its maximum value.

The XHV measurement systems require special care to choose proper materials and their conditioning. All the measurement system should be properly degassed to avoid the untimely outgassing from the filament. In our XHV test set-up, residual gas analyzer is used to measure the partial pressure as well as total pressure of the system in the XHV range.

5.3 Measurement of Secondary electron Yield (SEY)

When electrically charged particles (primary electrons) of sufficiently high kinetic energy strike a solid surface, the solid surface emits electrons. The emitted electrons are called secondary electrons (SE). The Secondary Electron Yield (SEY) is defined as the number of all the SE which are emitted per PE and as given by eq.(1),It is a three step process that includes the penetration of the PE into the target during which they produce SE through inelastic collisions with target materials, the next step is the transport of the generated SE to the surface, the third step is the escape of the SE through the surface into the vacuum. The secondary electron emission is a surface process and it is influenced by slight modifications of materials outer layers [132]. The mean escape depth of SE is of the order of 3 -5 nm [133] which is similar to the probing depth of XPS and AES. In electron spectroscopy, the electrons that contribute to the characteristic peak have a kinetic energy of more than 100 eV while vast majority of SE have energy of only a few eV. As a consequence the SE are work function influenced electrons which is not the case in AES or XPS. When measuring SEY, it is important to actually measure the yield of the material itself and not the yield from the contaminants that reside on the surface e.g. adsorbed gases and oxidation layers which can be removed by surface heating.

Secondary electron yield and surface outgassing are of special concern for accelerators and experiments undergo photo-electro diffraction [134]. Surfaces with greater secondary electron yield δ are more prone to provide multi-pacting or electron cloud instability [135]. This instability is excited by the interaction between successive charged bunches and secondary electron cloud around them multiplicatively generated by the interaction of charged bunches with the walls of vacuum pipes [136, 137]. One way to prevent these situations is to use inner surfaces with a low secondary electron yield. We have investigated the similar situation in our lab by investigating the effect of interaction of

electron beam of energy up to 2.5 keV on coated surfaces after heating at different temperatures. As the life-time of the accelerators also depends on the presence of residual gas molecules, the surfaces with high out gassing are culprit and are obstacle to increase the beam lifetime as residual molecules such as H_2 diffuses from the material due to concentration gradient. The residual molecules can also come out from the surface due to photon induced desorption [138]. These residual molecules not only act adversely with the main charge particle beams, but also reduce the life time of the beam. One of the effective solutions to this problem is to coat the whole inner wall of the vacuum pipe or chamber with non-evaporable getter (NEG) materials with an appropriate composition [139].

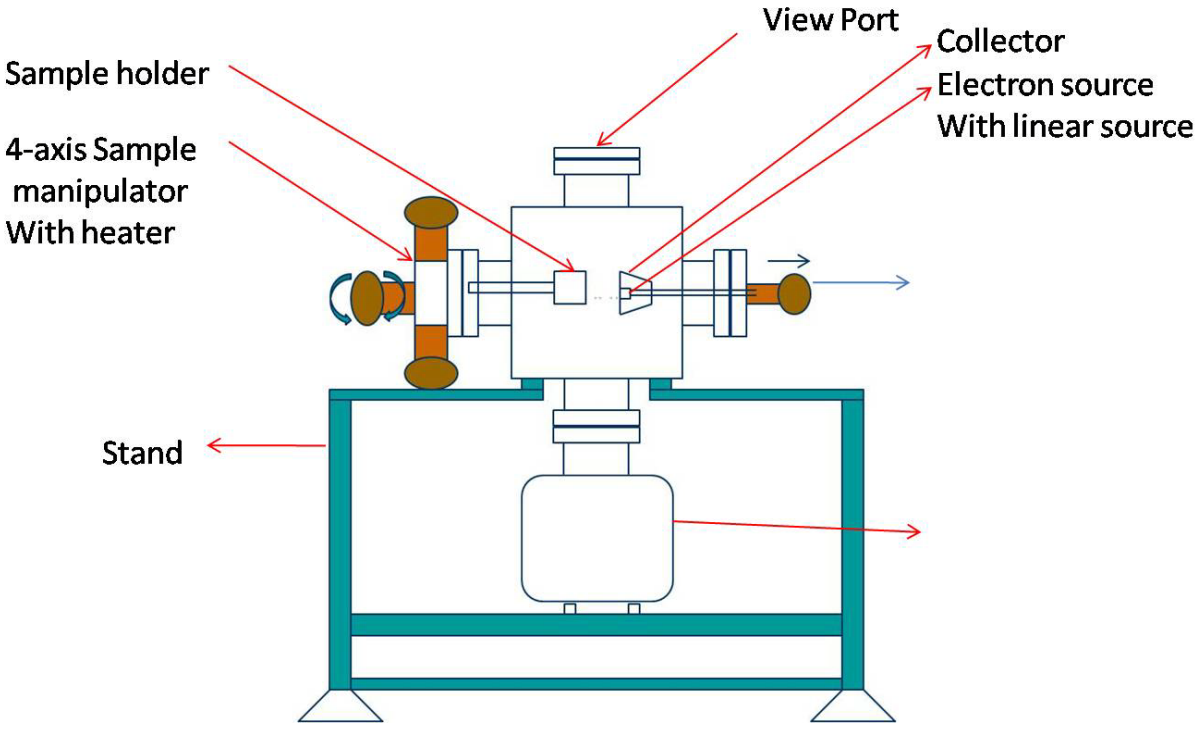

Fig. 5.8: Schematic of secondary electron yield measurement system.

5.3.1 Development of SEY Measurement System

Secondary electron yield measurement was done with an indigenously developed electron gun facilitated with inbuilt collector to collect the secondary electrons from the samples with increasing electron energy (0 -2.5keV). A current meter (Keithley make 6485) was utilized to

monitor the sample and scattered current. Schematic and actual photograph of the SEY measurement system has been shown in Fig. 5.8 and Fig. 5.9, respectively. These data basically provide secondary electron yield δ for the NEG coated samples which are calculated according to eq. (1), using the measured values of scattered and sample currents after heating the film at different temperatures. The collector voltage was set to 20V floating with theground and base pressure was < 10^{-9} mbar. The samples were prepared by sputtering technique as discussed in Chapter 2 and mounted on a 4-axes sample manipulator which is also facilitated with heating arrangements for the sample. The measurements were taken after heating the sample to different temperatures of 100ºC, 140ºC and 180ºC for two hours.

$$SEY(\delta) = \frac{I_c}{I_c + I_s} \qquad ----(1)$$

Where *Ic* is the Collector current and *Is* is the sample current.

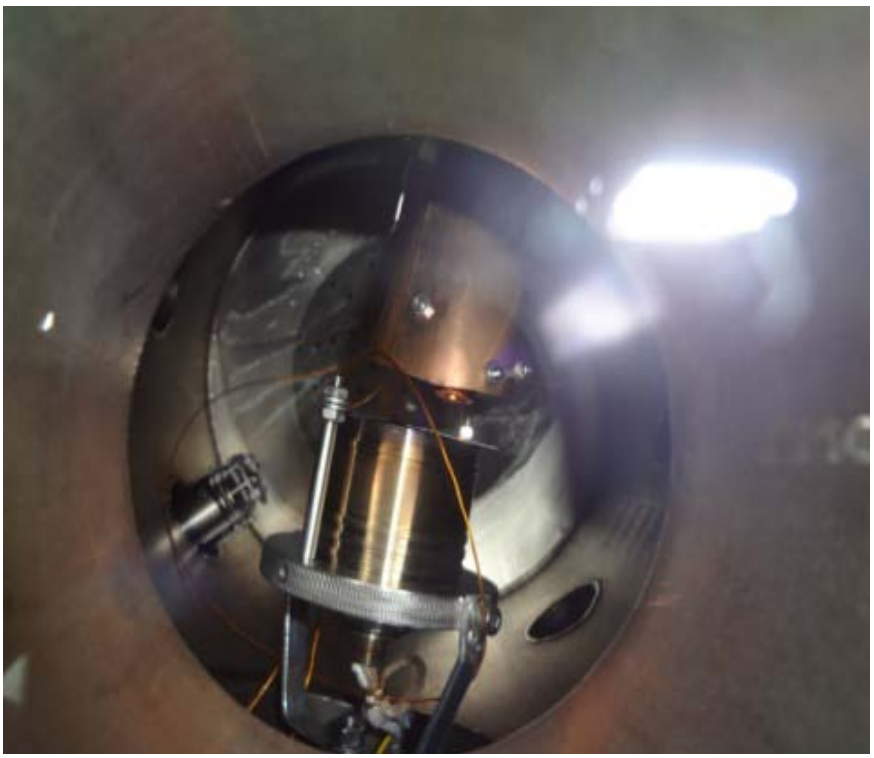

Fig. 5.9: Inside view of the secondary electron measurement set-up.

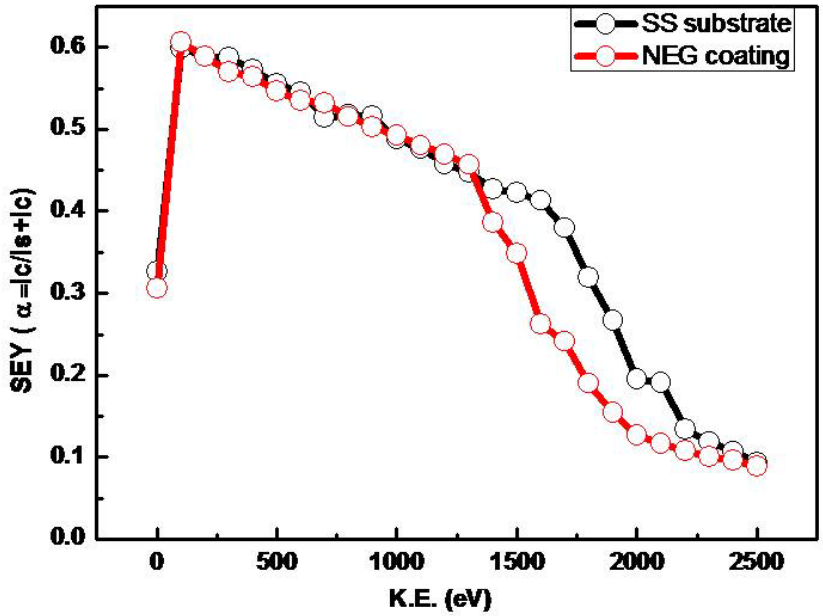

Fig. 5.10: Secondary Electron Yield (δ) as a function of K.E. for substrate and NEG coating.

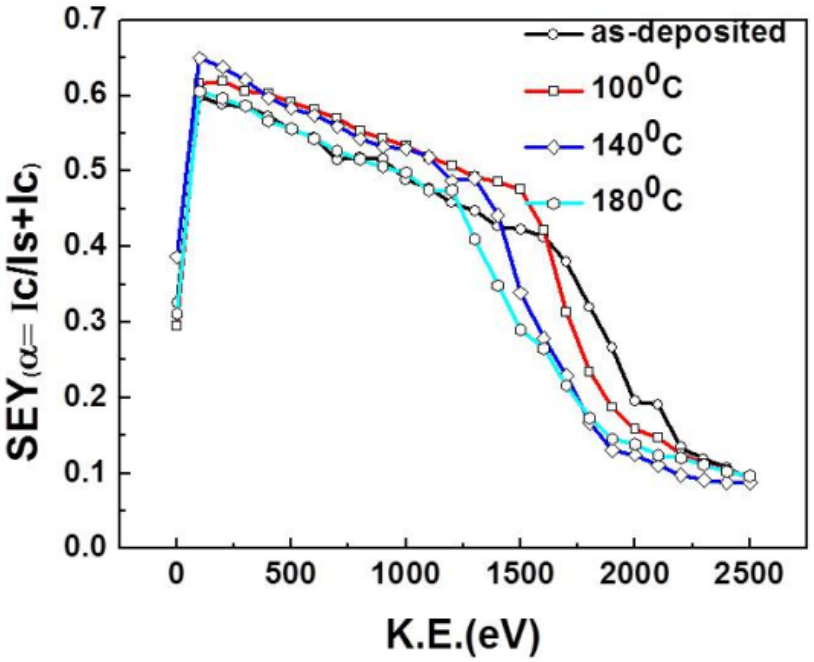

Fig. 5.11: Secondary Electron Yield (δ) as a function of K.E. for NEG coating maintained at different temperatures.

5.3.2 Results of SEY measurement of NEG thin film on SS304L substrate

A complete quantitative description of the SE emission process consists of the SEY versus PE spectrum and the energy distribution spectrum of the emitted SE at each PE energy as shown in Fig. 5.10 which shows the reduction of secondary electron yield of NEG coating on SS304L. The reduction of SEY of NEG coating after heating it to different temperature has been also shown in Fig. 5.11. The maximum reduction in the secondary electron yield of the NEG coated film on SS304L comes after heating the film at 180ºC for two hrs even at 1 keV of primary electron energy and characteristic of the results are similar to the result published by the group CERN group [140]. This is due to dissolution of surface oxides in the bulk after the heating. The SEY measurement shows a decrease in the SEY with increasing temperature of the coated surfaces which results in lowering the multi-pacting effect in accelerators.

5.4 Summary and Conclusions

A test set-up for the XHV was developed which consists of different vacuum pumps, vacuum gauges, UHV valves. The NEG coated pipe used to create XHV by pumping the different residual gases (H_2, CO_2, H_2O, N_2, CO) was also integrated in the set-up. The activation of the pipe was done by elevating the temperature of the NEG coated pipe to 180ºC. The NEG coated pipe was kept at this temperature for about 24 hrs. After the activation, a pressure of the order of 5 $X10^{-12}$ mbar was achieved which was measured by using the RGA. The evolution of partial pressures of H_2 down to 10^{-13} mbar and 10^{-14} for CO_2 which are pumped by the NEG coating are reported. A low secondary yield of the NEG coatings which is the additional benefit of NEG coated surfaces has been discussed. The secondary electron yield exhibits the multi-pacting effect in the accelerators which adversely affects the main beam. The lowering of the SEY of NEG coating as compared to SS has been demonstrated. It has been also achieved the lowering of NEG coating after activation.

CHAPTER 6

6.1 Summary and Conclusions

Development of the coatings of NEG materials in ternary alloy form has been carried out using the physical vapour deposition. The NEG coating has tremendous uses in the area of vacuum applications, production of very low secondary yield surfaces and surfaces with low photo-desorption yield. Systematic description of different types of NEG materials which have been developed till now are described in the thesis. The industries which are supplying NEG materials are few and they are using alloy St707 and St101 in the form of thick getter coatings that activate at relatively higher temperatures. In this thesis work on thin films of materials to develop NEG coatings with lower thicknesses and substantially low activation temperatures has been reported. These coatings deposited on SS substrates have been used in developing NEG pumps to efficiently create XHV conditions (pressures less than 10^{-12} mbar) in chambers.

The first ternary alloy film in this thesis was deposited by using a composite target of Ti-V-Zr on small size substrates (10mm X 10mm) of SS304L. The deposition was done using vacuum arc plasma at very high temperatures. Later, cylindrical type DC-magnetron sputtering technique was developed to deposit NEG films on inner surface of pipes of different sizes as well as big surface area substrates. This coating system was proved useful to coat narrow size tubes and longer pipes. Coatings of various chemical combinations on different substrates using various combinations of targets were deposited using the system.

The surface morphology that played a very important role in terms of adsorption sites and grain boundaries have been investigated and optimized to obtain desirable lower activation temperatures of the NEG films. The morphological study of films coated on different materials such as Cu, SS304 and Si using the same deposition parameters was done using FESEM technique revealed the nano-size grains on the film surface. A smaller size has

ensured a large number of grain boundaries on the film surface that are beneficial during the surface diffusion at elevated temperatures. The surface roughness had an important contribution in terms of increasing the actual surface area of the film. It also played very essential role as pores increase the trapping probability of the gaseous species by re-scattering from the walls of the pores. Activation studies on several compositions of coatings were conducted using the X-ray Photo electron spectroscopy. It was a sequential study carried over several days to take the XPS spectrum after heating the films in-situ under UHV conditions at different temperatures. The films were analyzed by the XPS technique at room temperature after each heating cycle. Several compositions in the ternary chemical combination of IVB (Ti, Zr, Hf) and V(V, Nb, Ta) have been investigated. The activation results of these coatings were discussed in Chapter 4.

Key features of the thesis:

- The first ternary alloy coating of NEG materials $Ti_{23}Zr_{47}V_{30}$ was deposited by a Vacuum plasma arc using a composite target of TiVZr on 10 x 10mm^2 SS304L substrates. The activation studies of the film using the XPS showed that the reduction of higher oxides of Ti, Zr and V into lower oxide and then to metallic, revealed the activation starts at 160ºC for this film.
- The ternary coating of chemical composition $Ti_{21}V_{55}Zr_{24}$ was deposited by cylindrical type DC-magnetron sputtering system using a target of Ti/V/Zr in twisted form on 300 X 200 mm^2 size substrate. The sequential activation studies of small portion of these coatings after heating at different temperatures were done by the XPS which revealed the activation temperature as 180ºC.
- The ternary alloy coating of chemical composition $Ti_{20}Nb_{55}Zr_{25}$ which was deposited by sputtering technique using different target. These coatings were activated after heating at temperature of 250ºC.

- Another ternary film of chemical composition $Ti_{28}V_{45}Zr_{27}$ was deposited by sputtering using different ratio of target materials. The activation studies of this coating by XPS revealed that film is activated after heating at 180ºC.
- NEG films of chemical composition of $Ti_{48}V_{20}Zr_{32}$were also deposited using a planar RF-sputtering technique. The activation studies of these coating by the XPS revealed the activation temperature as 200ºC.
- The GIXRD measurement of NEG coatings is done on an XRD beam line at a synchrotron radiation source. The XRD pattern showed the polycrystalline nature of the film. The average grain size calculated by Scherrer formula was about 35 nm.
- The chemical composition of all the films was studied using the EDX measurements and was reported in the Table 4.2 in Chapter 4.

The pumping action/sorption of the NEG films was attempted in an XHV test set-up which as described in Chapter 5. The inner surfaces of UHV compatible pipes of different diameters were deposited using the cylindrical magnetron sputtering using ternary inter-twisted target of getter materials. The pipe was integrated to the XHV test set-up to evaluate the pumping action of the NEG coatings. The NEG pump has been developed using NEG ribbon of size 1200 mm X 30 mm X 200 µm. An ultimate pressure below $1x10^{-12}$ (approx.) mbar has been achieved using this pump as discussed in Chapter 5. These coating have other benefits that may be useful in the energy accelerators and synchrotrons such as low secondary electron emission, low photo-desorption. The secondary electron measurement set-up has been developed and secondary electron yield of these coatings after heating at different temperature has been reported.The conclusions are given below.

- The ultimate pressure of 2 X 10^{-10} mbar (approx.) was achieved activation without NEG activation in the test set-up by continuous pumping using TSIP. This was measured by the total pressure of RGA.
- During the baking of the test set-up, the NEG coated pipe was kept at 100ºC with air cooling. Activation of the pipe was done for 24 hrs. The ultimate pressure of 5 X 10^{-12} mbar (approx.) was achieved after 10 hours of activation. During the activation only NEG coated chamber was heated externally at about 190ºC.
- Activation of the NEG pump that had an inbuilt heating arrangement and a thermocouple was deployed to create XHV in the test set-up. After activation of the pump the total ultimate pressure below 1 X 10^{-12} mbar (approx.) could be achieved. The evolution of partial pressures of H_2 and CO_2 has been reported in Chapter 5.
- The secondary electron yield (SEY) measurement of NEG coated samples was done after heating the samples at different temperatures. The calculated SEY from the measured values of scattered and sample currents, it is confirmed that the SEY yield is reduced due sorption of the surface oxide inside the bulk.

Future Scope

The development of new NEG coatings which can be activated at temperatures lower than 150ºC is still an open area of research. The development of such low temperature NEG coatings which could be fully activated with less number of hours will be useful in many applications. In order to develop such NEG films, it is suggested that quaternary and higher multi-component compositions of suitable elements may be attempted to form alloys. The deposition parameters should be such that to deposit films with a large effective surface area as well as increased number of grain boundaries.

BIBILIOGRAPHY

Chapter 1

[1]. P Della Porta, Vacuum, 4, 1954, 284.

[2]. J J B Fransen and H J R Perdijk, Vacuum, 10, 1960, 199.

[3]. M D Malev, Vacuum, 23, 1973, 359.

[4]. E. Fromm and H. Uchida, *J. Less-Common Met*. 131, 1 (1987).

[5]. J.M. Lafferty, "Foundations of Vacuum Science and Technology",John Wiley & Sons, Inc. (US), (1998) p.272.

[6]. P. Della Porta, in *Advances in Electron Tube Techniques*, edited by D. Slater, Proceedings of the Sixth National Conference, Sept. 1962 (Macmillan, New York, 1963).

[7]. C. Benvenuti and J. C. Decroux, *Proceedings of the 7th International Vacuum Congress and Jrd International Conference on Solid Surfaces* (International Atomic Energy Agency, Vienna, 1977), p. 85.

[8]. J. L. Cecchi, R. J. Knize, H. F. Dylla, R. J. Fonck, D. K. Owens, and J. J. Sredniawski, J. NucL Mater. 111&112, 305 (1982).

[9]. J. J. Reilly, in *Hydrogen: Its Technology and Implications, Transmission and Storage of Hydrogen,* edited by K. E. Cox and K. D. Williamson, Jr.(CRC, Boca Raton, 1977), Vol. II.

[10]. L. Rosai and M. Borghi, J. Vac. Sci. TechnoL 11, 347 (1974).

[11]. K. Ichimura, N. Inoue, K. Watanabe, T. Takeuchi, J. Vac. Sci. Technol.A 2 (3) (1984) 1341.

[12]. S. Dushman (revised by V. L. Stout and T. A. Vanderslice), in Scientific Foundations of Vacuum Technique, edited by J. M. Lafferty (Wiley, NewYork, 1962), p. 622.

[13]. B Kindl and E Rabusin, SupplNuovoCimento, 5, 1967, 36.

[14]. M. Sjöström, E. Wallén, M. Eriksson, and L.-J. Lindgren, Nucl. Instrum. Methods Phys. Res. A **601**, 229 (2009).

[15]. R..D. Penzhorn, M. Deviller, M. Sirch, J. Nucl. Mater. 170 (1990).

[16]. C Benvenuti, P Chiggiato, F Cicoira and V Ruzinov, Vacuum 50(1998) 57-63.

[17]. R.K.Sharma, N.Mithal, ShahshwatiSen, Jagannath, K.G.Bhushan, S.C. Gadkari, J.V. Yakhmi and V.C. Sahni, *Bulletin of Indian vacuum Society, Vol.9(2), 2006, pp. 11-14*, [2006].

[18]. R.K. Sharma, Jagannath, S. Bhattacharya, S.C. Gadkari, R. Mukund and S. K. Gupta ,*Journal of Physics: Conference Series 390 (2012) 012041*.

[19]. O.B. Malyshev, R. Valizadeh, R.M.A. Jones, A. Hannah, Vacuum 86 (2012) 2035-2039.

[20]. J. D. Fast, *Interaction of Metals and Gases*, Vol. 1. Macmillan, New York, 1965.

[21]. J. H. N. van Vucht, *Proc. Int. Vac. Congr*., Como, p. 170 (1959).

[22]. A. Sieverts, *Z. Metallkd*. 21, 37 (1929).

[23]. C. Benvenuti, J.M. Cazeneuve, P. Chiggiato, F. Cicoira, A. Escudeiro Santana, V. Johanek, V. Ruzinov, J. Fraxedas, "A nouvel route to extreme vacua: the non-evaporable getter thin filmcoatings", Vacuum **53**, (1999), 219-225.

[24]. A. E. Prodromides, "Influence of substrate material and coating temperature on the vacuum properties of Tix ZryV1-x-y getter films produced by magnetron sputtering", Presentation at the IUVSTA 15th international vacuum congress, San Francisco, (2001).

[25]. B. Predel "LandoltB¨ornstein", New series, Group IV "Macroscopic Properties of Matter",n◦ 5 "Phase Equilibria, Crystallographic and Thermodynamic Data of Binary Alloys",published by Springer-Verlag, Berlin, edited by O. Madelung (1990).

[26]. "Alloy Phase Diagrams", edited by H. Baker, ASM Handbook n◦ 3, ASM International,The Materials Information Society (1992).

[27]. P. Waldner, "Modelling of Oxygen Solubility in Titanium", ScriptaMaterialia, vol. 40,

n◦ 8, pp. 969–974 (1999).

[28]. S.A. Raspopov, A.G. Gusakov, A.G. Voropayev, M.L. Zheludkevich, A.S. Gritsovets, A.A. Vecher and V.K. Grishin, "Interactions of Zirconium with Atomic and Diatomic Oxygen", Journal of the Chemical Soc. Faraday Trans., vol. 93, pp. 2113-2116 (1997).

[29]. G. H¨orz, H. Speck, E. Fromm, H. Jehn "Physics Data. Gases and Carbon in Metals(Thermodynamics, Kinetics, and Properties)" vol. 5-7, "Part VII: Group V A Metals(1): (V) (1981).

[30]. H. Jehn, E. Fromm, "Oxygen Solubility in the Va-Metals Vanadium, Niobium, and Tantalum", Metallwissenschaft und Technik, vol. 26, n◦ 10, pp. 1007-1011 (1972).

[31]. D.L. Smith, "Solubility of Oxygen in Vanadium", Journal of Less-Common Metals, vol. 31, n◦ 3, pp. 345–358 (1973).

[32]. G. H¨orz, H. Speck, E. Fromm, H. Jehn “Physics Data. Gases and Carbon in Metals (Thermodynamics, Kinetics, and Properties)” vol. 5-8, “ Part VIII: Group V A Metals(2): (Nb)” (1981).

[33]. R. Bryant, “The Solubility of Oxygen in Transition Metal Alloys”, Journal of the Less-Common Metals, vol. 4, pp. 62–68 (1962).

[34]. “ASM Handbook (Formerly Ninth Edition, Metals Handbook), vol. 13, Corrosion, edited by J. Davis, ASM International, The Material Information Society (1993).

[35]. F. T. Sisco, E. Epremian, “Columbium and Tantalum”, in “Wiley Series on the Science and Technology of Materials”, published by JohnWiley and Sons, Inc., New York (1963).

[36]. C. Benvenuti, S. Calatroni, V. Ruzinov, “Diffusion of Oxygen in Niobium During Bake-Out”, SRF2001, Tsukuba, The 10th Workshop on RF Superconductivity, September 6–11 (2001).

[37]. A.U. Seybolt, “Solid Solubility of Oxygen in Columbium”, Journal of Metals, vol. 6, pp. 774–776 (1954).

[38]. A.Taylor, N. J. Doyle, “Solid-Solubility of Oxygen in Nb and Nb rich Nb-Hf, Nb-Mo and Nb-W Alloys. Part I: The Nb-O System”, Journal of the Less-Common Metals, vol. 13, pp. 313–330 (1967).

[39]. G. H orz, H. Speck, E. Fromm, H. Jehn “Physics Data. Gases and Carbon in Metals (Thermodynamics, Kinetics, and Properties)” vol. 5-9, “ Part IX: Group V A Metals (3): (Ta)” (1981).

[40]. S. Stecura, “Observation of Oxide Particles Below the Apparent Oxygen Solubility Limit in Tantalum”, Metallurgical Transactions, vol. 5, pp. 1337–1340 (1974).

[41]. R.J. Wasilewski, “The Solubility of Oxygen in, and the Oxides of, Tantalum”, Journal of the American Ceramic Society, vol. 75, pp. 1001–1002 (1953).

[42]. Y. Adda, J. Philibert “La diffusion dans les solides”, Presses Universitaires de France, Paris (1966).

[43]. H. Bakker, H. P. Bonzel, C. M. Bruff, M.A. Dayananda, W. Gust, J. Horv´ath, I. Kaur, G. Kidson, A. LeClair, H. Mehrer, G. Murch, G. Neumann, N. Stolica, N. A. Stolica, N. Stolwijk, “LandoltB¨ornstein”, New series, Group III “Condensed Matter”, n◦ 26 “Diffusion in Solid Metals and Alloys”, published by Springer-Verlag, Berlin, edited by H. Mehrer (1990), Chapter 8: “Diffusion of C, N, and O in metals” (A. LeClair), Chapiter 9: “The Diffusion of H, D, and T in Metals” (G. Kidson).

[44]. E. Fromm, H. Jehn, G. H¨orz, “Physics Data. Gases and Carbon in Metals (Thermodynamics, Kinetics, and Properties)” vol. 5-3, “ Part III: Group III A Metals. Rare EarthMetals (Sc, Y, La, Ce, Pr, Nd, Sm, Eu, Gd, Tb, Dy, Ho, Er, Tm, Yb, Lu)” (1978).

[45]. H. Jehn, E. Fromm, G. H¨orz, “Physics Data. Gases and Carbon in Metals (Thermodynamics,Kinetics, and Properties)” vol. 5-5, “Part V: Group IV A Metals (1): (Ti)”(1979).

[46]. S. Mozhaev, L. Sokiryanskii, “Some Laws of Oxygen Diffusion in Titanium” in “Mobilityof Atoms in Crystal Lattices”, edited by V. N. Svechnikov, Kiev (1965), translated intoEnglish by the Israel Program for Scientific Translations (1970).

[47]. H. Jehn, H. Speck, E. Fromm, G. H¨orz, “Physics Data. Gases and Carbon in Metals (Thermodynamics, Kinetics, and Properties)” vol. 5-6, “ Part VI: Group IV A Metals (2): (Zr, Hf)” (1979)152.

[48]. E. Samsonov, “Handbook of the Physicochemical Properties of the Elements”, Translatedfrom Russian, Plenum, New York (1968).

[49]. D. Fisher, “Defects and Diffusion in Metal. Five Years of Research and Annual RetrospectiveI”, Scitec Publications (1999).

[50]. G. H¨orz, H. Speck, E. Fromm, H. Jehn “Physics Data. Gases and Carbon in Metals(Thermodynamics, Kinetics, and Properties)” vol. 5-8, “ Part VIII: Group V A Metals (2): (Nb)” (1981).

[51]. “Diffusion Data. A Continuous Compilation of New Reference Data on Diffusion Processin Inorganic Solids and their Melts”, vol. 3, published by The Diffusion InformationCenter, Cleveland (1969).

[52]. B. Predel “LandoltB¨ornstein”, New series, Group IV “Macroscopic Properties

[53]. Young JoonYoona, KeunWookKima, Hong Koo Baika,*, Serk-Won Jangb, Sung-Man Lee Thin Solid Films 350 (1999) 138-142.

[54]. R. E. Honig and H. O. Hook, *RCA Rev*. 21, 360, 567 (1960).

[55]. Massimo, Sancrotti and Gabriele Trezzi, Paolo Manini, J. Vac. Sci. Technol. A, Vol. 9, No2, Mar/Apr 1991.

[56]. J. L. Cecchi, P. H. LaMarche, H. F. Dylla, and R. J. Knize, J. Vac. ScI. Technol. A 3 (3)(1985)765.

[57]. O. Grobner, Bunch induced multipactoring, in: Proceedings of the 10th International Conference on High Energy Acc., Protvino, July, vol. 2, 1977, pp. 277–282.

[58]. K Oide, Observations and cures of electron-cloud effects at TheKEKB low energy ring, CERN Report No. SL-2001-003, 2001.

[59]. L.F. Wang, H. Fukuma, K. Ohmi, S. Kurokawa, K. Oide, F.Zimmermann, Phys. Rev. ST Acc. Beams 5 (2002) 124402.

[60]. M. Hahn and the ESRF Vacuum Group, Vacuum **81**, 759 (2007).

[61]. P. DellaPorta, Kindl, B ; Ruetsch Ch.,Schonhuber M. J., JVST Vol.6 (1969) 40-44.

[62]. C. Boffito, B. Ferrario, P. DellaPorta, and L. Rosai, J. Vac. Sci. Technol. 15, 1117 (1981).

[63]. C. Benvenuti, P. Chiggiato, P. Costa Pinto, A. Escudeiro Santana, T. Hedley, A. Mongelluzzo, V. Ruzinov, I. Wevers, Vacuum 60 (2001) 57-65.

[64]. P. dellaPorta et aI., Transactions of the 8th National Symposium, 1962 (unpublished), Vol. I, p. 229.

[65]. B. Ferrario et aI., Proceedings of the 9th Symposium on Fusion Technology (Pergamon, New York, 1976), p. 51.

[66]. C. Benvenuti and F. Francia, J. Vac. Sci. Technol. A 6 (4)(1988)2528.

[67]. Massimo Sancrotti, Gabriele Trezzi, Paolo Manini, J. Vac. Sci. Technol. A 9(2)(1991)182.

[68]. C. Bevenuti, P. Chiggiato, F. Cicoira, and Y. L. 'Aminto, J. Vac. Sci. Technol. A, Vol. 16, No. 1, Jan/Feb 1998.

[69]. Chien-Cheng Li, Jow-Lay Huang, Ran-Jin Lin, Ding-Fwu Lin, Surface & Coatings Technology 201 (2006) 3977–3981.

[70]. Kenji Ichimura, Masao Matsuyama, and KuniakiWatanabe J. Vac. Sci. Technol. A 5 (2) (1987) 220.

[71]. Benvenuti C, Chiggiato P, Cicoira F, Ruzinov V, Vacuum (1998);50:57.

[72]. A High Energy Hemispherical Analyzer for Experimental Station of PES beamline at Indus-2", Jagannath, R.K.Sharma, U.K.Goutam, N. Mithal, U.S. Sule, S.C.Gadkari, J.V.Yakhmi and V.C. Sahni, *BARC/2009/E/006*, [2009].

[73]. Design and development of Toroidal shape analyzer", R.K. Sharma, U.K. Goutam, Jagannath, S.C. Gadkari, J.V. Yakhmi and V.C. Sahni, *EMSI (2009)47-48*, [2009].

[74]. Jagannath, U.S. Sule, R. Pradeep, RK Sharma, UK Goutam, VB Bhandarkar, SC Gadkari, JV Yakhmi and VC Sahni, *Asian J Phys 16(4)(2007)331-338*, [2007].

[75]. Design and development of Photo-emission electron microscope for ARPES/PEEM beamline on Indus-2", U.K. Gautam, R.K. Sharma, Jagannath, S.C. Gadkari, *EMSI (2009)76-77*, [2009].

Chapter 2

[76]. W. R. 1852 On the electro-chemical polarity of gases. Phil. Trans. R. Soc. Lond. 142, 87–101.

[77]. KiyotakaWasa, Makoto Kitabatake, Hideaki Adachi, "Thin film material technology" pp. 2 - 3 published, William Andrew, IncUSA(2004).

[78]. Mahan, J. E., Physical Vapor Deposition of Thin Films, p. 133, John Wiley & Sons, New York (2000).

[79]. E. Kay, Techniques of Metals Research, vol. 1, Chapter 31, "Thin Film Sputtering Techniques", pp. 1269–1309, published by Interscience, New York (1968). (Published a second time as proceedings: E. Kay, "Physics of Sputtering Processes", pp. 18–59, published by London MRC Materials Research Co in Transactions of the Conference and School on the Elements, Techniques and Applications of Sputtering, October 20–22, 1969, Grand Hotel, Brighton.).

[80]. .D. Smith, "Thin-film Deposition. Principles and Practice", McGraw-Hill, Inc., New York (1995) p. 371.

[81]. Idem as [83] p. 1274.

[82]. Stuart, R. V., and Wehner, G. K., *J. Appl. Phys.*, 33:2345 (1962).

[83]. Wasa, K., and Hayakawa, S., *Rev. Sci. Instrum.,* 40:693 (1969).

[84]. Wehner, G. K., *Phys. Rev.*, 102:690 (1956), ibid., l08:35 (1957), ibid.,112:1120 (1958)

[85]. Wehner, G. K., *Phys. Rev.*, 108:35 (1957).

[86]. Wehner, G. K., *J. Appl. Phys.*, 30:1762 (1959).

[87]. Wehner, G. K., and Rosenberg, D. L., *J. Appl. Phys.*, 31:177 (1960).

[88]. G. K. Wehner, in *Handbook of Thin Film Technology,* eds. L. I. Maissel and R. Glang. McGraw-Hill, New York, 1970.

[89]. Wasa, K., and Hayakawa, S., *Jpn. J. Electrical Engineering*, 85:130 (1965).

[90]. Brown, S. C., *Basic Data of Plasma Physics*, MIT Press, p. 258, Cambridge, MA (1959).

[91]. Von Engel, A., and Steenbeck, M., *ElektrischeGasentladunger*II:68, J. Springer, Berlin

[92]. N. Khan, I. H., in: *Handbook of Thin Film Technology,* (L. Maissel and R. Clang, eds.) 10-1, McGraw-Hill, New York (1970).

[93]. Penning, F. M., U.S. Patent 2,146,025 (Feb. 1935).

[94]. Wasa, K., and Hayakawa, S., *Proc. IEEE,* 55:2179 (1967).

[95]. R. K. Sharma, N. Mithal, Jagannath, K. G. Bhushan, D. Srivastava, H. R.Prabhakara3, S. C. Gadkari, J. V. Yakhmi and V. C. Sahni, Journal of Physics: Conference Series 114 (2008) 012050.

[96]. Nidhi Gupta, Jagannath, R. K. Sharma, S. C. Gadkari, K. P. Muthe, AIP Conf. Proc. 1512, 794 (2013); doi: 10.1063/1.4791277.

Chapter 3

[97]. Meli, F.; Sheng, Z.; Vedel, I.; Schlapbach, L. XPS analysis of the getter mechanism and getter activation process. *Vacuum* 1990, 41, 1938-1940.

[98]. Narducci, E.; Kovac, J.; Ghezzi, F.; Venkataramani, N.; Sancrotti, M. Water dissociation and selective absorption in the Zr[V0.5Fe0.5]2 gettering alloy: An x-ray photoemission spectroscopy investigation. *J. Vac. Sci. Technol.* 1991, A17(2), 385-390.

[99]. Henrist, B.; Hilleret, N.; Scheuerlein, C.; Taborelli, M. The secondary electron yield of TiZr and TiZrVnonevaporable getter thin film coatings. *Applied Surface Science* 2001, 172, 95-102.

[100]. C. R. Brundle: J. Vac. Sci. Technol. **11**, 212 (1974).

[101]. M. P. Seah and W. A, Dench: Surf. Interf. Anal. **1**, 2 (1979).

[102]. V. K. Zworykin, J. Hillier, R. L. Snyder, ASTM Bulletin **1942,** 11 **7,** 15.

[103]. T. E. Everhart, R. **F.** M. Thornley, J. Sci. Instrum. **1960, 37,** 246.

[104]. K .C. A. Smith, Proceedings *of*' the 5th Annual SEM Symposium (Ed: O. Johari), IITRI.Chicago1972, p. 1.

[105]. J. I. Goldstein, D. E. Newbury, P. Echlin, D. C. Joy, A. D. Romig, J. C.E. Lyman, C. Fiori, and E. Lifshin, "Scanning Electron Microscopy and X-ray Microanalysis, second edition", Plenum press 1992, New York,USA, chap.1, p.18.

[106]. Benvenuti C, J.M. Cazeneuve, P. Chiggiato, F. Cicoira, A. Escudeiro Santana, V. Johanek, V. Ruzinov, J. Fraxedas,Vacuum 53 (1999) 219-225.

[107]. C. Benvenuti, P. Chiggiato*, P. Costa Pinto, A. Prodromides, V. Ruzinov, Vacuum 71 (2003) 307–315.

[108]. Benvenuti C, Francia F. J Vac SciTechnol 1990; A8:3864.

[109]. Benvenuti C, Chiggiato P. J Vac SciTechnol 1996; A14:3278.

[110]. B.D.Cullity in elements of X-ray diffraction, Ed M. Cohen (Addison-Wesley publishing company, 1956).

[111]. C. Suryanarayan and M.G. Nortan in X-ray diffraction, a practical approach (New York: Plenem press 1998).

[112]. C. Kittel in introduction to solid state physics (John Wiley & Sons Inc.,1996)

Chapter 4

[113]. C. Benvenuti, P. Chiggiato, F. Cicoira, Y. L'Aminot, V. Ruzinov, Vacuum 73 (2004) 139.

[114]. V. Matolin, V. Dudr, S. Fabik, V. Chab, K. Masek, I. Matolinova, K.C. Prince, T. Skala, F.Sutara, N. Tsud, K. Veltruska, Appl. Surf. Sci. 243 (2005) 106.

[115]. S. Fabik, V. Chab, V. Dudr, K. Masek, K.C. Prince, F. Sutara, K. Veltruska, N. Tsud, M. Vondracek, V. Matolin, Surf. Sci. 566–568 (2004) 1246.

[116]. C. Scheuerlein, M. Taborelli, J. Vac. Sci. Technol. A 20 (2002) 93.

[117]. XPS studies on Non-Evaporable Getter(NEG) thin films of Zr and Ti-Zr for possible applications in production of extreme high vacuum(XHV), **R.K.Sharma**, N.Mithal, Shahshwati Sen, Jagannath, K.G.Bhushan, S.C. Gadkari, J.V. Yakhmi and V.C. Sahni, *Bulletin of Indian vacuum Society*, Vol.9(2), 2006, pp. 11-14.

[118]. R. K. Sharma, N. Mithal, Jagannath, K. G. Bhushan, D. Srivastava, H. R.Prabhakara, S. C. Gadkari, J. V. Yakhmi and V. C. Sahni, Journal of Physics: Conference Series 114 (2008) 012050.

[119]. J.F. Moulder, W.F. Stickle, P.E. Sobol, K.D. Bomben, Handbook of X-ray PhotoelectronSpectroscopy, Perkin-Elmer Corporation Physical Electronics Division,Minnesota, U.S.A, 1992, p. 40.

[120]. Chien-Cheng Li, Jow-Lay Huang, Ran-Jin Lin, Ding-FwuLii, Chia-Hao Chen,Li-Chyong Chen, Kuei-Hsien Chen, Thin Solid Films 517 (2009) 3672–3676.

[121]. T.B. Massalaki, J.L. Murray, L.H. Bennett, H. Baker, L. Kacprzak, Binary alloy phasediagrams, vol. 2, American Society for Metals, Metals Park, Ohio, 1986, p. 593.

[122]. V. Matolin, V. Johanek, Vacuum 67 (2002) 177–184

[123]. "Concise Encyclopedia of Materials Characterization", edited by R. Cahn, E. Lifshin,

Series: Advances in Materials Science and Engineering, Oxford, Pergamon Press Ltd.

(1993).

[124]. J.-P. Eberhart, "Analyse StructuraleetChimique des Mat´eriaux", Dunod, Paris (1989).

[125]. Idem as [124] pp. 109–111.

[126]. N. Cusack, "The Physics of Structurally Disordered Matter: an Introduction", IOPPublishing Ltd, Bristol (1987).

[127]. D. Brandon, W. Kaplan, "Microstructural Characterization of Materials", published by John Wiley & Sons Ltd, Chichester (1999).

[128]. J.-P. Lauriat, "Introduction `a la Cristallographie et `a la Diffraction Rayons X - Neutrons",edited by Paris Onze Edition, Orsay (1996).

[129]. L. Dent Glasser, "Crystallography and its Applications", published by Van Nostrand Reinhold Company, New York (1977).

[130]. H. Klug, L. Alexander, "X-ray Diffraction Procedures: for Polycrystalline and Amorphous Materials", Wiley Interscience, New York, second edition (1974), p. 562.

[131]. H. Lipson, H. Steeple, "Interpretation of X-Ray Powder Diffraction Patterns", Macmillan,London (1970), pp. 246–263.

Chapter-5

[132]. B. Henrist, N. Hilleret, C. Scheuerlein, M. Taborelli, and G. Vorlaufer, "The variation of the secondary electron yield of copper under electron bombargemnt: Origin and impact on the conditioning of the LHC," CERN. Geneva, Switzerland, Proc. EPAC 2002.

[133]. C. Kunz, "Synchrotron Radiation Overview", in "*Photoemission in Solids II*", edited by L.Ley and M. Cardona, Springer Verlag, (1979), 322.

[134]. M. P. Brown and K. Austin, *The New Physique*, Publisher City: Publisher Name, 2005, pp. 25-30.

[135]. O. Grobner, Bunch induced multipactoring, in: Proceedings of the 10th International Conference on High Energy Acc., Protvino, July, vol. 2, 1977, pp. 277–282.

[136]. K Oide, Observations and cures of electron-cloud effects at The KEKB low energy ring, CERN Report No. SL-2001-003, 2001.

[137]. L.F. Wang, H. Fukuma, K. Ohmi, S. Kurokawa, K. Oide, F.Zimmermann, Phys. Rev. ST Acc. Beams 5 (2002) 124402.

[138]. M. P. Brown and K. Austin, *Appl. Phys. Letters* **85**, 2503-2504 (2004).

[139]. R. T. Wang, "Title of Chapter," in *Classic Physiques*, edited by R. B. Hamil, Publisher City: Publisher Name, 1999, pp. 212-213.

[140]. B. Henrist, N. Hilleret, C. Scheuerlein, M. Taborelli, Applied Surface Science 172 (2001) 95 - 102.